MinEx CRC Limited
26 Dick Perry Avenue, Kensington, WA, 6151
PO Box 1130, Bentley, WA, 6102, Australia
admin@minexcrc.com.au

ABN: 66 625 533 913

MinEx CRC provides financial support to the value of $1K to promote Honours and Masters by Coursework projects that are aligned with the mission of MinEx CRC and to encourage young researchers toward a career in mineral exploration research. Projects are not restricted to MinEx CRC Participants and Affiliates.

Please note that the content of this thesis has not been subjected to peer-review and subsequent corrections.

Australian Government
Department of Industry, Science and Resources
Cooperative Research Centres Program

SCHOOL OF WASM: MINERALS, ENERGY AND CHEMICAL ENGINEERING

CHEMICAL ENGINEERING

SOFTWARE SIMULATION OF REVERSE CIRCULATION AIR DRILLING

BY

CHLOE THIEL

19478078

NOVEMBER 2021

To the best of my knowledge and belief, this report contains no material previously published by any other person except where due acknowledgement has been made. This report contains no material which has been accepted for the award of any other degree or diploma in any university.

Signature	:	
Name	:	Chloe Thiel
Date	:	04/11/2021

ABSTRACT

Title: Software Simulation of Reverse Circulation Air Drilling

Author: Chloe Thiel

Date: 4/11/2021

Supervisors: Dr Dimple Quyn and Dr Masood Mostofi

The research project objective was to simulate single phase, compressible air and water, and two-phase air-water, compressible, steady state flow in the vertical, inner and outer annulus pipes of a reverse circulation air drilling rig through software, with investigation into pressure drops profiles, velocity profiles, liquid holdup, and flow pattern. The software simulations were validated using analytical model data.

The simulations were developed using Schlumberger's PIPESIM and ANSYS Fluent software, following the standard simulation procedure and specifying appropriate models. The inner and outer annulus drill string pipe was simulated for single-phase air and water flow using PIPESIM and ANSYS Fluent, and two-phase air-water flow using PIPESIM. Several sensitivity studies at different drilling depths with vary total mass flowrate and varying liquid-gas ratios (LGRs) were also conducted through PIPESIM. The single-phase air and water flow results were validated between the software simulations and against the Drilling Mechanics Group (DMG) analytical and Simulink models, while the initial two-phase flow simulation in PIPESIM was validated against the DMG analytical and Simulink models.

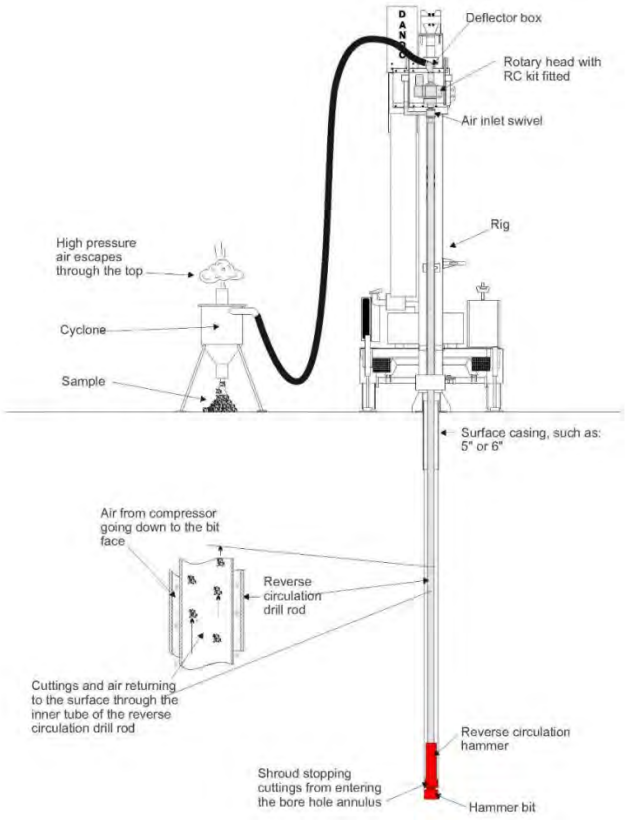

The major findings of the research project were the development of a series of operating regime charts for identifying the optimal volumetric flowrate of water to be added to compressed air at a standard 1500 SCFM for the inner pipe, outer annulus pipe and overall operation, to obtain the most desirable flow pattern, for example *annular* or *mist* with reduced liquid holdup. It was concluded for overall operation of a 90 m wellbore, a maximum of 11.38 L/min of water can be added to maintain *annular* and *annular-mist* flow patterns in the inner and outer annular pipes, respectively. The operating regime charts have the potential to decrease fuel consumption during operation with decreased liquid holdup and hence, increasing mineral cuttings transportation and RC drilling production.

ACKNOWLEDGEMENTS

Throughout my engineering industry research project, I have obtained extensive knowledge and received continuous guidance and support from my supervisors and the Drilling Mechanics Group at Technology Park. I would like to acknowledge and thank my supervisors; Dr Dimple Quyn for her endless support, guidance, and motivation, through weekly meetings, email communications and review of my research project submissions, and Dr Masood Mostofi for his support and valuable technical contributions. I would also like to acknowledge Dr Thomas Richard for his support, critical review, and contributions towards my research. The Drilling Mechanics Group at Technology Park are acknowledged for welcoming and accommodating my research studies.

TABLE OF CONTENTS

LIST OF FIGURES ..... **VII**
LIST OF TABLES ..... **IX**
NOTATION ..... **X**
ACRONYMS ..... **XI**
1. INTRODUCTION **1**
1.1. Background 1
1.2. Problem Statement and Objectives 4
1.2.1. Research Problem Statement 4
1.2.2. Research Objectives 5
1.3. Significance of the Research 7
1.4. Scope and Limitations 7
1.4.1. Scope of the Research 7
1.4.2. Limitations of the Research 8
2. LITERATURE REVIEW **9**
2.1. Content of the Literature Review 9
2.1.1. Mineral Drilling Background 9
2.1.2. RC Air Drilling 9
2.1.3. Fundamentals of Multiphase Flow 12
2.1.4. Fundamentals of Pneumatic Cuttings Transport 14
2.2. Research Gap 16
3. METHODOLOGY **17**
3.1. Simulation Software 17
3.1.1. ANSYS Fluent 2020 R2 Software 17
3.1.2. Schlumberger's PIPESIM Software 18
3.2. ANSYS Fluent Simulation Procedure 18
3.2.1. Preliminary Conceptual Design and Planning 19
3.2.2. Construction of Drill String Geometry 20
3.2.3. Generation of Drill String Mesh 20
3.2.4. Simulation of Drill String Fluid Flow 21
3.3. PIPESIM Simulation Procedure 21
3.3.1. Preliminary Conceptual Planning 22
3.3.2. Construction of Drill String Geometry 22
3.3.3. Simulation of Drill String Fluid Flow 22

3.4. Analysis and Validation of Simulation Results 23
3.5. Evaluation of Methodology 24
4. RESULTS AND DISCUSSION 25
4.1. Single Phase Air Flow in RC Drilling 25
4.1.1. Single Phase Air Flow in Inner Drill String Pipe 25
4.1.2. Single Phase Air Flow in Outer Annulus Drill String Pipe 28
4.1.3. Single Phase Air Flow Modelling Evaluation 30
4.2. Single Phase Water Flow in RC Drilling 31
4.2.1. Single Phase Water Flow in Inner Drill String Pipe 31
4.2.2. Single Phase Water Flow in Outer Annulus Drill String Pipe 33
4.2.3. Single Phase Water Flow Modelling Evaluation 35
4.3. Two-Phase Air-Water Flow in RC Drilling 35
4.3.1. Two-Phase Air-Water Flow in Inner Drill String Pipe 35
4.3.2. Two-Phase Air-Water Flow in Outer Annulus Drill String Pipe 38
4.3.3. Two-Phase Air-Water Flow Modelling Evaluation 41
4.4. Two-Phase Air-Water Flow in RC Drilling Sensitivity Studies 42
4.4.1. Two-Phase Air-Water Flow in Inner Drilling Pipe Sensitivity Studies 42
4.4.2. Two-Phase Air-Water Flow in Outer Annulus Drilling Pipe Sensitivity Studies 44
4.4.3. Two-Phase Air-Water Flow Model Sensitivity Studies Evaluation 47
4.5. Operating Regime Charts for RC Air Drilling 48
4.5.1. Two-Phase Air-Water Flow in RC Drill String Pipes Operating Regime Charts 48
4.5.2. RC Air Drilling Operating Regime Charts Evaluation 53
5. CONCLUSIONS 54
6. RECOMMENDATIONS 56
REFERENCES 57
APPENDIX A – RESEARCH PROJECT GANTT CHART 60
APPENDIX B – DATA MANAGEMENT PLAN (DMP) 64
APPENDIX C – ANSYS FLUENT SIMULATION MODELLING 67
APPENDIX D – ANSARI MULTIPHASE, VERTICAL FLOW CORRELATION 69
APPENDIX E – ORKISZEWSKI MULTIPHASE, VERTICAL FLOW CORRELATION 79

LIST OF FIGURES

FIGURE 1.1.1: RC AIR DRILLING RIG DIAGRAM. 2
FIGURE 2.1.2.1: RC AIR DRILLING PROCESS DIAGRAM. 10
FIGURE 3.2.1: FLOW DIAGRAM OF ANSYS FLUENT SIMULATION PROCEDURE. 19
FIGURE 3.2.1.1: PRELIMINARY DESIGN FOR SOFTWARE SIMULATION 20
FIGURE 3.3.1: FLOW DIAGRAM OF PIPESIM SIMULATION PROCEDURE. 22
FIGURE 4.1.1.1: COMPARISON OF SINGLE-PHASE AIR, INNER PIPE FLOW PRESSURE DROP PROFILES FROM PIPESIM, ANSYS FLUENT, DMG ANALYTICAL MODEL AND DMG SIMULINK MODEL. 26
FIGURE 4.1.1.2: COMPARISON OF SINGLE-PHASE AIR, INNER PIPE FLOW VELOCITY PROFILES FROM PIPESIM, ANSYS FLUENT, DMG ANALYTICAL MODEL AND DMG SIMULINK MODEL. 27
FIGURE 4.1.2.1: COMPARISON OF SINGLE-PHASE AIR, OUTER ANNULUS PIPE FLOW PRESSURE DROP PROFILES FROM PIPESIM AND ANSYS FLUENT. 29
FIGURE 4.1.2.2: COMPARISON OF SINGLE-PHASE AIR, OUTER ANNULUS PIPE FLOW VELOCITY PROFILES FROM PIPESIM AND ANSYS FLUENT. 29
FIGURE 4.2.1.1: COMPARISON OF SINGLE-PHASE WATER, INNER PIPE FLOW PRESSURE DROP PROFILES FROM PIPESIM, ANSYS FLUENT, DMG ANALYTICAL MODEL AND DMG SIMULINK MODEL. 32
FIGURE 4.2.1.2: COMPARISON OF SINGLE-PHASE WATER, INNER PIPE FLOW VELOCITY PROFILES FROM PIPESIM, ANSYS FLUENT, DMG ANALYTICAL MODEL AND DMG SIMULINK MODEL... 32
FIGURE 4.2.2.1: SINGLE-PHASE WATER, OUTER ANNULAR PIPE FLOW PRESSURE DROP PROFILES FROM PIPESIM AND ANSYS FLUENT. 34
FIGURE 4.2.2.2: SINGLE-PHASE WATER, OUTER ANNULAR PIPE FLOW VELOCITY PROFILES FROM PIPESIM AND ANSYS FLUENT. 34
FIGURE 4.3.1.1: COMPARISON OF TWO-PHASE AIR-WATER, INNER PIPE FLOW PRESSURE DROP PROFILES USING THE ANSARI AND NO SLIP PIPESIM CORRELATIONS, DMG ANALYTICAL MODEL AND DMG SIMULINK MODEL. 36
FIGURE 4.3.2.1: COMPARISON OF TWO-PHASE AIR-WATER, OUTER ANNULUS PIPE FLOW PRESSURE DROP PROFILES USING THE ORKISZEWSKI AND NO SLIP PIPESIM CORRELATIONS. 39
FIGURE 4.4.1.1: TWO-PHASE AIR-WATER, INNER PIPE FLOW OVERALL PRESSURE DROP USING THE ANSARI AND NO SLIP PIPESIM CORRELATIONS WITH VARYING MASS FLOWRATE. 42

FIGURE 4.4.1.2: TWO-PHASE AIR-WATER, INNER PIPE FLOW PATTERNS USING THE ANSARI PIPESIM CORRELATION WITH VARYING TOTAL MASS FLOWRATE. 43
FIGURE 4.4.2.1: TWO-PHASE AIR-WATER, OUTER ANNULAR PIPE FLOW OVERALL PRESSURE DROP USING THE ORKISZEWSKI AND NO SLIP PIPESIM CORRELATIONS WITH VARYING TOTAL MASS FLOWRATE. 45
FIGURE 4.4.2.2: TWO-PHASE AIR-WATER, OUTER ANNULAR PIPE FLOW PATTERN USING THE ORKISZEWSKI AND NO SLIP PIPESIM CORRELATIONS WITH VARYING TOTAL MASS FLOWRATE. 45
FIGURE 4.5.1.1: TWO-PHASE AIR-WATER, INNER PIPE OPERATING REGIME CHART. 49
FIGURE 4.5.1.2: TWO-PHASE AIR-WATER, INNER PIPE OPERATING REGIME CHART ASSOCIATED FLOW PATTERNS. 49
FIGURE 4.5.1.3: TWO-PHASE AIR-WATER, OUTER ANNULAR PIPE OPERATING REGIME CHART..... 51
FIGURE 4.5.1.4: TWO-PHASE AIR-WATER, OUTER ANNULAR PIPE OPERATING REGIME CHART ASSOCIATED FLOW PATTERNS. 51
FIGURE C.1: ANSYS FLUENT SIMULATION REALIZED K-EPSILON VISCOUS MODEL AND CONSTRAINTS. 67
FIGURE C.2: ANSYS FLUENT SIMULATION REALIZED K-EPSILON VISCOUS MODEL WITH ENHANCED WALL TREATMENT..... 68

LIST OF TABLES

TABLE 3.3.1: SUMMARY OF THE AVAILABLE PIPESIM MULTIPHASE FLOW CORRELATIONS..... 23

NOTATION

VARIABLE	DESCRIPTION	UNITS
A (IP)	Cross sectional area of inner drilling pipe	m^2
A (OP)	Cross sectional area of outer annulus drilling pipe	m^2
Di (DB)	Inside diameter of drill bit	*mm*
Di (IP)	Inside diameter of inner drilling pipe	*mm*
Di (OP)	Inside diameter of outer annulus drilling pipe	*mm*
Di (W)	Inside diameter of wellbore	*mm*
Do (IP)	Outside diameter of inner drilling pipe	*mm*
Do (OP)	Outside diameter of outer annulus drilling pipe	*mm*
h	Depth from drilling surface	*m*
L (DB)	Vertical length of drill bit	*m*
L (IP)	Vertical length of inner drilling pipe	*m*
L (OP)	Vertical length of outer annulus drilling pipe	*m*
m(air, bot)	Mass flowrate of air into the bottom of the inner drilling pipe	*kg/s*
m(air, in)	Mass flowrate of air into the drill string	*kg/s*
m(air, out)	Mass flowrate of air out of the drill string	*kg/s*
m(water, bot)	Mass flowrate of water into the bottom of the inner drilling pipe	*kg/s*
m(water, in)	Mass flowrate of water into the drill string	*kg/s*
m(water, out)	Mass flowrate of water out of the drill string	*kg/s*
P(in)	Pressure of fluid at drill string inlet	*Pa*
P(out)	Pressure at drill string outlet	*Pa*
P0	Standard atmospheric pressure	*Pa*
Q(air, bot)	Volumetric flowrate of air into the bottom of the inner drilling pipe	m^3/s
Q(air, in)	Volumetric flowrate of air into the drill string	m^3/s
Q(air, out)	Volumetric flowrate of air out of the drill string	m^3/s
Q(water, bot)	Volumetric flowrate of water into the bottom of the inner drilling pipe	m^3/s
Q(water, in)	Volumetric flowrate of water into the drill string	m^3/s
Q(water, out)	Volumetric flowrate of water out of the drill string	m^3/s
T(in)	Temperature of fluid at drill string inlet	*K*
T(out)	Temperature of fluid at drill string outlet	*K*
T0	Standard ambient temperature	*K*
v(air, bot)	Velocity of air into the bottom of the inner drilling pipe	*m/s*
v(air, in)	Velocity of air into the drill string	*m/s*
v(water, bot)	Velocity of water into the bottom of the inner drilling pipe	*m/s*
v(water, in)	Velocity of water into the drill string	*m/s*
dP	Pressure drop	*kPa or bar*
ε (IP)	Absolute inner drilling pipe roughness	*mm*
ε (OP)	Absolute outer annulus drilling pipe roughness	*mm*
ρ(water, in)	Density of water into the drill string	kg/m^3

ACRONYMS

ACRONYM	ANTONYM
2D	Two Dimensional
3D	Three Dimensional
CAD	Computer-Aided Design
CFD	Computation Fluid Dynamics
DMG	Drilling Mechanics Group
IPR	Inflow Performance Relationship
LGR	Liquid to Gas Ratio
RC	Reverse Circulation
SCFM	Standard Cubic Feet per Minute
VC	Vertical Correlation

1. INTRODUCTION

1.1. Background

In modern mineral drilling, the use of air (or other available gas) is commonly used as the drilling fluid. This technique requires compressed air to transport rock cuttings accumulated at the bottom of a wellbore to the drilling surface. This approach to mineral drilling was established in the 1950s and continues to be used today, especially for the drilling of extremely hard mineral surfaces to increase boring rates and for its ability to maintain continuous circulation. Air drilling applications can be categorised into two main techniques; direct air drilling and reverse circulation (RC) air drilling (Zhu et al. 2015). RC air drilling is a relatively new technology when compared to traditional direct drilling methods, with increasing industry popularity in recent years.

Generally, RC air drilling is utilised for the creation of both vertical and horizontal, straight wellbores. In vertical RC configurations, compressed air enters at the top of the outer annulus drilling pipe, flowing down towards the bottom of the wellbore. The air flowing across the surface of the rock cuttings, lifts and carries the cuttings up through the inner drilling pipe to the surface for discharge, as seen in Figure 1.1.1 (Zhu et al. 2015). The continuous nature of RC air drilling is highly time efficient, while optimal pressure conditions allow for a long drill bit life and stable wellbore. Due to the efficiency and stability of this technique, it requires low intensity labour and is reliable in the most complex of drilling situations, including geothermal wellbore drilling (Xiumin, Yue, and Luheng 2014).

The technique of RC air drilling for minerals is based on key engineering fundamentals, including multiphase, compressible flow in pipes, which is the foundation of all drilling applications (Cao et al. 2019). Multiphase, compressible flow, in particular gas-liquid two-phase flow, is a concept present in an extensive range of applications in industry, including oil and gas, nuclear and chemical processes. Hence, it has been studied thoroughly, for both horizontal and vertical pipe configurations to determine the flow pattern, liquid holdup, velocity profile and pressure drop (López et al. 2016). Recently, (Ganat et al. 2019) theoretically studied upward, two-phase, compressible flow in a vertical pipe configuration, while (López et al. 2016) conducted experimental and numerical modelling studies in horizontal pipes for two-phase flow. However, it can be observed in the vertical flow study by (Ganat et al. 2019), as opposed to the horizontal flow study by (López et al. 2016), multiphase vertical flow is largely influenced by buoyancy and gravitational forces, resulting in highly symmetric radial properties, and

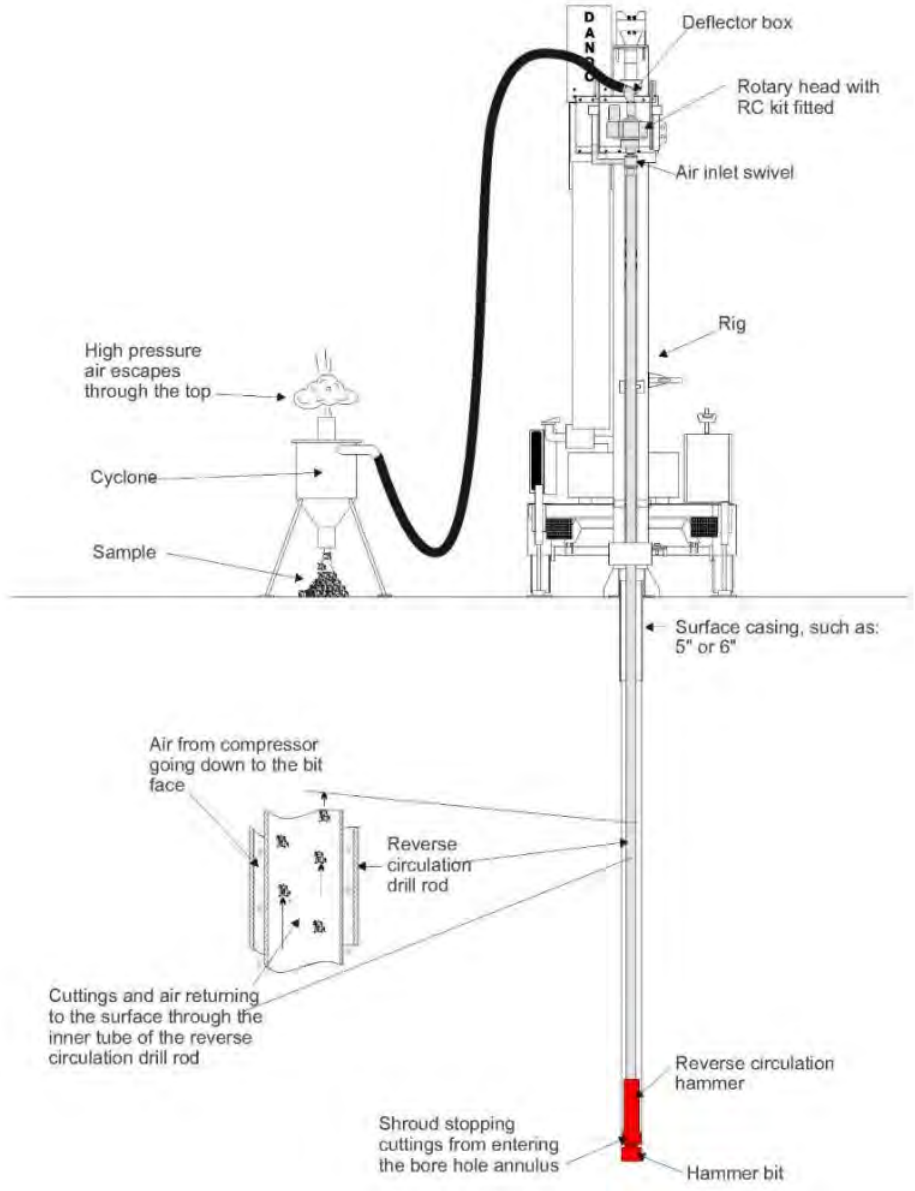

Figure 1.1.1: RC air drilling rig diagram.

Source: Figure reproduced from Dando Drilling International (2016).

making hydrostatic pressure drop during drilling the major cause of pressure loss. Therefore, the liquid holdup and pressure drop modelling is vital to vertical RC drilling (Eissa and James 2017) and different to that of horzontal multiphase flow. It also diffs to that of direct drilling, as the pressure drop increases as a function of distance travelled, and can therefore impact the vertical flow regimes significantly, impacting cuttings transportation.

While modelling single-phase properties and flowrates is relatively easy, multiphase fluid flow modelling uses the individual phases properties and flowrates to determine complex

multiphase variables, such as liquid holdup and void fraction, that affect multiphase mixture properties, including flow pattern, and therefore, the pressure drop of the system (Ben Mahmud 2012). Hence, for complex multiphase flow modelling, several correlations must be collated for each individual phase before the multiphase mixture variables and properties can be determined. This may give rise to various numerical difficulties and disconnected variable predictions, if the initial individual phase variables are calculated incorrectly (Ellul, Saether, and Shippen 2004).

The other key engineering fundamental in RC air drilling is pneumatic cuttings transport, which is dependent on the systems pressure drop. Cuttings transportation is the basis of improved drilling rates and optimisation, evidently, pneumatic cuttings transport has been studied thoroughly across the engineering literature. Most recently, (Zhang et al. 2021) conducted a series of experiments on gas-solid multiphase flow in horizontal drilling pipes. This study investigated the pressure drop of the system and calculated the minimum pneumatic conveying pressure. Hence, validating the vital relationship between pressure drop and cuttings transport. While many available studies explore cuttings transport in horizontal flow configurations, some studies for vertical configuration have been conducted.

Considering the board range of multiphase, compressible flow and cuttings transport literature, modelling RC air drilling has been attempted for some oil and gas applications. In the past year, (Krishna et al. 2020) theoretically modelled fluid velocity in a concentric annulus to determine surge and swage pressure gradients for oil and gas industry RC drilling. (Wang et al. 2020) studied the drilling gas in coal seam extraction using a dynamic inversion model. This study is important to the research of RC drilling and relevant to many of its applications, as drilling performance is based on the carrying capacity of drilling fluid and hence, the drilling fluid properties (i.e.: flowrate). (Han, Li, and Li 2020) also simulated pneumatic, reverse circulating cuttings removal for coal seam drilling to determine flow characteristic of the cuttings, flow characteristics of the air, forces between cuttings and air, the effects of cuttings removal and two-phase flow pressure drop. Similarly, (Han, Song, and Li 2020) determined the influence of air flowrate, cuttings flowrate and cuttings particle sizes on the system pressure drop during reverse circulating pneumatic cuttings removal of coal seam through experiments. However, these studies conducted by (Krishna et al. 2020), (Wang et al. 2020), (Han, Li, and Li 2020) and (Han, Song, and Li 2020) do not aim to model RC air drilling for mineral drilling applications, but rather for general oil and gas well drilling without cuttings transport, or for multiphase, seam coal gas drilling with cuttings transport – both of which are significantly different to that in mineral drilling. Hence, solid mineral cuttings flow within a two-phase, air-water system has not been modelled, to the author’s knowledge.

Based on the studies previously discussed, multiphase, compressible flow, pneumatic cuttings transport and oil and gas industry drilling applications of RC air drilling require fitting together several correlations which are often empirical into a heterogeneous multiphase model (Moshfeghian 2008). The compilation of these theories and techniques to simulate multiphase, compressible, steady state flow in vertical RC air drilling of minerals requires determining individual phase properties from which multiphase flow properties and variables can be calculated, for both a simple vertical pipe and a vertical annulus pipe, including piping components (i.e.: expansions), as well as solid cuttings transport properties. However, in the last decade drilling research has extended to include simulation software to comprehensively determine fluid flow through a system for critical analysis and performance review. The advancements in readily available software systems, increased computer speed and memory capabilities, have made software simulation more economical, time efficient and safer than traditional experiments and pilot plant studies (Ben Mahmud 2012).

To obtain a comprehensive understanding of mineral RC air drilling in industry, a software simulation is to be developed for vertical, multiphase, compressible, steady state flow through a drill string. Based on the key fundamentals previously discussed, the simulation will allow the study of the influence of hydrostatic pressure and major head loss due to pipe surface friction on pressure drop, the influence of different drilling depths and other parameters (i.e.: total mass flowrate, liquid gas ratio (LGR)) on flow pattern, pressure drop and velocity profile, and to investigate other key RC air drilling variables, such as liquid holdup, computed by the software.

1.2. Problem Statement and Objectives

1.2.1. Research Problem Statement

There have been no previous software simulations used to model multiphase, compressible, steady state flow in vertical RC air drilling of minerals. The related studies conducted are based on multiphase, compressible flow in vertical pipes, pneumatic cuttings transportation or oil and gas industry drilling applications alone. Hence, the underlying fundamental engineering theory, assumptions, and software capabilities used in these studies have not been studied collaboratively to represent the flow phenomena occurring in mineral RC drilling applications. Furthermore, studies into the pressure loss in RC air drilling including hydrostatic and major head loss caused by pipe surface friction have not been conducted. A software simulation that can comprehensively represent hydrostatic and major head loss in the modelling of pressure drop, velocity profile and flow pattern with varied drilling depth and other variables, such as

total mass flowrate and LGR, and compute other key drilling performance related variables, including liquid holdup in mineral RC air drilling will create a strong foundation for optimisation and automation in industry.

1.2.2. Research Objectives

The overall aim of this research project is to simulate multiphase, compressible, steady state flow in vertical RC air drilling of minerals through software. The research conducted will not determine a new numerical model, but instead use a combination of suitable existing engineering theory and valid assumptions to create a comprehensive simulation. This software simulation will be validated using analytical modelling data sourced external to this study. The objectives of this research project are:

1. To establish a software simulation to model two-phase, compressible, steady state flow in vertical RC air drilling of mineral and study the influence of hydrostatic pressure and major head losses on the overall drill string pressure drop.
2. To investigate the influence of other system variables, including drilling depth, total mass flowrate and LGR, on the system flow pattern, pressure drop and velocity profile through sensitivity studies and explore key RC drilling performance related variables, such as liquid holdup, computed by the software.
3. To validate the software simulation data by comparing analytical modelling data from multiple sources.

1.2.2.1. Research Activities and Elements

The objectives of this study will be achieved through the standard stages and elements of a research study. A Gantt chart of the various project activities outlined below can be seen as per Appendix A, which has been developed for clarity of the research process and tasks to be completed.

For objective 1, preliminary work is to be conducted to have a deeper understanding of the associated context, through background reading on RC air drilling, drilling simulation software applications and fluid flow, in particular multiphase, compressible flow and pipe pressure drop correlations. Preliminary tasks also include research and familiarisation of multiphase flow simulation software packages to be utilised, including Schlumberger's PIPESIM and ANSYS Fluent, by self-study of the software controls, assistance from supervisors and online tutorials. The first research stage is the planning of the research project, including the research topic, objectives, and scope, by performing a comprehensive literature review to critically interpret

associated theory and modelling from multiphase pipe flow, cuttings transportation and oil and gas industry studies, and determination of the research gap. The next stage of research is to establish a methodology, by writing a clear research project procedure based on the project objectives and software functionality, with revisions and further explanations provided throughout the progression of the project. The next research stage is modelling and data collection, which is the foundation of the research project and includes selecting fundamental models and making valid assumptions in the software to obtain a simulation that represents two-phase air-water, compressible, steady state flow in a specified vertical RC air drill string. The validity of the two-phase flow simulation will be investigated by determining the suitability of the underlying theoretical model assumptions and variable values used for a simple vertical pipe and a vertical annulus pipe through literature studies. Objective 1 is also part of the analysis and interpretation of data stage, which is the majority of the research project and includes the investigation of hydrostatic pressure and major head loss influences on the drilling pressure drop through simulations. The flow simulations internally compute pressure readings at a given node or series of nodes across the drill string pipes that can be easily exported to Microsoft Excel for further investigation.

For objective 2, the modelling and data collection research stage also includes conducting several sensitivity studies of the multiphase flow at different drilling depth, to obtain a clear and comprehensive understanding of the RC air drilling flow patterns, pressure drop and velocity profiles, which are internally generated within the software. These sensitivity studies may also be repeated with alternative varied parameters, including total mass flowrate and LGR. Other key RC drilling variables, such as liquid holdup of the drilling fluid, that are computed by the software are to be explored, to allow for a more comprehensive study of the simulation and drill string. If the simulation of mineral RC air drilling and the associated data cannot be obtained using the specified software, other software packages have also been made readily available with sufficient prior knowledge to complete the research.

For objective 3, the analysis and interpretation of data stage also includes the validation of the software simulation developed, through comparative analysis of the results collected against analytical models, including the Drilling Mechanics Group (DMG) analytical model and DMG Simulink model. From which, a clear conclusion of the model validity and recommendations for further research studies into other drilling variables or varied applications may be deduced. Preparation of an article or report for publication or submission is the final research stage, which requires evidence of all previous research stages and elements, compiled in a professional format.

1.3. Significance of the Research

The significance of this research project is the development of a software simulation that can model multiphase, compressible, steady state flow in vertical RC air drilling of minerals accurately, as there are no published models to date. Further understanding of hydrostatic pressure and major head losses on pressure drop, flow pattern, pressure drop and velocity profiles with drilling depth and other variables, and investigation of key performance-based variables in mineral RC air drilling may be applied and utilised by operators in the drilling industry, specifically onshore mineral exploration projects.

The economic benefits of this study in improved drilling production, optimisation, and automation are significant contributions to the mining industry, in particular onshore mineral RC drilling exploration companies. This is achieved through operation within the ideal, two-phase operating regime, reducing the pumping and diesel requirements accountings for majority of drilling exploration operation costs. For a 25-day drilling campaign for RC drilling, at a typical cost of $1.75 million, reducing downtime, diesel requirements and blockage due to reduced cuttings transportation can save thousands of dollars (DET CRC 2014). Hence, this study can is mainly classed within the mining industry as the field of endeavour under drilling and completions, with utilisations for onshore mineral explorations.

1.4. Scope and Limitations

1.4.1. Scope of the Research

This research project aims to construct simulations of two-phase air-water, compressible, steady state flow in vertical RC air drilling of minerals, using commercially available software. This will allow the determination of the wellbore flow pattern, pressure drop, velocity profile and liquid holdup of the drilling system. The simulation will be used to study the influence of hydrostatic pressure and major head loss caused by friction on the pressure drop of a specified drilling pipe. The influence of other variables, including drilling depth, total mass flowrate and LGR on the flow pattern, pressure drop, and velocity profile is also to be thoroughly investigated through a series of extensive sensitivity studies. Exploration into other key performance related variables in RC drilling, including liquid holdup of drilling fluid, is to be conducted for a complete analysis of the drilling simulation. The software simulation will be validated using analytical model data from unpublished DMG studies. This simulation of RC

air drilling will satisfy the modelling requirements for use in industry operations and optimisation.

1.4.2. Limitations of the Research

This study aims to develop and validate an accurate software simulation for further research studies and industry utilisation; however, this project has some limitations. While literature is available on multiphase, compressible flow in vertical pipes, pneumatic cuttings transport and oil and gas drilling applications, there is no prior, published studies compiling this literature for mineral RC air drilling and consequently, there is no available published theoretical modelling, software simulations or experimental field data for validation purposes. Research studies on RC air drilling of minerals are currently being conducted analytically and by simulations using engineering fundamentals within the DMG, however, the reliability of this data is unknown. The availability of simulation software for use may also be a research limitation, however, it should be noted that several simulation software packages, including readily available software used predominantly in the oil & gas industry, have been considered for this study.

2. LITERATURE REVIEW

2.1. Content of the Literature Review

2.1.1. Mineral Drilling Background

In the mining industry, drilling and blasting operations are the initial and foundation stages of the mining production or value cycle and have proven to be the most productive method of mineral mining, compared to traditional primary breaking techniques (Marjoribanks 2010). Drilling operations are largely executed using percussive or rotary drills, which are selected based on the specific application. Percussive drilling uses a hydraulic (or sometimes, pneumatic) pressurised top hammer and drill bit to cut into hard rock formations, while rotary drilling use purely rotating drills with specialised drill bits (Bustillo Revuelta 2018). Rotary drilling is most commonly utilised in mineral drilling applications.

As a rotary drill string progresses into mineral rock, cuttings or particles are created. Drilling fluid, most commonly compressed air or other gas, transports the cuttings or particles from the wellbore bottom to the drilling surface (Zhu et al. 2015). If the drilling fluid does not have a sufficient carrying capacity, the mineral cuttings will not be removed from the bottom of the wellbore and will build up causing abrasion and erosion of the drill bit. The flow of the drilling fluid also dissipates the heat generated from the friction between the drill bit cones and mineral rock layer (Bustillo Revuelta 2018). The use of air-lift technology in rotary drilling was established in the 1950s and continues to be used today, due to its continuous circulation even in fractured or depleted ore reservoirs. In rotary drilling, the air-lifted or pneumatic cuttings transportation can operate in a direct or reverse circulating configurations (Zhu et al. 2015).

2.1.2. RC Air Drilling

The principle behind RC air drilling is that the flow of drilling fluid and mineral cuttings is in the opposite direction to conventional direct circulation configurations. During the drilling cycle, as seen in Figure 2.1.2.1, the drilling air enters the top of the drilling rig through the annulus area between the inner vertical pipe and wellbore wall pipe, and continuously flows through this dual-walled pipe section by compressive power. The compressed air then enters the drill bit opening at the bottom of the wellbore, where the flow of air across the surface of mineral cuttings entrains the solid material, allowing the cuttings to be transported through the inner

drill string pipe to the drilling surface pneumatically (Xiumin, Yue, and Luheng 2014; Lyons et al. 2009).

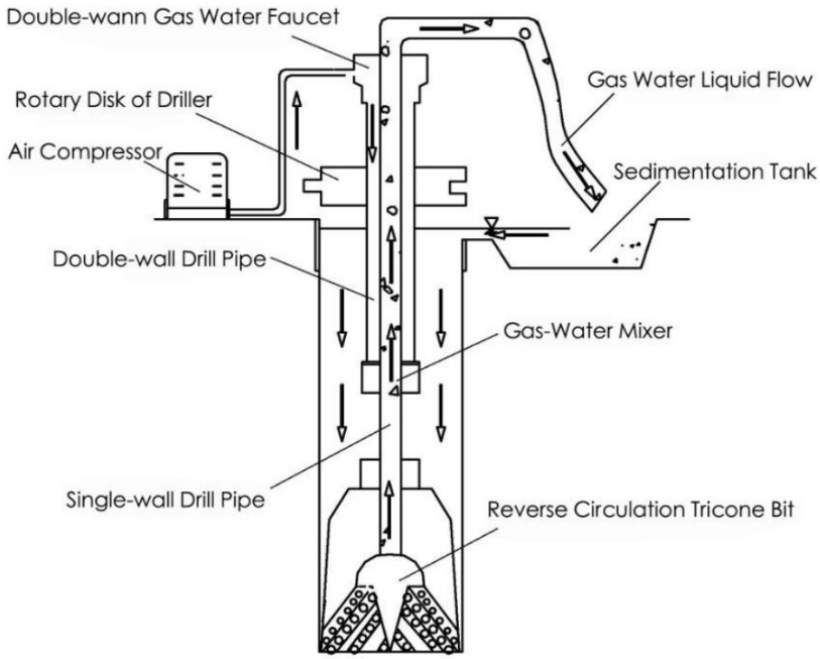

Figure 2.1.2.1: RC air drilling process diagram.

Source: Figure reproduced from Xiumin, Yue, and Luheng (2014).

In gas-lift drilling operations, such as RC air drilling, two-phase flow occurs through the annulus dual-wall pipe which consists of a compressible gas (i.e.: air) phase and incompressible liquid (i.e.: fresh water) phase. While three-phase flow occurs during pneumatic transport of mineral cuttings through the drill bit opening and upwards through the inner drill string pipe to the surface of the wellbore, which consists of a compressible gas phase, incompressible liquid phase and solid rock (i.e.: mineral) cuttings or particles phase (Lyons et al. 2009).

The continuous flow of fluid and return of mineral cuttings makes this technique highly efficient with a high time efficiency and low labour intensity (Xiumin, Yue, and Luheng 2014). The advanced techniques involved in RC drilling also allows for the creation of reliable straight vertical and horizontal wellbore configurations, even in complex drilling applications (Zhu et al. 2015). While, the flow of the drilling fluid and the regulation of optimal drilling rig pressures allow for a long drill bit life and overall wellbore stability (Xiumin, Yue, and Luheng 2014).

As the volumetric flowrate of the compressed drilling air is directly proportional to the velocity of the air, the productivity of a drilling application is dependent on the rate in which the mineral cuttings are transported from the bottom of the wellbore through the inner drilling pipe to the

surface. Thus, as the air velocity allows for the continuous removal of solid cuttings from the bottom of the wellbore, drilling fluid flow and cuttings transport is vital to effective and productive drilling applications (Zhu et al. 2015).

Modelling of RC drilling techniques in industry scenarios continue to be studied, however, the completeness of the models is problematic. Recently, (Dong et al. 2020) conducted a performance analysis on RC drilling techniques in horizontal configurations through experimentation, with the addition of a jet-pump design in the laboratory drilling rig prototype. This allowed for the study of the impact of drilling fluid flowrate, drilling fluid pressure and drill bit rotation on overall drilling performance and the impact of particle size and drilling fluid type on cuttings removal capabilities. However, this study by (Dong et al. 2020) has limited applications as it only investigates cuttings transport characteristics in a specified inner drilling pipe, excluding any study into three-phase characteristics. It also only considers horizontal flow configurations, hence, the pressure drop in the central drilling pipe is not the same as that for a vertical pipe, as it does not account for hydrostatic pressure drop. (Ganat et al. 2019) developed an analytical model for the frictional pressure drop in upward, two-phase, homogeneous, vertical flow in a wellbore. As friction on the central drill pipe surface decreases the flow velocity and creates a pressure drop with pipe length, the pressure drop was modelled for multiphase flow using fluid mechanic principles and empirical correlations, including the Darcy and Colebrook friction factor correlations. Sensitivity studies were also conducted for different drilling fluid flowrates, fluid properties and pipe diameters, which were validated using OLGA simulation software. While, this study by (Ganat et al. 2019) was able to investigate upward, vertical, two-phase flow numerically and by software simulation, the multiphase flow modelled was for two-phase water-oil flow. This presents different flow pattern modelling to that of air-water two-phase flow, because the compressibility of air impacts the density and pressure drop calculations significantly. This study also assumes homogeneous multiphase flow characteristics, which limits the frictional pressure drop data accuracy due to highly non-homogeneous nature of the gas-water multiphase flow. In real-world mineral drilling scenarios, non-homogeneous, three-phase flow would occur in the inner pipe and should be consider in frictional pressure loss modelling.

Some researchers also applied RC drilling to ice drilling and ice core extraction. (Cao et al. 2018) conducted theoretical calculations for the air drilling fluid flow in RC drilling of ice cores, as ice chips and core transport to the drilling surface depends on the air flow properties. A series of studies on the central drill string pipe with different diameters were also conducted to determine the minimum air input pressure, using several fluid mechanics equations, such as the Bernoulli equation to determine the total pressure drop of the central drilling pipe, the drill

bit area and annulus drilling pipe, and therefore the influence of the pressure drop on ice cuttings and core transport. The study by (Cao et al. 2018) investigated pressure drop of the entire drill string, however, it only considers single-phase gas flow as opposed to multiphase flow, making this study limited to ice drilling and other unique applications. The studies by (Dong et al. 2020), (Ganat et al. 2019) and (Cao et al. 2018) discussed above, show that a complete model of multiphase and compressible RC drilling has not been developed, in part due to the complexity of modelling.

2.1.3. Fundamentals of Multiphase Flow

Multiphase flow is based on fluid mechanics theory of the flow of two or more phases simultaneously. With continuous technological advancements, the importance of studying and developing cheap multiphase transport of resources from reservoir is increasing, in particular multiphase flow in a drill string. However, the variation in flow properties present in wellbore drilling is difficult to predict and model. The multiphase flow phenomena in vertical wellbores, as previously mentioned, may be modelled assuming that the compressible gas phase follows the ideal gas law, that the two-phase gas-liquid drilling fluid mixture is uniform and homogenous, and that the solid mineral cuttings are uniform in density and size with a uniform distribution (Lyons et al. 2009). However, this is not a realistic representation of real-world drilling flow for many scenarios. The use of homogeneous and uniform flow assumptions limit the accuracy of flow models, including pressure drop that varies drastically between homogeneous and non-homogenous flow, and the applications in which the model may be applied (Eissa and James 2017).

The analysis of multiphase flow in a pipe can also be divided into two complexity levels: steady state flow and transient or dynamic flow. Steady state flow refers to a pipe system which experiences no major flow changes with time, which can be calculated through theoretical principles or empirical correlations developed from experiments and is applicable for many applications, including drilling operations due to the continuous drill string flow (Ellul, Saether, and Shippen 2004).

2.1.3.1. Non-Homogeneous, Two-Phase Flow Modelling in Vertical Pipes

The modelling of multiphase flow is greatly dependent on flow pattern. Flow pattern in a vertical pipe is defined as the vertical and radial distribution of gas and liquid. Gas-liquid flow patterns in non-homogeneous flow may be classified as dispersed flow, bubble flow, dispersed bubble flow, churn flow, annular flow, mist flow or slug flow. The most widely used empirical method to determine vertical flow patterns is the (Ros 1961) empirical flow pattern map, which requires

the calculation of the flow liquid velocity flux and gas velocity flux. While, the most common theoretical modelling approach for determining flow pattern in vertical pipe flow is the (Taitel, Bornea, and Dukler 1980) flow pattern map, which requires the calculation of the superficial gas and liquid velocities.

Another key characteristic in non-homogeneous, multiphase flow is liquid holdup, which can also be calculated using empirical correlations and theoretical models. The (Beggs and Brill 1973) empirical correlation is commonly used to calculate liquid holdup in vertical and deviated wellbores. While theoretical approaches are dependent on flow pattern. Hence, a hydrodynamic liquid holdup model is required for each of the flow patterns previously discussed. Similar to the liquid holdup models, non-homogeneous, multiphase pressure drop may be determined using the empirical (Beggs and Brill 1973) correlation or using the theoretical approaches dependent on flow pattern. The equations discussed above in the determination of flow pattern, liquid holdup and pressure drop may also be applied to annulus pipe configurations by the use of effective variables, such as effective diameter, and correction factors (Lyons et al. 2009).

Numerous researchers have investigated non-homogeneous, multiphase flow in vertical pipe configurations over the last few decades. Most recently, (Adaze, Badr, and Al-Sarkhi 2019) developed a computational fluid dynamic (CFD) model for annular pattern, two-phase flow in a vertical pipe towards the onset of liquid film reversal. The model incorporated the use of the mass and momentum conservation equations, turbulence modelling, surface tension modelling and single-phase properties, to investigate the superficial gas and liquid velocities, and the impact of superficial velocities on the two-phase velocity profile, liquid volume fraction and slip velocity. This study by (Adaze, Badr, and Al-Sarkhi 2019) modelled non-homogeneous, multiphase flow in a vertical pipe configuration, however, flow was only modelled for the annular flow pattern with a mean fluid velocity up to 38 m/s within the CFD model. Multiphase flow through the inner drilling rod experiences changes in flow pattern with drilling depth due to the change in air density, typically from a well-mixed pattern, such as annular or mist flow, to a flow pattern with high liquid holdup, such as slug flow. This results in a significant decrease in mean fluid velocity and increase in liquid holdup, which is not considered by the single flow pattern CFD simulation.

Research on the effects of shockwaves on compressible, multiphase flow has become an area of great endeavour in the last year, which is highly applicable to mineral RC drilling due to blasting operations in close proximity. (Nguyen et al. 2021) and (Nguyen, Phan, and Park 2021) studied the shock and interface capturing method to simulate compressible multiphase

flow with shockwaves, using multi-dimension curvilinear coordinated framework for finite-volume differencing scheme of high order and a Godunov-type numerical scheme, respectively. However, these models only consider transient, highly turbulent mixing as a result of underwater explosions and shockwaves which limits the results applicability. (Aslani and Regele 2018) analytically modelled compressible, multiphase flow using mass, momentum and energy continuity equations and (Le Métayer, Massoni, and Saurel 2005)'s stiffened gas equation of state, which is used for modelling compressible flow with interfaces and has been validated by various experimental research studies. This model developed by (Aslani and Regele 2018) is also limited to transient, highly turbulent flow with extensive modelling of eddy propagation. (Houim and Oran 2016) modelled compressible, multiphase gas-solid flow to predict flow behaviour with shockwaves, using Euler equations for gas and solid phases. However, this study has limited applicability due to its single-phase drilling fluid and turbulent, transient flow modelling. These studies discussed above, investigated the impact of shockwaves on a single phase and multiphase flow, which could be a great direction for further research from standard RC air drilling simulation.

2.1.3.2. Multiphase Flow with Variations in Pipe Diameter

When a multiphase flow mixture is expanded through a pipe component, it diverges due the increase flow cross sectional area, decreasing the fluid velocity and hence, increasing the static pressure in the pipe due to conservation of energy. Flow expanders and restrictors can include flowmeters, safety flow valves, tubing centralisers, wellhead chokes and pipe components, such as valves, elbows and drill bit openings (Eissa and James 2017).

The multiphase flow pressure drop through various pipe components and fittings is based primarily on resistance in the specified type of component, for example a globe valve. The (Sookprasong, Brill, and Schmidt 1986) two-phase flow pressure drop over piping components and fittings equation, and the (Crane 2009) single-phase resistance coefficients, K can be used for a large range of scenarios, including components and fitting on wellbore drilling rigs. However, no recent studies have been conducted to calculate pipe component pressure drop in multiphase flow or drilling industry applications.

2.1.4. Fundamentals of Pneumatic Cuttings Transport

For effective mineral drilling, solid cuttings created at the bottom of a wellbore must be carried to the drilling surface by entrainment into the drilling fluid (Caenn, Darley, and Gray 2017). Therefore, the flow of a drilling fluid and solid cuttings must both be modelled in the inner drill string pipe by three-phase flow (Lyons et al. 2009). The flow properties of the compressible

gas and incompressible liquid phases in the drilling fluid and size, shape and type of solid cuttings must be considered in three-phase modelling, as well as the operating conditions, such as temperature and pressure (Pedrosa, Saasen, and Ytrehus 2021).

2.1.4.1. Cuttings Transport Modelling in Vertical Pipes

The underlying principles of pneumatic cuttings transport are the internal forces imposed on and by the solid cuttings. Hence, for upward, three-phase, flow in a vertical drilling pipe, a number of variables must be calculated through continuity equations and fluid mechanic principles, including individual phase mass and volumetric flowrates, total mass flowrate, specific weight of the three-phase mixture, velocity of the three-phase mixture and friction factor for the laminar, transitional or turbulent flow based on the Reynolds number, to model the cuttings transport phenomena (Lyons et al. 2009).

Pneumatic cuttings transport in simple, vertical pipe configurations has been thoroughly researched throughout industry. Research has also been conducted in modelling pneumatic cuttings transport for RC air drilling applications. (Zhu et al. 2015) mathematically modelling the motion of solid cuttings and particles in RC air drilling in both the axial and radial directions. The axial motion considered aerodynamic drag, friction, and weight forces of the solid cuttings, while the radial motion was modelled by considering aerodynamic drag and friction forces. The research by (Zhu et al. 2015) modelled pneumatic cuttings transport in mineral RC air drilling, however, this model is limited to the single-phase drilling fluids, which is not common in real world drilling applications. Hence, the accuracy of this model and results for use in multiphase drilling fluid cuttings transport is limited.

Some researchers have extended general pneumatic cuttings transport modelling to specific RC air drilling applications in the exploration of resources and other scientific endeavours. In the last year, (Han, Song, and Li 2020) numerically modelled pneumatic cuttings removal in the inner drilling pipe during RC drilling of coal seam. This enabled further experimental analysis of the velocity profile and the effect of drilling fluid air velocity, solid cuttings mass flowrate and solid cuttings particle size on overall pressure to be investigated through a series of sensitivity studies. However, this study by (Han, Song, and Li 2020) modelled the flow characteristics of cuttings in a single gas phase. The numerical model was also based on a series of uniform particle flow and size assumptions, which limits the result accuracy. (Han, Li, and Li 2020) developed a CFD simulation using the QUICK and SIMPLE algorithms for pneumatic cuttings transport in RC drilling of a coal seam. The simulation encompassed two-phase air-cuttings flow in the inner drill string pipe, from which the impact of air velocity and

solid cuttings mass flowrate on flow behaviour and cuttings removal rate was studied. Similarly, (Xiao-ming et al. 2017) analytically modelled mineral cuttings transport phenomena in RC drilling for a coal seam. A pressure drop model was developed from a combination of continuity equations (i.e.: mass, momentum, energy) and two-phase gas-solid flow theory. The model was used to conduct sensitivity studies for varying inlet pressures, solid cuttings mass flowrate and solid cuttings size. These studies by (Han, Li, and Li 2020) and (Xiao-ming et al. 2017) modelled multiphase flow in the inner drilling pipe, however, the models and results obtained have limited applications due to the single phase drilling fluid flow.

Alternatively, (Cao et al. 2019) theoretically studied pneumatic transport of ice chips and cores in RC air drilling. Thorough analytical investigation and modelling of the air and ice properties, and flow characteristics were conducted for vertical, non-homogenous, two-phase gas-solid in the inner drilling pipe. This also allowed the determination of the minimum required volumetric flowrate of gas to meet the desired quantity of ice chips and cores. While the research by (Cao et al. 2019) was able to study pneumatic cuttings transport in RC drilling, the model did not attempt to model multiphase flow scenarios. The models and results obtained in the studies mentioned above are highly specific to oil and gas, and ice drilling applications which varies significantly from mineral applications, due to the complexity involved in compressible, multiphase flow modelling.

2.2. Research Gap

For the research and mining industries to obtain a comprehensive understanding of mineral RC air drilling, and to assist in automation and in-situ monitoring of RC drilling, a software simulation is to be developed and validated against analytical data. Currently, there is no software or complete simulation that has been published in open literature for vertical, non-homogeneous, multiphase, compressible, steady state flow with or without cuttings transportation in a dual wall drill string (i.e.: central pipe and outer annulus) to investigate flow pattern, pressure drop, velocity profile and liquid holdup. Many chemical engineering multiphase compressible flow applications are for steady state horizontal pipes. However, the hydrostatic pressure in a vertical pipe account for a significant part of the pressure drop calculations, which has not been addressed in the literature. Based on the research gap identified, the significance, scope and limitations of this research project were revised as previously detailed in sections *1.3. Significance of the Research* and *1.4. Scope and Limitation.*

3. METHODOLOGY

The following section introduces the simulation software utilised for the simulation of multiphase, compressible, steady state flow in vertical RC air drilling. The software chosen will allow for the study of the influence of hydrostatic pressure and major head losses on the overall drill string pressure drop, influence of specific variables, such as drilling depth, total mass flowrate and LGR on the flow pattern, pressure drop and velocity profiles, and other performance-related variables, such as liquid holdup. The simulation software selected were ANSYS Fluent 2020 R2 and Schlumberger's PIPESIM, in which their advantageous features, applications, and methodology have been discussed below.

The stages involved in each of the simulation methodologies are also specified for the creation of the drilling system geometry, convergence of a modelling solution and validation of the model. The general simulation methodology for ANSYS Fluent has been applied to single-phase air and water flow through the inner and outer annulus drill pipe. The methodology for the PIPESIM simulations has been to be applied to single-phase air and water flow, and two-phase air-water flow for the inner and outer annulus drill pipe. The single-phase flow simulations have been validated by comparative analysis of ANSYS Fluent, PIPESIM, the DMG analytical model and DMG Simulink results for the inner drilling pipe, and ANSYS Fluent and PIPESIM results for the outer annulus drilling pipe. The two-phase flow simulations were validated by comparison between PIPESIM, the DMG analytical and DMG Simulink model results for the inner drill string pipe, while the outer annulus pipe PIPESIM results were considered valid based on the various validation made previously, however, further validation may be conducted. All simulations results and analyses have been saved and organised as per a Data Management Plan (DMP), which can be seen as per Appendix B.

3.1. Simulation Software

3.1.1. ANSYS Fluent 2020 R2 Software

ANSYS Fluent is a fluid simulating software, highly regarded in industry for its extensive physics modelling applications and renown accuracy (ANSYS 2021). ANSYS Fluent was primarily selected as simulation software for the modelling of vertical RC air drilling due to its array of multiphase flow modelling capabilities, including for homogeneous and non-homogeneous, compressible gas-liquid and particle flows, in the most challenging flow

geometries, such as drill string. This software was also readily available for students through university facilities. ANSYS Fluent has been utilised for a series of multiphase flow studies, including the study previously discussed by (Adaze, Badr, and Al-Sarkhi 2019) on two-phase, vertical flow modelling towards the onset of liquid film reversal, which utilised commercial ANSYS Fluent version 16.1 to construct and run two-dimensional (2D) axisymmetric simulations. Research conducted by (Ben Mahmud 2012) on three-dimensional (3D), two-phase flow in a horizontal pipe modelling used the Eulerian (i.e.: non-homogeneous) model in ANSYS Fluent version 12.1 to conduct CFD calculations. Studies as early as beginning of the 21st century have used ANSYS Fluent, including studies by (Ghorai and Nigam 2006) on two-phase CFD modelling in vertical pipes which utilised the Eulerian model in ANSYS Fluent version 6 to determine flow patterns and interfacial phenomena. The extensive array of research studies on flow phenomena present in a drill string validates the applicability of this software for RC air drilling simulation.

3.1.2. Schlumberger's PIPESIM Software

PIPESIM by Schlumberger is a multiphase, steady state flow simulator for the analysis and optimisation of wellbore drilling and drilling surface networks. PIPESIM was selected based on its wide array of single and multiphase flow correlations capable of determining flow pattern, pressure drop and liquid holdup for vertical and horizontal wellbore configurations (Schlumberger 2020). This software was also selected based on readily available university licensing provided by Schlumberger. PIPESIM has not been utilised in any research studies for pipeline or wellbore drilling applications at present, therefore, the uniqueness of utilising this software was another means for the selection of the software. This software was selected as the primary software for simulation and validation at this stage of research, as the large simulation solving time and common divergence of solutions in ANSYS Fluent was considered as potentially limiting to the research progress. Hence, ANSYS Fluent was only utilised for the simulation of single phase air and water flow.

3.2. ANSYS Fluent Simulation Procedure

The ANSYS Fluent simulation software follows a standard procedure for the creation and analysis of any fluid flow, which can be followed below as per Figure 3.2.1. Each stage of the procedure has been specifically detailed in subsequent sections for the simulation of compressible, multiphase, steady state flow in RC air drilling.

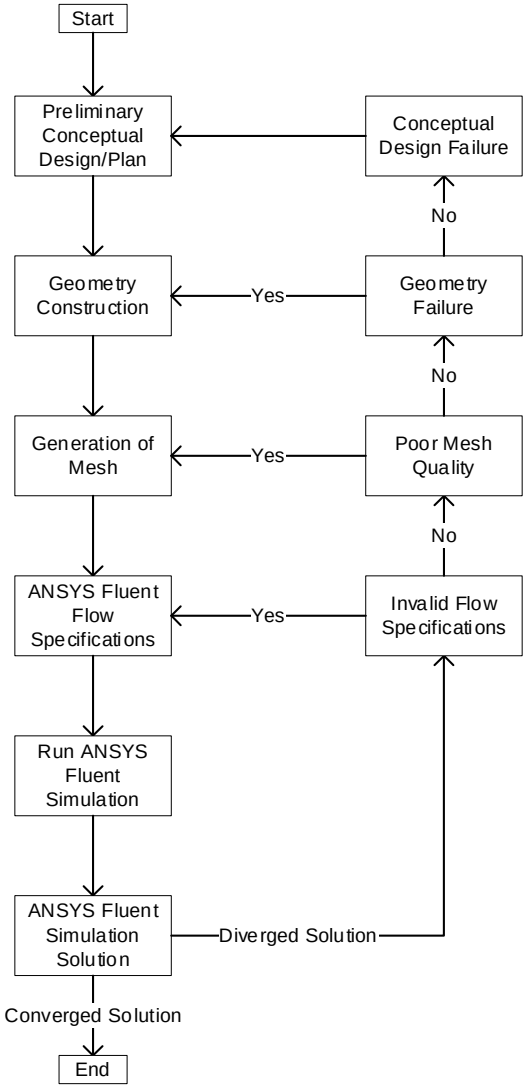

Figure 3.2.1: Flow diagram of ANSYS Fluent simulation procedure.

Source: Figure reproduced from Ben Mahmud (2012).

3.2.1. Preliminary Conceptual Design and Planning

Before any ANSYS Fluent software simulation could be initiated, a thorough understanding of the drill string geometry, including dimensions, boundary conditions, such as single-phase velocity and gauge pressure, and flow characteristics, such as homogeneous or non-homogeneous flow were required. Based on field data and the requirements for simulation, a preliminary design was developed, as seen by Figure 3.2.1.1.

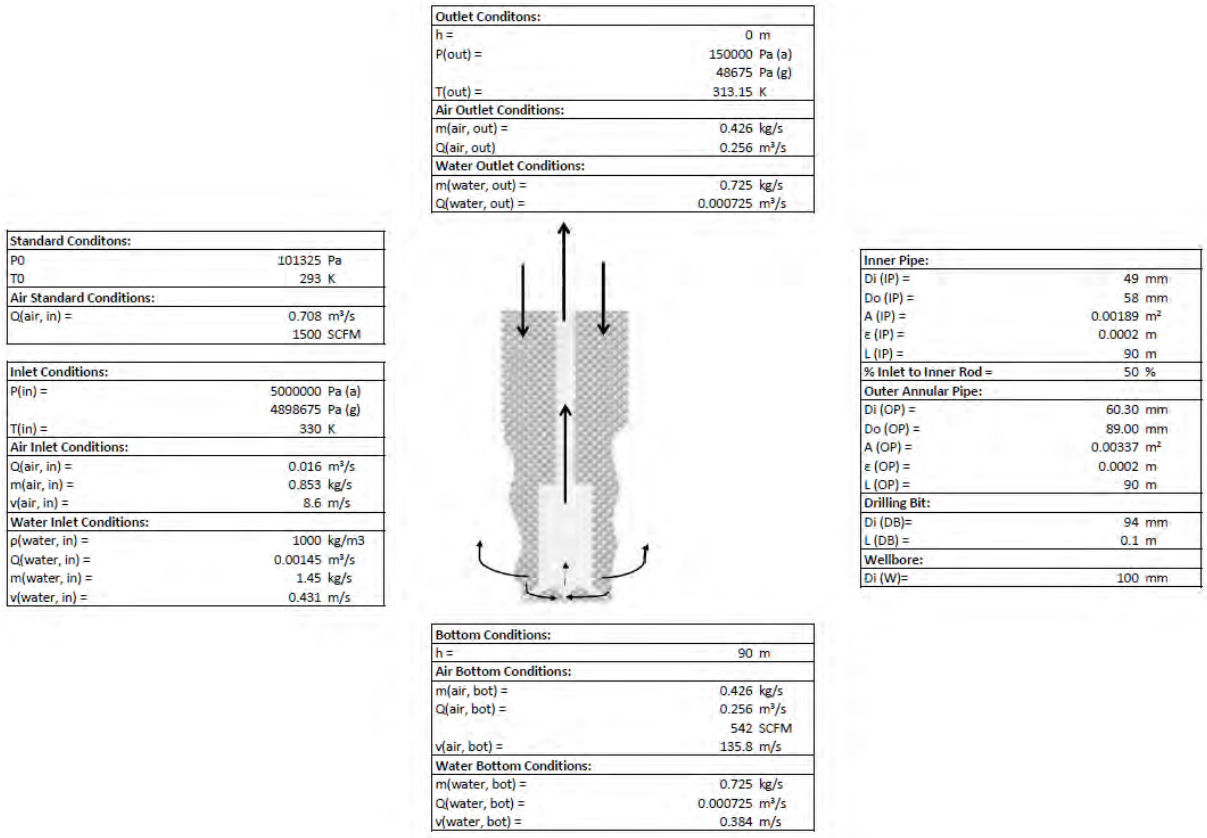

Figure 3.2.1.1: Preliminary design for software simulation

Source: Figure reproduced from Quyn (2020).

3.2.2. Construction of Drill String Geometry

Each simulation was set up initially through ANSYS Workbench, which is an interface that allows the communication between major ANSYS software, including the connection of the simulation base geometry, mesh geometry and Fluent flow analysis, to obtain an effective and complete simulation. The creation of all geometry was performed using ANSYS DesignModeler, which is the original ANSYS computer-aided design (CAD) program, which allows the creation of simple 2D geometry to highly complex 3D geometry. This program was used to develop the inner cylindrical and outer annulus drilling pipe geometries as per the preliminary conceptual design (Figure 3.2.1.1).

3.2.3. Generation of Drill String Mesh

Once the complete geometry was created and updated in ANSYS Workbench, a mesh geometry with a 1 m element size was generated for the inner cylindrical and outer annulus

drilling pipe flow geometries. During this stage, the geometry boundaries were also specified as flow inlet, flow outlet, fluid wall and internal fluid.

3.2.4. Simulation of Drill String Fluid Flow

Using the previously constructed drill string meshes, ANSYS Fluent was used to analyse the flow of single-phase air and water through the inner cylindrical and outer annulus drill pipe individually. The ANSYS Fluent solver was set up systematically by specifying general setup, such as steady state flow, fluid materials and boundary conditions, and solution settings, including the flow phenomena present and analytical models selected, as prompted by the program.

The ANSYS Fluent analysis was initialised using the boundary condition data and solved for a minimum of 100 iterations. If the solution diverged and the calculations were not completed, the flow diagram in Figure 3.2.1 was followed for problem identification and simulation repetition. However, if the solution converged, the simulation results were analysed and validated.

3.3. PIPESIM Simulation Procedure

The PIPESIM simulation software uses a slightly different procedure from other simulation software, as it is only applicable for wellbore drilling systems. This procedure can be followed below as per Figure 3.3.1, where each stage of the procedure has been described in subsequent sections.

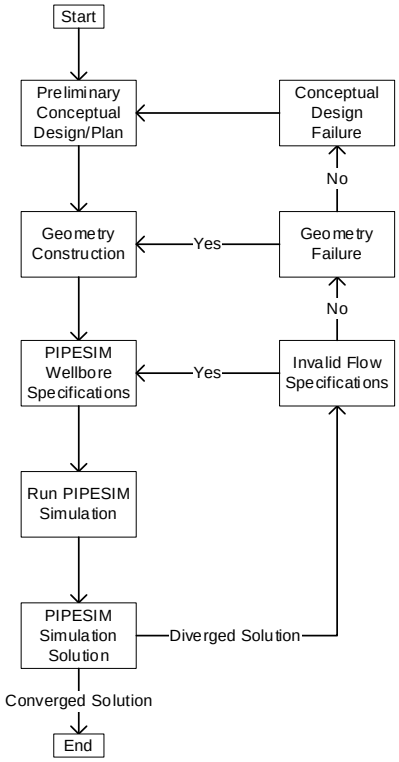

Figure 3.3.1: Flow diagram of PIPESIM simulation procedure.
Source: Figure reproduced from Ben Mahmud (2012).

3.3.1. Preliminary Conceptual Planning

Before creating a PIPESIM simulation, the drill string geometry, such as dimensions, and boundary conditions, such as single-phase volumetric flowrates, mixture mass flowrate and absolute pressure were specified. These specification for PIPESIM simulations, have also been detailed in the preliminary design as per Figure 3.2.1.1.

3.3.2. Construction of Drill String Geometry

All PIPESIM simulations were set up as a ‘New Centric Wellbore’, which has a simple user interface that allows the creation of a 2D schematic wellbore and drill string geometry through drag and drop of components, such as inner pipe tubing, completions, and surface equipment. This function was used to develop wellbore and complete drill string geometries, as per the preliminary conceptual design (Figure 3.2.1.1).

3.3.3. Simulation of Drill String Fluid Flow

The PIPESIM software was then used to analyse the flow of single-phase air and water, and two-phase, air-water through the inner cylindrical and outer annulus drill pipe. The PIPESIM

flow analyser function was easily utilised, as it only required the use of the 'Model Calibration – Data Comparison' function and specification of the outlet pressure and single-phase volumetric flowrate or multiphase mass flowrate, to determine the inlet or wellbore bottom pressure and various other system variables. This function also allowed for the selection of the calculation correlation used, in which multiple models can be selected and results compared. The complete list of 24 available correlations and acronyms used can be seen as per Table 3.3.1. The correlations utilised were chosen based on the whether the correlation was homogeneous or non-homogenous, other key assumptions such as for vertical or horizontal flow, the age of the most revised version and the extent of use in similar multiphase flow research studies. If the solution diverged and the results could not be obtained, the flow diagram for PIPESIM simulations in Figure 3.2.1 was used to identify the root cause and the simulation was repeated. If the solution converged, the simulation results were analysed and validated, as in the ANSYS Fluent simulations.

Table 3.3.1: Summary of the available PIPESIM multiphase flow correlations.

Correlation	Acronym	Source
Aziz Govier Fogarasi	Agf1	Neotec
Govier, Aziz & Fogarasi	GA	Baker Jardine
Govier, Aziz [Tulsa (Legacy 1989)]	TGA	Tulsa (Legacy 1989)
Ansari	ANSARI	Tulsa (Legacy 1989)
Beggs & Brill Original	BBO	Baker Jardine
Beggs & Brill Revised	BBR	Baker Jardine
Beggs & Brill Revised [Tulsa (Legacy 1989)]	TBB	Tulsa (Legacy 1989)
Duns & Ros [Baker Jardine]	DR	Baker Jardine
Duns & Ros [Tulsa (Legacy 1989)]	TDR	Tulsa (Legacy 1989)
Gomez	Gomez1	Neotec
Gomez Enhanced	Gomez2	Neotec
Hagedorn & Brown (Original) [Tulsa (Legacy 1989)]	THB	Tulsa (Legacy 1989)
Hagedorn & Brown (Revised)	HBR	Baker Jardine
Hagedorn & Brown (Revised), Duns & Ros map	HBRDR	Baker Jardine
Hagedorn & Brown (Revised) [Tulsa (Legacy 1989)]	TBHR	Tulsa (Legacy 1989)
Mukherjee & Brill [Baker Jardine]	MB	Baker Jardine
Mukherjee & Brill [Tulsa (Legacy 1989)]	TMB	Tulsa (Legacy 1989)
No Slip Assumption	NO SLIP	Baker Jardine
Orkiszewski [Baker Jardine]	ORK	Baker Jardine
Orkiszewski [Tulsa (Legacy 1989)]	TORK	Tulsa (Legacy 1989)

3.4. Analysis and Validation of Simulation Results

The results generated from the single-phase and two-phase flow simulations in the inner and outer annulus drilling pipes using ANSYS Fluent and PIPESIM, were analysed and validated based mainly on the pressure drop (and velocity profiles) with depth inside the drilling pipe, as

it is the primary variable of study. For single-phase flow within the inner and outer drill pipes, the ANSYS Fluent and PIPESIM simulations pressure drop and velocity profiles with depth inside the drill pipe were compared for analysis and validation based on deviations and correlation assumptions. For two-phase air-water flow within the inner and outer drill pipes, the PIPESIM simulation pressure drop with depth inside the drill pipe were compared to the DMG analytical and DMG Simulink model for analysis and were validation based on variations between pressure values, as well as model applicability and assumptions.

3.5. Evaluation of Methodology

The selection of the ANSYS Fluent and PIPESIM software for the simulation of RC air drilling show conclusive results for both single- and two-phase, steady state flow in the inner and outer drill string pipes. The procedures used in both software are generic and based on systematic simulation requirements, however, due to only recent software access and inexperience in the ANSYS Fluent and PIPESIM software, the repetition of procedures in Figure 3.2.1 and Figure 3.3.1 during divergent solution problems proved to be significantly time consuming and it was sometimes difficult identify root causes. The capabilities of ANSYS Fluent and PIPESIM to predict temperature change in the wellbore is also to be further investigated, as the homogeneous DMG analytical model assumes that the temperature profile is isothermal for a wellbore depth of 90 m. The temperature profile is significant in the simulation of compressible, multiphase flow as it impacts the air density and pressure drop of the overall drill string.

Upon use of the PIPESIM software, it was found that there were several limitations to the analysis capabilities. PIPESIM uses nodal analysis which is only capable of determining variables at a single node, in this case the wellbore bottom. Therefore, variable profiles such as pressure and velocity profiles could not be obtained by a single geometry. Rather several simulations had to be run with various depths to obtain appropriate pressure drop and velocity profiles. This program also allowed for the development of a wellbore and complete drill string geometry however, it is only designed to analyse flow from the wellbore bottom to drilling surface. Hence, the outer annulus drill string pipe geometry construction was only made possible through an unconventional, equivalent-based approach. Due to these limitations, the ANSYS Fluent, DMG analytical model and DMG Simulink results for single-phase and DMG analytical model and DMG Simulink results for two-phase flow utilised for validation of the result obtained by the PIPESIM simulations are vital to the research feasibility.

4. RESULTS AND DISCUSSION

The following section critically analyses the results obtained from the simulations of the inner and outer drill string pipes using PIPESIM. Based on the pressure drop and velocity profiles, the simulation results have been compared to the ANSYS Fluent, DMG analytical model and DMG Simulink results for validation and explanation for variations between results have been addressed. It should be noted that the validation of each of the single-phase and two-phase simulations stages are important to ensure the validity and accuracy of the final complete drill string simulation. The impact of the simulation methodology and software models on the research results, and the gaps in the research results have been discussed. The learnings from the simulation results and objectives achieved include successful simulation of single-phase air and water flow, and simulation of two-phase air-water flow through the inner and outer pipe of a RC drill string as specified in the research project objectives. The creation of the complete drill string pipe simulations and various sensitivity studies allowed for the development of a series of operational charts applicable for utilisation by mineral drilling operators for process optimisation and future automation of RC drilling applications. The operational boundaries identified will allow for reduced pressure drop due to decreased liquid holdup leading to a reduction in fuel consumption, increased cuttings transportation and removal and hence, greater RC drilling profitability in industry.

4.1. Single Phase Air Flow in RC Drilling

4.1.1. Single Phase Air Flow in Inner Drill String Pipe

The inner drilling rod was simulated in PIPESIM for pure, single-phase air flow based on a mass flowrate of 0.426 kg/s, which is the mass flowrate of the air within the two-phase air-water flow from field data and outlet pressure of 1.5 bar(a), as summarised in Figure 3.2.1.1. The composition of air was specified as 79 volume% nitrogen and 21 volume% oxygen gases with a LGR, which is the ratio of the liquid water mass flowrate over the gas air mass flowrate, of zero. The air properties were then specified by the inbuild PIPESIM functions. The friction factor correlation was specified by the inflow performance relationship (IPR) model selected. The Well PI model was used for all PIPESIM simulations, which required user specification of the IPR basis of either gas or liquid phase, in which gas phase was selected and the associated productivity index of 1.14E-11 $m^3/(s.Pa^2)$ was used. The PIPESIM overall pressure drop and change in velocity of the single-phase, air flow in the inner pipe from a wellbore depth of 90 m

to the drilling surface are presented in Figures 4.1.1.1 and 4.1.1.2. As PIPESIM can only perform nodal analysis for a single point, the figures below are not a representation of the pressure drop or velocity profiles, but rather an indication of the overall change with drilling depth. The inner drilling rod was also simulated in ANSYS Fluent for pure, single-phase air flow based on an outlet single-phase velocity of 135.8 m/s and outlet pressure of 1.5 bar(a), as per Figure 3.2.1.1. The composition and properties of air was specified by the ANSYS Fluent Database Materials based on the outlet conditions. The friction factor correlation was specified by the viscous model selected in ANSYS Fluent. The realised k-epsilon viscous model with enhanced wall treatment was used for this simulation as per Appendix C – Figure C.1, in which the wall roughness was specified as 0.0002 m and the remaining equation variables were left as the default values, as seen in Appendix C – Figure C.2. The pressure drop and velocity profiles of the single-phase air flow from a wellbore depth of 90 m to the drilling surface are also presented in Figures 4.1.1.1 to 4.1.1.2.

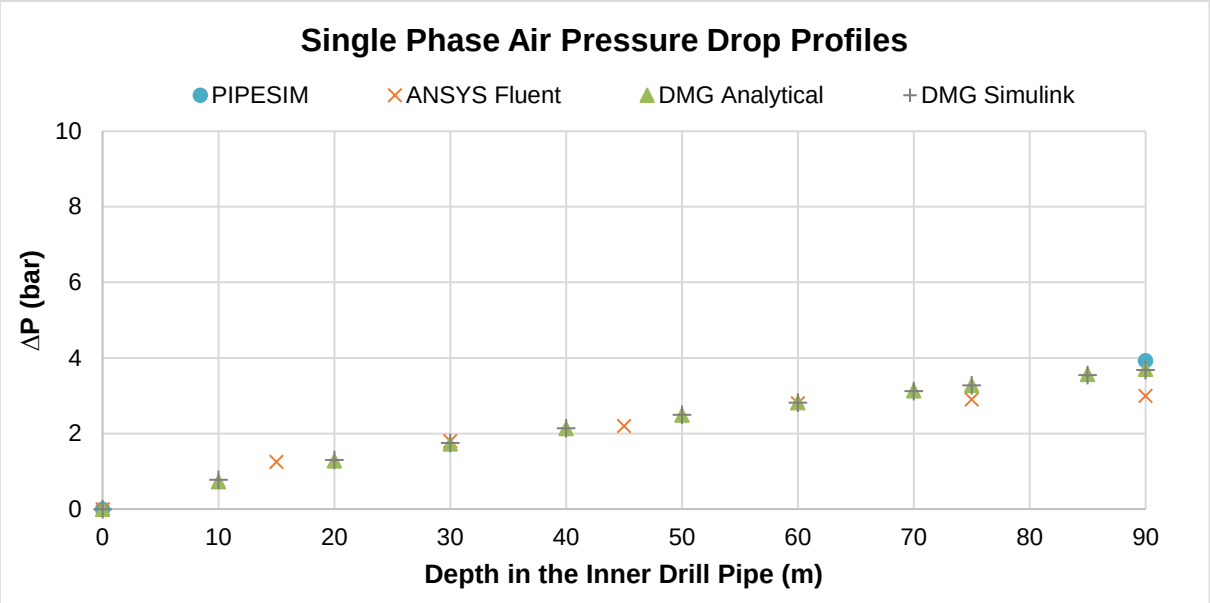

Figure 4.1.1.1: Comparison of single-phase air, inner pipe flow pressure drop profiles from PIPESIM, ANSYS Fluent, DMG analytical model and DMG Simulink model.

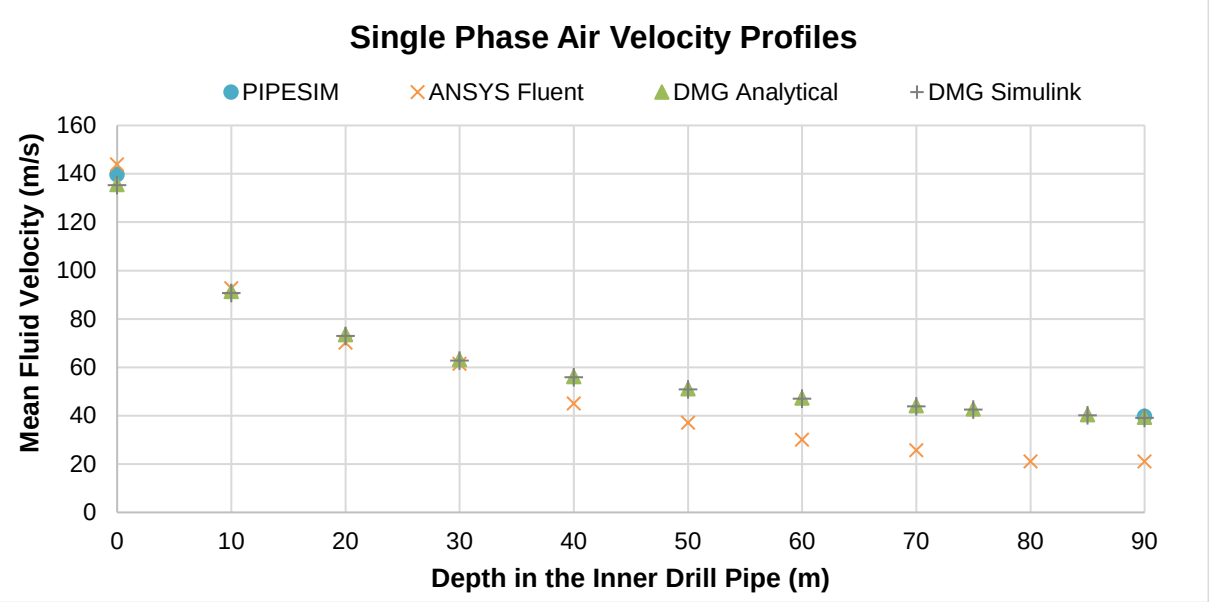

Figure 4.1.1.2: Comparison of single-phase air, inner pipe flow velocity profiles from PIPESIM, ANSYS Fluent, DMG analytical model and DMG Simulink model.

The results obtained from PIPESIM and ANSYS Fluent for the single-phase compressible air flow in the inner drill pipe can be compared against each other and the DMG analytical and Simulink models for a complete validation of the results. The comparison of the pressure drop results (Figure 4.1.1.1) and velocity change results (Figure 4.1.1.2) from PIPESIM and ANSYS Fluent show some variation from the DMG analytical and Simulink model with an overall pressure drop of 3.70 bar(a) and 3.69 bar(a), respectively. Figure 4.1.1.1 shows a difference of 0.23 bar(a) and 0.71 bar(a) between the DMG analytical model pressure drop and pressure drops calculated by the PIPESIM and ANSYS Fluent simulations, respectively. The graph also shows a difference of 0.24 bar(a) and 0.70 bar(a) between the DMG Simulink model pressure drop and pressure drops calculated by the PIPESIM and ANSYS Fluent simulations, respectively. These variations may be attributed to differences in the frictional pressure loss models, that may account for a lower pressure loss in the case of the ANSYS Fluent results, and the non-isothermal temperature models, that influence the density of the compressible air and hence, hydrostatic pressure loss. Figure 4.1.1.2 presents a variation of 2.97% and 6.10% for the air flow at the bottom of the wellbore and a variation of 0.86% and 46.64% for air flow at the drill string surface, for the PIPESIM and ANSYS Fluent simulations against the DMG analytical model, respectively. The graph also shows a difference of 3.22% and 6.35% for the air flow at the bottom of the wellbore and a variation of 1.49% and 46.31% for air flow at the drill string surface, for the PIPESIM and ANSYS Fluent simulations against the DMG Simulink

model, respectively. These are also attributed to the frictional pressure loss models which may account for increased wall friction and a greater decrease in gas velocity, in the case of the ANSYS Fluent simulation results, as well as variations in non-isothermal temperature profile. Hence, this range of variation in the pressure drop and velocity values for the PIPESIM results can be considered acceptable for further research and simulation, while ANSYS Fluent requires additional validation studies.

4.1.2. Single Phase Air Flow in Outer Annulus Drill String Pipe

The outer annulus drilling pipe was simulated in PIPESIM for pure, single-phase air flow based on a mass flowrate of 0.853 kg/s, which is the mass flowrate of the air within the two-phase air-water flow from field data and inlet pressure of 50 bar(a), as summarised in Figure 3.2.1.1. The composition of air was specified as 79 volume% nitrogen and 21 volume% oxygen gases with a LGR, which is the ratio of the liquid water mass flowrate over the gas air mass flowrate, of zero. The air properties were then specified by the inbuild PIPESIM functions. The friction factor correlation was specified by the inflow performance relationship (IPR) model selected. The Well PI model was used for all PIPESIM simulations, which required user specification of the IPR basis of either gas or liquid phase, in which gas phase was selected and the associated productivity index of 1.14E-11 $m^3/(s.Pa^2)$ was used. The PIPESIM overall pressure drop and change in velocity of the single-phase air flow in the outer annulus pipe from the drilling surface to a wellbore depth of 90 m are presented in Figures 4.1.2.1 and 4.1.2.2. As PIPESIM can only perform nodal analysis for a single point, the figures below are not a representation of the pressure drop or velocity profiles, but rather an indication of the overall change with drilling depth as previously stated. The outer annulus drill pipe was also simulated in ANSYS Fluent for pure, single-phase air flow based on an inlet single-phase velocity of 18.3 m/s and outlet pressure of 1.5 bar(a), as per Figure 3.2.1.1. The composition and properties of air was specified by the ANSYS Fluent Database Materials based on the inlet conditions. The friction factor correlation was specified by the viscous model selected in ANSYS Fluent. The realised k-epsilon viscous model with enhanced wall treatment was used for this simulation as per Appendix C – Figure C.1, in which the wall roughness was specified as 0.0002 m and the remaining equation variables were left as the default values, as seen in Appendix C – Figure C.2. The pressure drop and velocity profiles of the single-phase, annulus pipe air flow from the drilling surface to a wellbore depth of 90 m are also presented in Figures 4.1.2.1 to 4.1.2.2.

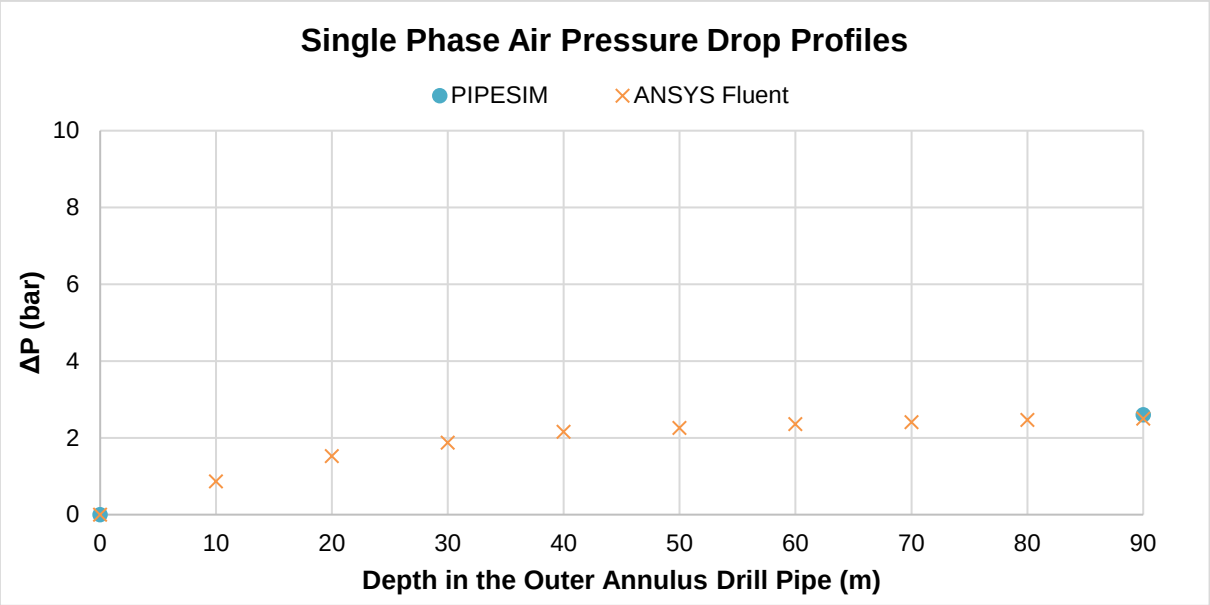

Figure 4.1.2.1: Comparison of single-phase air, outer annulus pipe flow pressure drop profiles from PIPESIM and ANSYS Fluent.

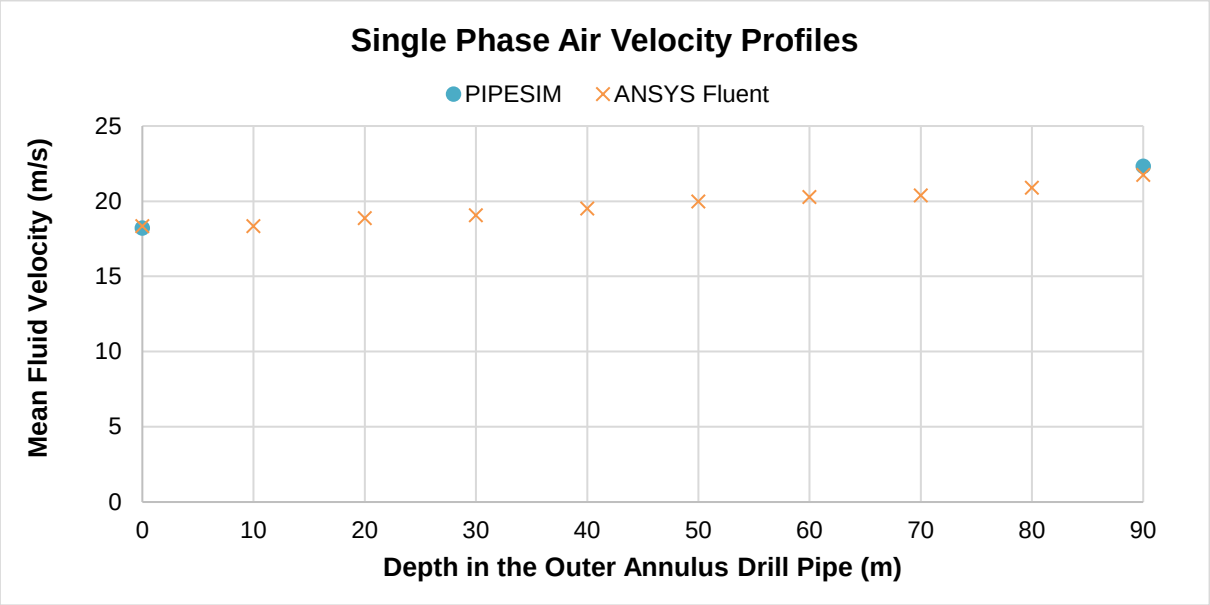

Figure 4.1.2.2: Comparison of single-phase air, outer annulus pipe flow velocity profiles from PIPESIM and ANSYS Fluent.

The results obtained from PIPESIM and ANSYS Fluent for the single-phase compressible air flow can be compared against each other for validation of the results. The comparison of the pressure drop results (Figure 4.1.2.1) and velocity change results (Figure 4.1.2.2) from PIPESIM and ANSYS Fluent show some variation. Figure 4.1.2.1 shows a difference of 0.1 bar(a) in overall pressure drops. This may be attributed to variations in the frictional pressure

loss models, that may account for a lower pressure loss in the case of the ANSYS Fluent results, and the on-isothermal temperature models, that influence the density of the compressible air and hence, hydrostatic pressure loss. Figure 4.1.2.2 presents a variation of 0.65% and 2.60% in wellbore surface velocities and 90 m wellbore bottom velocities, respectively. This is also attributed to the frictional pressure loss models which may account for decreased wall friction and a greater increase in gas velocity, in the case of the PIPESIM simulation results, as well as variations in non-isothermal temperature profile. Hence, this range of variation in the pressure drop and velocity values can be considered as acceptable for PIPESIM and ANSYS Fluent, due to previous preliminary validation of single phase, compressible air flow modelling using PIPESIM and ANSYS Fluent for the inner drill string rod geometry.

4.1.3. Single Phase Air Flow Modelling Evaluation

The approach to selecting the simulation basis, including density or pressure and simulation models, such as the Well PI IPR model in PIPESIM and realised k-epsilon viscous model in ANSYS Fluent, were mainly iterative and extremely time consuming due to the unfamiliarity of the array of models that may be used in compressible gas modelling and the inexperience with the PIPESIM and ANSYS Fluent software. Due to these aspects of the simulation methodologies, the simulation results obtained were impacted particularly for the ANSYS Fluent simulations, as more appropriate and accurate models may have been selected. Therefore, the quality, quantity and range of results may have been increased with greater knowledge and experience.

The key learnings developed from this aspect of the research project were the fundamental basis for accuracy and validity of the simulation of multiphase vertical flow in a RC drilling rig. These learnings include use of the PIPESIM and ANSYS Fluent software for compressible gas flow, familiarity with vertical flow correlations, and general knowledge on what pressure drop and velocity profiles may be expected. The results and overall findings obtained from the flow of compressible air in the inner and outer drill pipes were the basis data for the simulation of two-phase air-water flow.

4.2. Single Phase Water Flow in RC Drilling

4.2.1. Single Phase Water Flow in Inner Drill String Pipe

The inner drilling rod was simulated in PIPESIM for pure, single-phase water flow based on a mass flowrate of 0.725 kg/s, which is the mass flowrate of the water within the two-phase air-water flow from field data and outlet pressure of 1.5 bar(a), as summarised in Figure 3.2.1.1. The properties of water were specified by built in PIPESIM functions, with an infinite LGR, which is the ratio of the liquid water mass flowrate over the gas air mass flowrate. The friction factor correlation was specified by the IPR model as previously discussed, in which the Well PI model was also used for this PIPESIM simulation on a liquid phase basis and using a productivity index of 4.83E-9 m^3/(s.Pa). The overall pressure drop and change in velocity of the upward vertical water flow from a depth of 90 m to the drilling surface are presented in Figures 4.2.1.1 and 4.2.1.2. The inner drilling rod was also simulated in ANSYS Fluent for pure, single-phase water flow based an outlet single-phase liquid velocity of 0.38 m/s and outlet pressure of 1.5 bar(a), as per Figure 3.2.1.1. The properties of water were specified by the ANSYS Fluent Database Materials based on the outlet conditions. The friction factor correlation was specified by the viscous model selected in ANSYS Fluent, similar to the single-phase air flow simulation. The realised k-epsilon viscous model with enhanced wall treatment was used for this simulation as per Appendix C – Tables C.1, in which the wall roughness was specified as 0.0002 m and the remaining equation variables were left as default, which can be seen in Appendix C – Table C.2. The pressure drop and velocity profiles of the single-phase water flow from a depth of 90 m to the drilling surface are also presented in Figures 4.2.1.1 to 4.2.1.2.

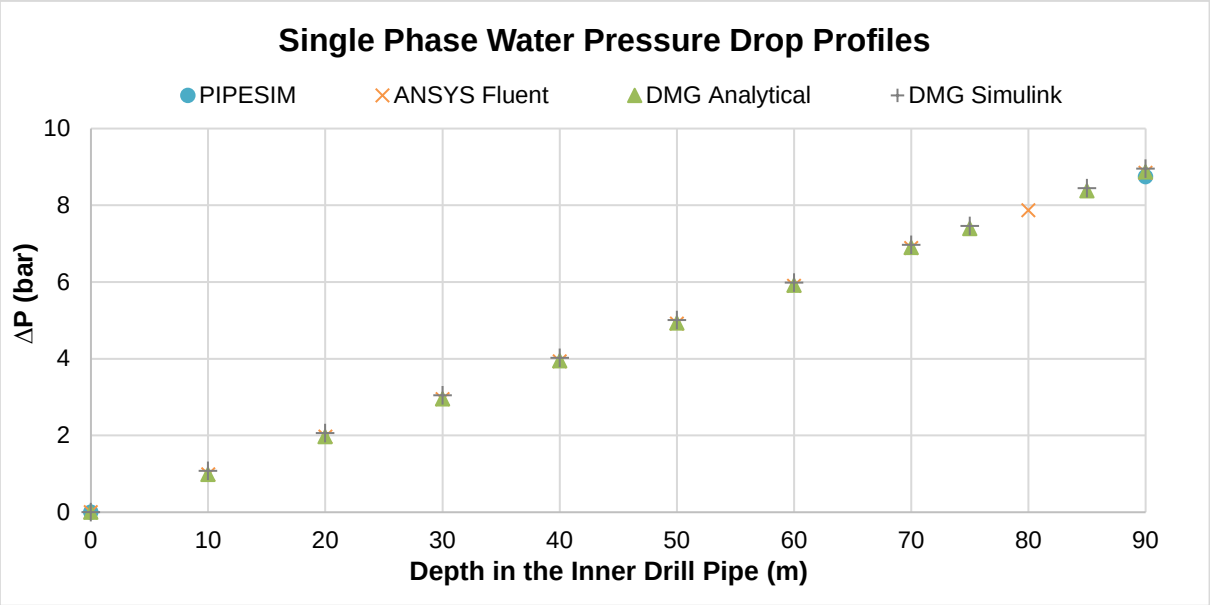

Figure 4.2.1.1: Comparison of single-phase water, inner pipe flow pressure drop profiles from PIPESIM, ANSYS Fluent, DMG analytical model and DMG Simulink model.

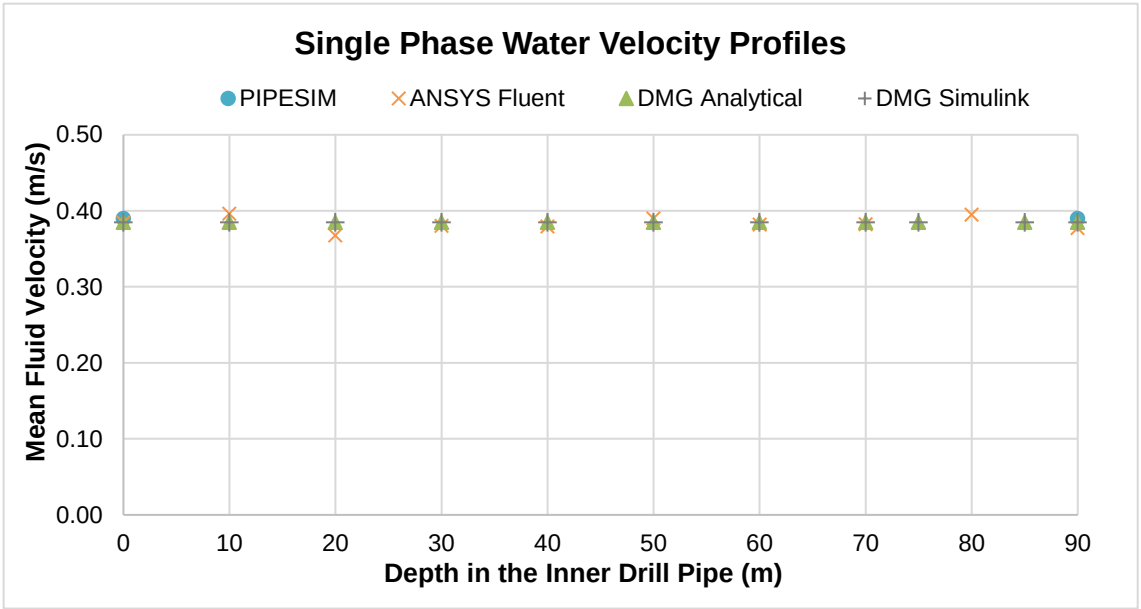

Figure 4.2.1.2: Comparison of single-phase water, inner pipe flow velocity profiles from PIPESIM, ANSYS Fluent, DMG analytical model and DMG Simulink model.

The results obtained from PIPESIM and ANSYS Fluent for the single-phase liquid water flow can be comparatively analysed against the DMG analytical and DMG Simulink models for a complete validation of the simulation results obtained. The comparison of the pressure drop

results in Figure 4.2.1.1 and velocity change results in Figure 4.2.1.2 from PIPESIM and ANSYS Fluent show some variation. The overall pressure drops from the PIPESIM and ANSYS Fluent simulations show a difference of 1.40 bar(a) and 0.27 bar(a) from the DMG analytical model, respectively. While the overall pressure drops from the PIPESIM and ANSYS Fluent simulations show a difference of 2.33 bar(a) and 1.20 bar(a) from the DMG Simulink model, respectively. This is attributed to the frictional pressure loss models used, that may account for a greater pressure loss in the case of PIPESIM and hence, increase the hydrostatic pressure loss. The overall velocity changes presented in Figure 4.2.1.2 show a variation of 1.30% and 0.14% for the water flow at the wellbore bottom and a variation of 1.30% and 2.06% for the water flow at the drill string surface between the PIPESIM and ANSYS Fluent simulation results and both the DMG analytical and Simulink models. This may also be attributed to the frictional pressure loss models which may account for increased wall friction and a greater decrease in liquid velocity, in the case of the ANSYS Fluent simulations.

4.2.2. Single Phase Water Flow in Outer Annulus Drill String Pipe

The outer annulus drill pipe was simulated in PIPESIM for pure, single-phase water flow based on a mass flowrate of 1.45 kg/s, which is the mass flowrate of the water within the two-phase air-water flow from field data and inlet pressure of 50 bar(a) as summarised in Figure 3.2.1.1. The properties of water were specified by built in PIPESIM functions, with an infinite LGR, which is the ratio of the liquid water mass flowrate over the gas air mass flowrate. The friction factor correlation was specified by the IPR model as previously discussed, in which the Well PI model was also used for this PIPESIM simulation on a liquid phase basis and using a productivity index of 4.83E-9 m^3/(s.Pa). The overall pressure drop and change in velocity of the downward water flow in an annulus pipe from the drilling surface to a drilling depth of 90 m are presented in Figures 4.2.2.1 and 4.2.2.2.

The inner drilling rod was also simulated in ANSYS Fluent for pure, single-phase water flow based an inlet single-phase liquid velocity of 0.44 m/s and inlet pressure of 50 bar(a), as per Figure 3.2.1.1. The properties of water were specified by the ANSYS Fluent Database Materials based on the inlet conditions. The friction factor correlation was specified by the viscous model selected in ANSYS Fluent, similar to the single-phase air flow simulation. The realised k-epsilon viscous model with enhanced wall treatment was used for this simulation as per Appendix C – Figures C.1 and C.2, in which the wall roughness was specified as 0.0002 m and the remaining equation variables were left as default, which can be seen in Appendix C – Table C.2. The pressure drop and velocity profiles of the single-phase water flow in an

annulus pipe from a depth of 90 m to the drilling surface are also presented in Figures 4.2.2.1 to 4.2.2.2.

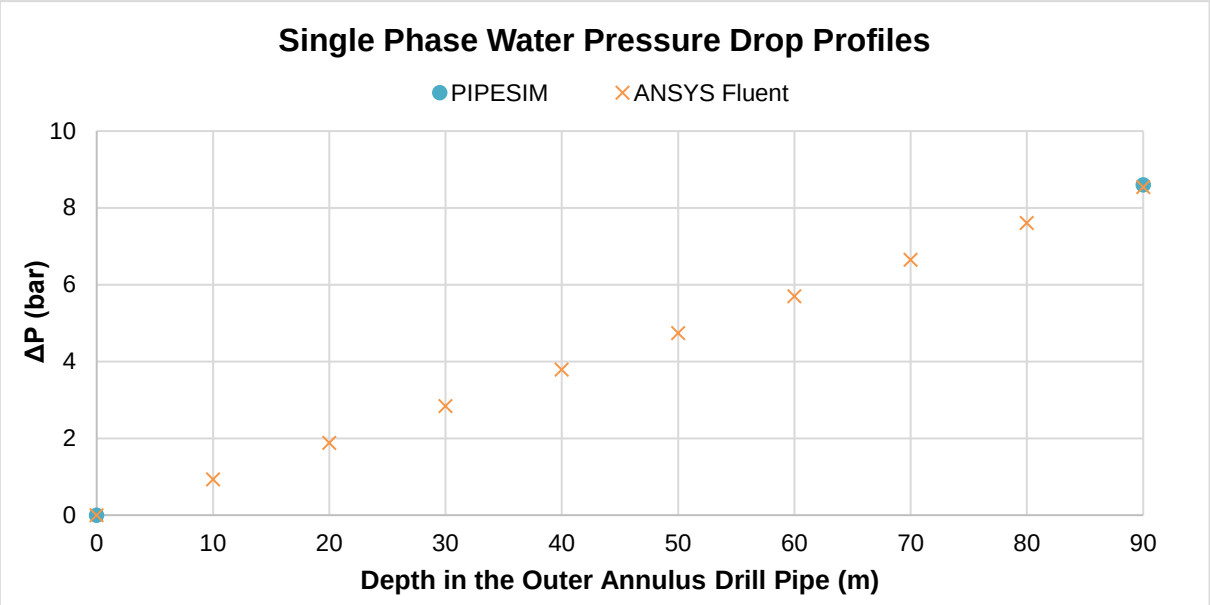

Figure 4.2.2.1: Comparison of single-phase water, outer annulus pipe flow pressure drop profiles from PIPESIM and ANSYS Fluent.

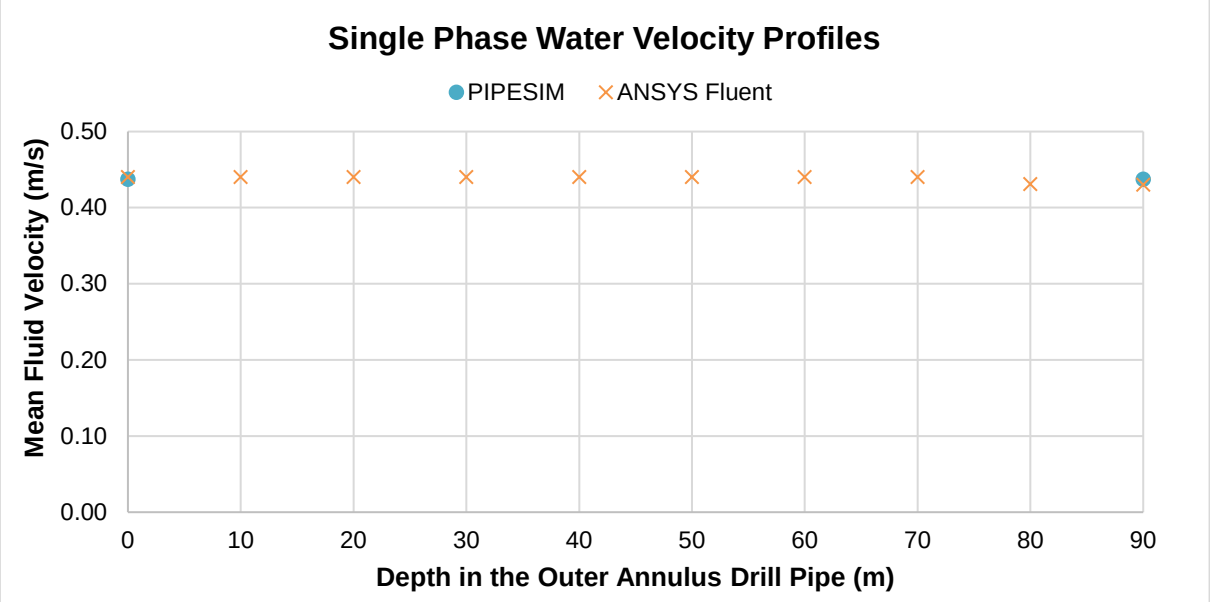

Figure 4.2.2.2: Comparison of single-phase water, outer annulus pipe flow velocity profiles from PIPESIM and ANSYS Fluent.

The results obtained from PIPESIM and ANSYS Fluent for the single-phase liquid water flow can be comparatively analysed against each other for a complete validation of the simulation

results obtained. The comparison of the pressure drop results in Figure 4.2.2.1 and velocity change results in Figure 4.2.2.2 from PIPESIM and ANSYS Fluent show minimal variation. The overall pressure drops from the PIPESIM and ANSYS Fluent simulations show a difference of 0.05 bar(a). This is attributed to the frictional pressure loss models used, that may account for a greater pressure loss in the case of PIPESIM and hence, increase the hydrostatic pressure loss. The overall velocity changes presented in Figure 4.2.2.2 show a variation of 0% for the water flow at the drilling surface and a variation of 1.6% for the water flow at the wellbore bottom between the PIPESIM and ANSYS Fluent simulation results. This may also be attributed to the frictional pressure loss models which may account for increased wall friction and a decrease in liquid velocity, in the case of the ANSYS Fluent simulations.

4.2.3. Single Phase Water Flow Modelling Evaluation

The approach to selecting the simulation models, such as the Well PI IPR model in PIPESIM and realised k-epsilon viscous model in ANSYS Fluent, was iterative and very time consuming as previously discussed for the simulation single-phase air flow. Therefore, a greater array of results, may have been possible with greater knowledge and experience using the software. Based on improvements identified above, predicting potential problems and scheduling longer time periods to complete tasks, in particular simulation modelling and data collection, were implemented.

The key learnings obtained from this section of the research project are the basis for ensuring the validity of the simulation of multiphase vertical flow and in a complete RC drilling rig. These learnings include use of the PIPESIM and ANSYS Fluent software for liquid flow, familiarity with vertical flow correlations, and general understanding of expected results in the inner and outer annulus drill pipe flows, similar to the single-phase air simulation. The simulation findings from liquid water flow in the inner and outer annulus drill pipe were also utilised as the foundation data for the simulation of two-phase air-water flow, similar to the single phase compressible air simulation data.

4.3. Two-Phase Air-Water Flow in RC Drilling

4.3.1. Two-Phase Air-Water Flow in Inner Drill String Pipe

The inner drilling rod was simulated for two-phase air-water flow with a mass flowrate of 1.151 kg/s and outlet pressure of 1.5 bar(a), based on the field data presented in Figure 3.2.1.1. The two-phase air-water flow composition was specified by a gas mass flowrate of 0.426 kg/s and

liquid mass flowrate of 0.725 kg/s, and properties of air-water flow were specified by built in PIPESIM functions, based on a constant LGR of 1.702 kg water/kg air obtained from the basis field data (Figure 3.2.1.1). As PIPESIM can only perform nodal analysis for a single point, several geometries were created for drill depths of 15 m, 30 m, 45 m, 60 m, 75 m and 90 m and simulated to obtain complete pressure drop profiles from 90 m to the drilling surface (i.e.: 0 m). The multiphase pressure drop and velocity profiles for the vertical air-water flow using the Ansari correlation and No Slip correlation were graphed against the DMG analytical model and DMG Simulink model in Figures 4.3.1.1 and 4.3.2.2. The full list of available multiphase correlations can be seen as per Table 3.3.1.

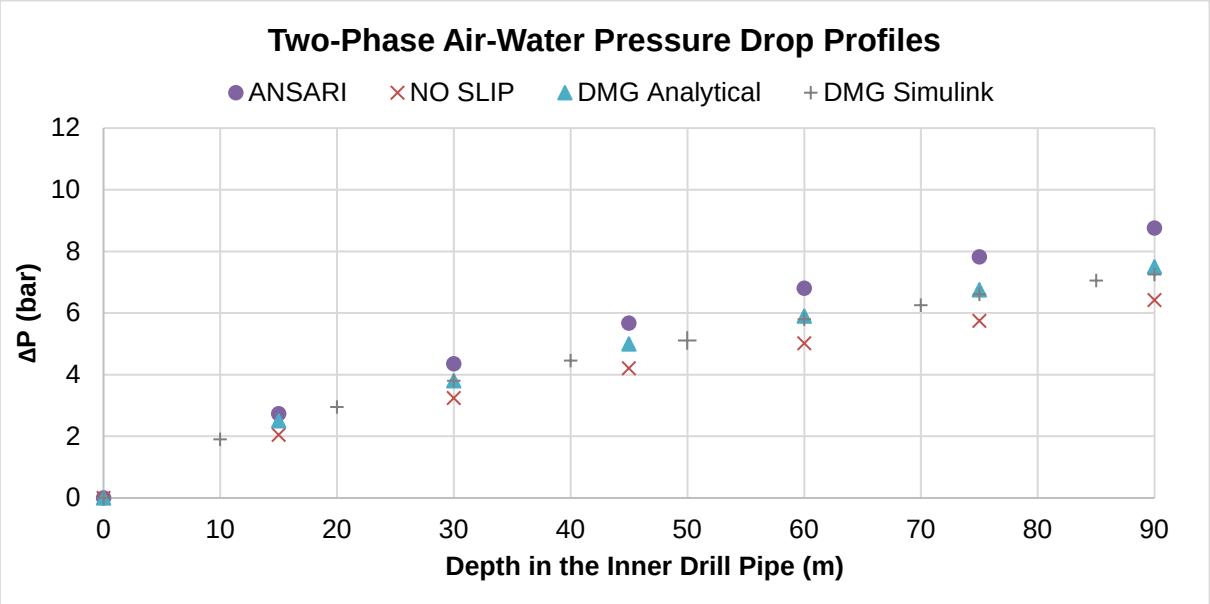

Figure 4.3.1.1: Comparison of two-phase air-water, inner pipe flow pressure drop profiles using the Ansari and No Slip PIPESIM correlations, DMG analytical model and DMG Simulink model.

The Ansari correlation was selected out of the 24 available PIPESIM correlations for analysis as is a most commonly utilised non-homogeneous, multiphase flow correlations with various research studies on standard vertical pipe and vertical wellbore flow scenarios, including by Ping, Wang, and Wei (2006), Ben Mahmud (2012) and Ganat et al. (2019). The No Slip correlation was also selected as it was the only homogenous (i.e.: non-heterogeneous, no slip) vertical flow model available in PIPESIM and would allow for the analysis and comparison against the DMG analytical model and DMG Simulink model, which also assumes homogenous flow behaviour. The various other multiphase flow correlations were excluded for flow in the inner drill pipe based on series of variables including year of development,

correlation sources, correlation types, typical applications, flow patterns modelled and some limited correlation boundary conditions for gas flowrate, liquid flowrate and LGR. For example, the Gomez [Neotec], Gomez Enhanced [Neotec], Mukherjee & Brill [Baker Jardine] and Mukherjee & Brill [Tulsa (Legacy 1989)] correlations were excluded due to their applicability in inclined or horizontal, two-phase flow scenarios. While the Aziz Govier Fogarasi [Neotec], Govier, Aziz & Fogarasi [Baker Jardine], Govier, Aziz [Tulsa (Legacy 1989)], Duns & Ros [Baker Jardine], Buns & Ros [Tulsa (Legacy 1989)], Hagedorn & Brown (Original) [Tulsa (Legacy 1989)], Hagedorn & Brown (Revised) [Baker Jardine], Hagedorn & Brown (Revised) with Duns & Ros map [Baker Jardine], Hagedorn & Brown (Revised) [Tulsa (Legacy 1989)] and TUFFP (v. 2011 2-Phase) [TUFFP Unified] correlations were excluded due to their inability to model two-phase flow with a notable quantity of water present. The Beggs & Brill Original [Baker Jardine], Beggs & Brill Revised [Baker Jardine] and Beggs & Brill Revised [Tulsa (Legacy 1989)] correlations are generally the most reliable and widely utilised correlations; however, they are only applicable over short pipes with reduced overall pressure drop. The Orkiszewski [Baker Jardine] and Orkiszewski [Tulsa (Legacy 1989)] were simply excluded due to the high applicability of the Ansari [Tulsa (Legacy 1989)] correlation for the upward, vertical flow in the inner drill string rod.

The pressure drop profiles presented in Figure 4.3.1.1 for two-phase air-water, vertical flow in the inner pipe of a 90 m wellbore show pressure drop of 8.75 bar(a) for the Ansari correlation and 6.42 bar(a) for the No Slip correlation, compared to a 7.50 bar(a) pressure drop and 7.25 bar(a) pressure drop for the DMG analytical model and DMG Simulink model, respectively, at a constant mass flowrate of 1.151kg/s and an output pressure of 1.5 bar(a). The mass flowrates of each phase were specified under the fluid manager composition and remained constant at 0.426 kg/s of compressible air and 0.725 kg/s of liquid water. The pressure drop profiles all follow the expected curved shape approaching an equilibrium value, which is typical of multiphase, compressible vertical flow and reflects the pressure drop due to decrease in two-phase flow density. This pressure drop values account for the hydrostatic and frictional pressure losses experienced by the compressible two-phase air-water flow from the bottom of a 90 m wellbore to the drilling surface, assuming an inner drilling rod wall roughness of 0.0002 m. The friction factor correlation was specified by the IPR model, in which the Well PI model was selected for all multiphase PIPESIM simulations, similar to the single-phase water simulations, which required user specification of the IPR basis in which liquid phase was selected and the associated productivity index was specified as 4.83E-9 m^3/(s.Pa). This two-phase air-water flow was also assumed to be non-isothermal, with an observed temperature drop from 329.71 K to 322.41 K for the Ansari correlation and 329.53 K to 321.18 K for the No Slip correlation.

The variation in the pressure drop profiles, and the change in non-isothermal temperature can attributed to the key assumptions and applicability of the correlations discussed. The No Slip correlation in PIPESIM is a basic homogenous or no slip model for vertical multiphase flow, which considers acceleration, frictional and hydrostatic pressure loss on the assumption that the vapour and liquid phases in multiphase flow are well mixed or are a continuous phase and travel at the same velocity (Awad and Muzychka 2008). However, this is not true or valid for at least some sections of the inner drilling rod. Therefore, heterogeneous, multiphase flow simulation is extremely important in this research. The Ansari correlation is a non-homogenous mechanistic model specialised for upward, vertical flow application and considers acceleration, frictional and hydrostatic pressure difference, based on the appropriately determined gas-liquid flow regime. This correlation was one of many models developed by the Tulsa University Fluid Flow Projects (TUFFP) research projects which utilises a number of independent model to predict pressure drop, hydrostatic and frictional pressure losses, and liquid holdup (Fetoui 2017). The inner drill string pipe two-phase pressure drop is highly dependent on the determined flow regime of the air-water flow for the Ansari correlation. For the 90 m wellbore at the conditions specified by field data (Figure 3.2.1.1), the flow regime determined by the Ansari correlation was *annular* flow for the complete 90 m vertical flow.

As the No Slip correlation, DMG analytical model and DMG Simulink model are homogeneous models, they are expected to calculate a similar pressure drop which has been observed. The pressure drop is also expected to be a lower value when compared to heterogenous models, as the increased wall friction imposed by two phases is not considered, which is consistent with the Ansari correlation results. For the two-phase air-water flow in a vertical, inner drill rod, the simulation data using the Ansari correlation reflects the expected results to a high degree, based on the overall pressure drop magnitude and pressure drop profile shape, and was utilised in further sensitivity studies with varying total mass flowrates and the creation of “operating regime” graphs for RC drilling operation.

4.3.2. Two-Phase Air-Water Flow in Outer Annulus Drill String Pipe

The outer annulus drill pipe was simulated for two-phase air-water flow with a mass flowrate of 2.303 kg/s and an inlet pressure of 50 bar(a), based on the field data presented in Figure 3.2.1.1. The two-phase air-water flow composition was specified by a gas mass flowrate of 0.853 kg/s and liquid mass flowrate of 1.45 kg/s, and properties of air-water flow were specified by built in PIPESIM functions, based on a constant LGR of 1.702 kg water/kg air obtained from the basis field data (Figure 3.2.1.1). As PIPESIM can only perform nodal analysis for a single point, several geometries were created for drill depths of 15 m, 30 m, 45 m, 60 m, 75 m and

90 m and simulated to obtain complete pressure drop profiles, as previously explained. The multiphase pressure drop profile for the air-water flow in the outer annulus pipe using the Orkiszewski correlation and No Slip Assumption correlation were graphed against each other in Figure 4.3.2.1. The full list of available vertical, multiphase correlations can be seen as per Table 3.3.1.

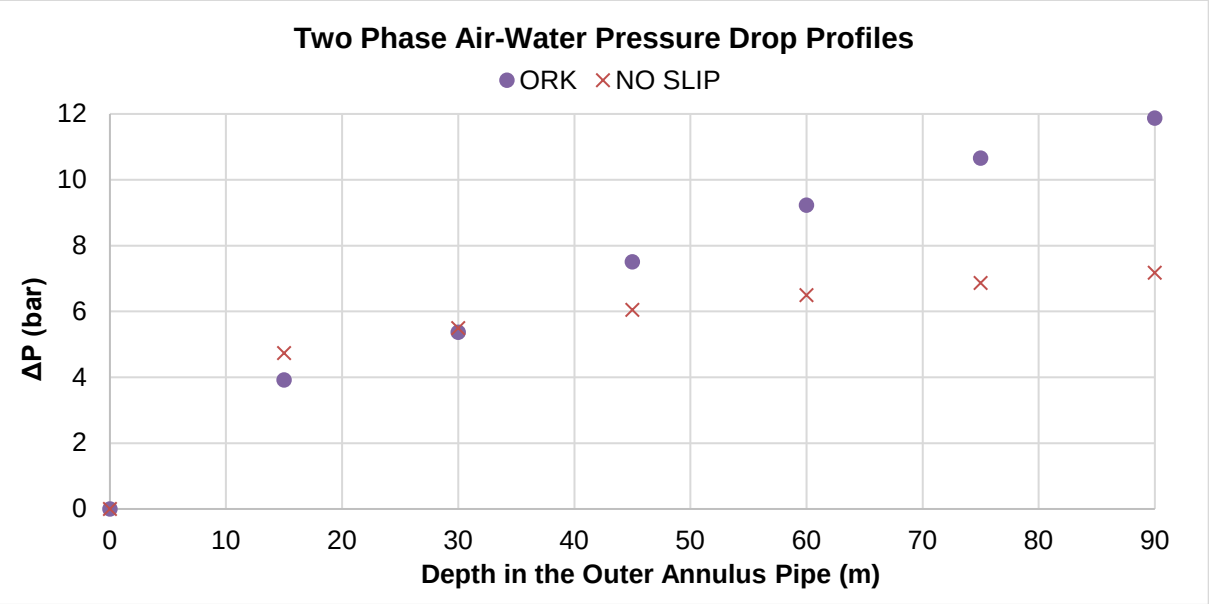

Figure 4.3.2.1: Comparison of two-phase air-water, outer annulus pipe flow pressure drop profiles using the Orkiszewski and No Slip PIPESIM correlations.

The Orkiszewski correlation was selected out of the 24 available PIPESIM correlations for analysis, as it was developed based on a new flow regime map and a combination of aspects from existing multiphase flow correlations, including the Duns and Ros (1963) correlation and Hagedorn and Brown (1965), which made the correlation most applicable for the unique annulus pipe flow conditions. The No Slip correlation was also selected once again as it was the only homogenous (i.e.: no slip) vertical flow model available in PIPESIM as previously discussed. The various other multiphase flow correlations were excluded for flow in the inner drill pipe based on series of variables including year of development, correlation sources, correlation types, typical applications, flow patterns modelled and some limited correlation boundary conditions for gas flowrate, liquid flowrate and LGR as utilised for the inner drill strong pipe flow correlations. For example, the Gomez [Neotec], Gomez Enhanced [Neotec], Mukherjee & Brill [Baker Jardine] and Mukherjee & Brill [Tulsa (Legacy 1989)] correlations were excluded due to their applicability in inclined or horizontal, two-phase flow scenarios, as previously specified for the inner drill string pipe flow. While the Aziz Govier Fogarasi [Neotec],

Govier, Aziz & Fogarasi [Baker Jardine], Govier, Aziz [Tulsa (Legacy 1989)], Duns & Ros [Baker Jardine], Buns & Ros [Tulsa (Legacy 1989)], Hagedorn & Brown (Original) [Tulsa (Legacy 1989)], Hagedorn & Brown (Revised) [Baker Jardine], Hagedorn & Brown (Revised) with Duns & Ros map [Baker Jardine], Hagedorn & Brown (Revised) [Tulsa (Legacy 1989)] and TUFFP (v. 2011 2-Phase) [TUFFP Unified] correlations were excluded due to their inability to model two-phase flow with a notable quantity of water present, as specified for the inner drill string pipe flow. The Beggs & Brill Original [Baker Jardine], Beggs & Brill Revised [Baker Jardine] and Beggs & Brill Revised [Tulsa (Legacy 1989)] correlations are generally the most reliable and widely utilised correlations; however, they are only applicable over short pipes with reduced overall pressure drop. The Ansari [Tulsa (Legacy 1989)] correlation was then excluded as it is only applicable for the upward, vertical flow. Hence, the Orkiszewski [Baker Jardine] and Orkiszewski [Tulsa (Legacy 1989)] were remaining and the Orkiszewski [Baker Jardine] variation was simply selected.

The pressure drop profiles presented in Figure 4.3.2.1 for two-phase air-water, vertical flow in the inner pipe of a 90 m wellbore show pressure drop of 11.87 bar(a) for the Orkiszewski correlation and 7.18 bar(a) for the No Slip correlation, at a constant mass flowrate of 2.303 kg/s and an input pressure of 50 bar(a). The mass flowrates of each phase were specified under the fluid manager composition and remained constant at 0.853 kg/s of compressible air and 1.45 kg/s of liquid water. The pressure drop profiles all follow the expected curved shape approaching an equilibrium value, which is typical of multiphase, compressible vertical flow and reflects the pressure drop due to decrease in two-phase flow density. This pressure drop account for the hydrostatic and frictional pressure losses experienced by the compressible two-phase air-water flow from the drilling surface to the bottom of a 90 m wellbore, assuming an inner and outer annulus drill pipe wall roughness of 0.0002 m. The friction factor correlation was specified by the IPR model, in which the Well PI model was selected for all multiphase PIPESIM simulations, similar to the single-phase water simulations, which required user specification of the IPR basis in which liquid phase was selected and the associated productivity index was specified as 4.83E-9 m^3/(s.Pa). This two-phase air-water flow was also assumed to be non-isothermal, with an observed temperature drop from 329.83 K to 328.00 K for the Orkiszewski correlation and 329.86 K to 328.97 K for the No Slip correlation.

The variation in the pressure drop profiles, and the change in non-isothermal temperature can attributed to the key assumptions and applicability of the correlations discussed. The No Slip correlation in PIPESIM is a basic homogenous or no slip model for vertical multiphase flow, which considers acceleration, frictional and hydrostatic pressure loss on the assumption that the vapour and liquid phases in multiphase flow are well mixed or are a continuous phase and

travel at the same velocity (Awad and Muzychka 2008). However, this is not true or valid for at least some sections of the outer annulus drill pipe. Therefore, heterogeneous, multiphase flow simulation is extremely important in this research. The Orkiszewski correlation is a heterogenous, empirical model applicable for gas lift production wells, in which a wide range of operating conditions can be appropriately modelled. This correlation is typically accurate with minimal variation from measured, experimental data. It also utilises a number of established and new models to predict density, pressure drop including hydrostatic and frictional pressure losses, superficial mixture velocity and liquid holdup (Fetoui 2017). The outer annulus drill pipe two-phase pressure drop is highly dependent on the determined flow regime of the air-water flow for the Orkiszewski correlation. For the 90 m wellbore at the conditions specified by field data (Figure 3.2.1.1), the flow regime determined by the Orkiszewski correlation was *slug* flow for the first 15 m, then changed to *transition* flow for the remaining outer pipe from 15 m to the bottom of the wellbore.

As the No Slip correlation is a homogeneous model, the pressure drop is expected to be a lower value when compared to heterogenous models, as the increased wall friction imposed by two phases is not considered, which is consistent with the Orkiszewski correlation results. For the two-phase air-water flow in a vertical, outer annulus drill pipe, the simulation data using the Orkiszewski correlation reflects the expected results to a high degree, based on the overall pressure drop magnitude and pressure drop profile shape, and hence, was utilised in further sensitivity studies with varying total mass flowrates and the creation of “operating regime” graphs for RC drilling operation.

4.3.3. Two-Phase Air-Water Flow Modelling Evaluation

The method for selecting the PIPESIM vertical, multiphase flow correlations for analysis was mainly qualitative. Therefore, correlation selection to obtain results of maximum accuracy would require extended knowledge on vertical, multiphase flow correlations and their quantitative boundary conditions and experience using the PIPESIM software. Based on these potential improvements identified, the project considered periods to further learn the capabilities and specific models of PIPESIM and ANSYS Fluent, and complete simulation modelling tasks. The key learnings obtained from this aspect of research project are to ensure the validity of the simulation of multiphase vertical flow in a complete RC drilling rig. These learnings include use of basic PIPESIM software functions for two-phase flow, familiarity with some vertical, multiphase flow correlations, and general understanding of expected pressure drop and velocity profiles for multiphase flow in the inner and outer annulus drill pipe flow. The simulation results obtained from two-phase air-water flow in the inner and outer drill pipes will

be utilised for sensitivity study simulation. The PIPESIM simulation results obtained can be considered as valid for continued utilisation, as the previous single phase compressible air, single phase water and two-phase air-water flow simulation data have been extensively validated and all two-phase air-water flow simulation data follows the expected heuristics.

4.4. Two-Phase Air-Water Flow in RC Drilling Sensitivity Studies

4.4.1. Two-Phase Air-Water Flow in Inner Drilling Pipe Sensitivity Studies

The inner drilling rod was simulated for two-phase air-water flow for a constant LGR of 1.702 kg water/kg air and outlet pressure of 1.5 bar(a), based on a series of sensitivity studies with varying total mass flowrate. The two-phase air-water flow composition were specified on a molar basis and the physical properties of air-water flow were specified by built in PIPESIM functions, for total mass flowrates of 0.576 kg/s, 1.151 kg/s and 2.303 kg/s. The specified total mass flowrates were based on basis air volumetric flowrates of 375 SCFM, 750 SCFM and 1500 SCFM. The overall pressure drop and associated flow patterns of the vertical air-water flow in an inner drill pipe for a depth of 300 m are presented in Figures 4.4.1.1 to 4.4.1.2, using the Ansari correlation and No Slip correlations. As PIPESIM can only perform nodal analysis for a single point, Figure 4.4.1.1 was created through a series of individual simulations, as previously explained for the basis two-phase air-water flow simulations.

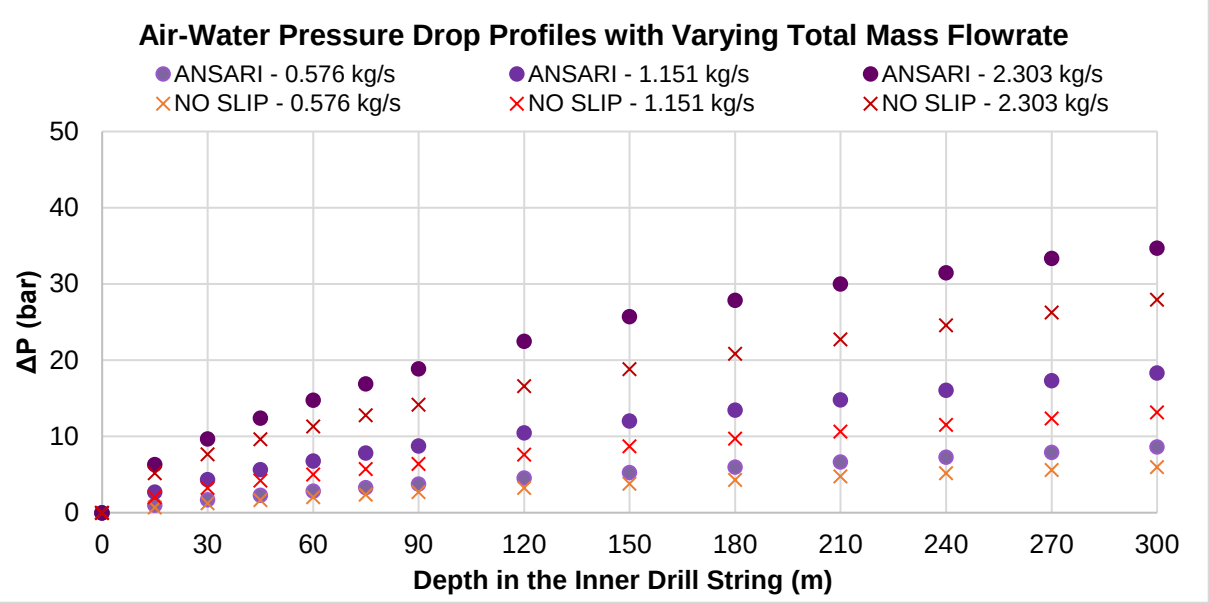

Figure 4.4.1.1: Two-phase air-water, inner pipe flow overall pressure drop using the Ansari and No Slip PIPESIM correlations with varying mass flowrate.

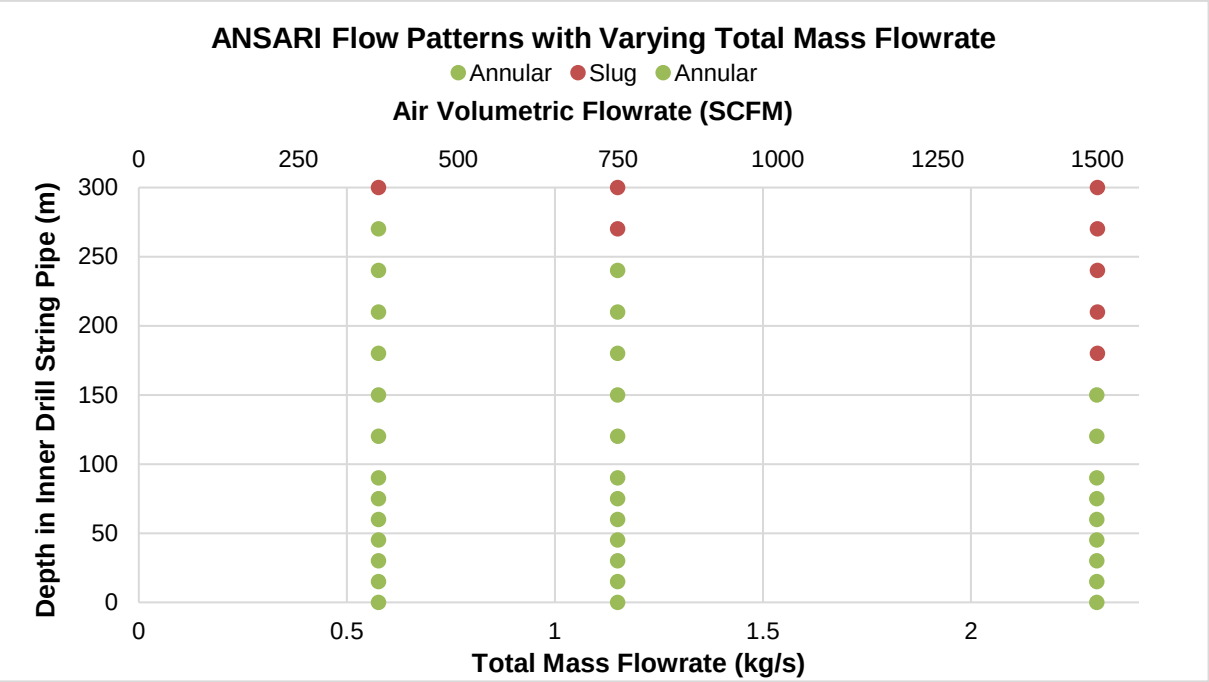

Figure 4.4.1.2: Two-phase air-water, inner pipe flow patterns using the Ansari PIPESIM correlation with varying total mass flowrate.

The Ansari and No Slip correlations were selected for sensitivity studies with variation in the total mass flowrate to compare the results between homogeneous and non-homogeneous flow assumptions. The overall pressure drops in Figure 4.4.1.1 for two-phase air-water flow in a 300 m wellbore show an array of values from 8.64 bar(a) for a total mass flowrate of 0.576 kg/s (i.e.: 375 SCFM), 18.31 bar(a) for 1.151 kg/s (i.e.: 750 SCFM) and 34.70 bar(a) for 2.303 kg/s (i.e.: 1500 SCFM) using the Ansari correlation and 5.98 bar(a) for a total mass flowrate of 0.576 kg/s, 13.18 bar(a) for 1.151 kg/s and 27.93 bar(a) for 2.303 kg/so using the No Slip correlation, at a constant LGR of 1.702 kg water/kg air and outlet pressure of 1.5 bar(a) though the inner drill string pipe. It can be observed that the pressure drop values for the varying total mass flowrate are greater for the Ansari correlation compared to the No Slip correlation, which can be attributed to increased frictional pressure losses calculated in the heterogeneous Ansari correlation, as previously discussed in detail. The LGR was specified under the fluid manager composition for the varying mass flowrates studied. The friction factor correlation was specified by the IPR model as specified previously for two-phase air-water flow simulation. This two-phase air-water flow was also assumed to be non-isothermal in all sensitivity studies, with a temperature variation from 329.9 K to 322.4 K for the Ansari correlation and 329.9 K to 322.8 K for the No Slip correlation, as the temperature changes through the outer annulus pipe from 330 K was considered negligible.

The associated flow patterns for the varying total mass flowrate can be seen in Figure 4.4.1.2, which for two-phase air-water flow in a 300 m wellbore, at a total mass flowrate of 0.576 kg/s from 0 m to 270 m the flow was *annular* and from 270 m to 300 m the flow was *slug*. While at a total mass flowrate of 1.151 kg/s from 0 m to 240 m, the flow was *annular* and from 240 m to 300 m, the flow was *slug*. At the greater total mass flowrate of 2.303 kg/s from 0 m to 150 m, the flow was *annular* and then from 150 m to 300 m was *slug* flow. It is clear from Figure 4.4.1.2, that for increasing total mass flowrate using the Ansari correlation, the earlier the formation and hence, the greater the presence of *slug* flow throughout the 300 m wellbore. For the 300 m vertical wellbore with a total mass flowrate of 0.576 kg/s through the inner drill pipe, the Ansari correlation predicts a change in liquid holdup from 2.6% to 13.8%, while the No Slip correlation predicts 0.4% to 1.8%. For a total mass flowrate of 1.151 kg/s, the Ansari correlation predicts a change in liquid holdup from 1.4% to 15.7%, while the No Slip correlation predicts 0.4% to 3.5%. For the greatest total mass flowrate of 2.303 kg/s, the Ansari correlation shows a liquid holdup variation from 0.7% to 18.4% and the No Slip correlation shows 0.4% to 6.9%.Therefore, the relationship between total mass flowrate, liquid holdup and unstable flow pattern has been determined, that for increasing total mass flowrate, the liquid holdup increased and the unstable, Slug flow pattern is developed. This is due to the increased mean fluid velocity with increasing total mass flowrate, resulting in increased two-phase air-water pressure drop, including hydrostatic and frictional pressure drops (Figure 4.4.1.1), and the frequency of eddies and turbulent flow with distance from the wellbore bottom.

4.4.2. Two-Phase Air-Water Flow in Outer Annulus Drilling Pipe Sensitivity Studies

The outer annulus drilling pipe was simulated for two-phase air-water flow for a constant LGR of 1.702 kg water/kg air and inlet pressure of 50 bar(a), based on a series of sensitivity studies with varying total mass flowrate. The two-phase air-water flow composition were specified on a molar basis and the physical properties of air-water flow were specified by built in PIPESIM functions as previously utilised, for total mass flowrates of 1.151 kg/s, 2.303 kg/s and 4.606 kg/s. The specified total mass flowrates were based on basis air volumetric flowrates of 750 SCFM, 1500 SCFM and 3000 SCFM. The overall pressure drop and associated flow patterns of the vertical air-water flow in an outer annulus drill pipe for a depth of 300 m are presented in Figures 4.4.2.1 to 4.4.2.2, using the Orkiszewski correlation and No Slip correlations. As previously explained, Figure 4.4.2.1 was created through a series of individual simulations due to PIPESIM simulation limitations.

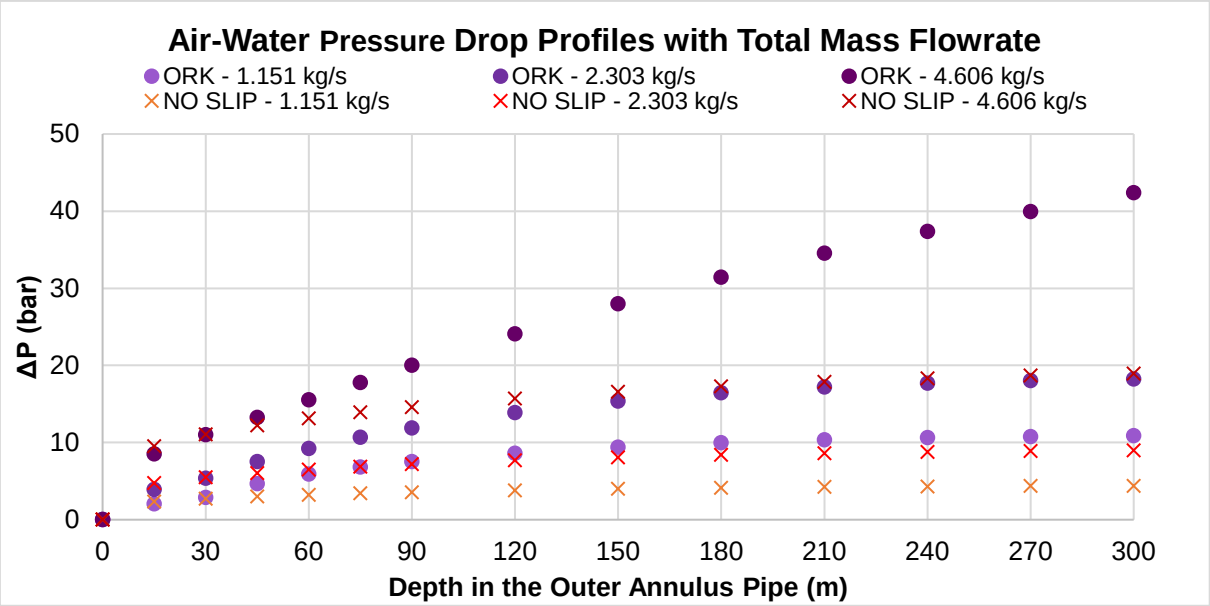

Figure 4.4.2.1: Two-phase air-water, outer annulus pipe flow overall pressure drop using the Orkiszewski and No Slip PIPESIM correlations with varying total mass flowrate.

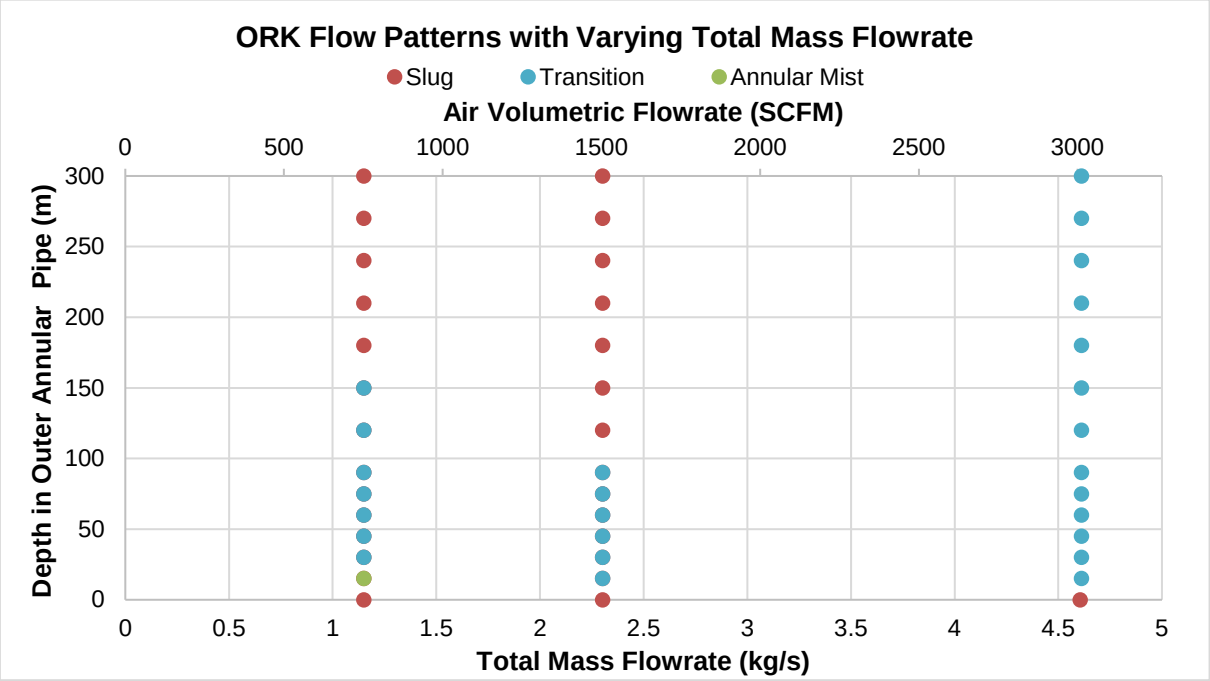

Figure 4.4.2.2: Two-phase air-water, outer annulus pipe flow pattern using the Orkiszewski and No Slip PIPESIM correlations with varying total mass flowrate.

The Orkiszewski correlation and No Slip correlations were selected for sensitivity studies with variation in the total mass flowrate to compare the results between homogeneous and non-homogeneous flow assumptions, once again, for the outer annulus drill pipe. The overall pressure drops in Figure 4.4.2.1 for two-phase air-water flow in a 300 m wellbore show an array of values from 10.89 bar(a) for a total mass flowrate of 1.151 kg/s (i.e.: 750 SCFM), 18.22 bar(a) for 2.303 kg/s (i.e.: 1500 SCFM) and 42.37 bar(a) for 4.606 kg/s (i.e.: 3000 SCFM) using the Orkiszewski correlation and 4.38 bar(a) for a total mass flowrate of 1.151 kg/s, 8.99 bar(a) for 2.303 kg/s and 18.95 bar(a) for 4.606 kg/so using the No Slip correlation, at a constant LGR of 1.702 kg water/kg air and inlet pressure of 50 bar(a) though the outer annulus drill string pipe. It can be observed that the pressure drop values for the varying total mass flowrate are greater for the Orkiszewski correlation compared to the No Slip correlation, as seen for the inner drill pipe Ansari correlation and No Slip correlation, which can be attributed to increased frictional pressure losses calculated in the heterogeneous Orkiszewski correlation, as previously discussed. The LGR was specified under the fluid manager composition for the varying mass flowrates studied. The friction factor correlation was specified by the IPR model as specified previously for two-phase air-water flow simulation. This two-phase air-water flow was also assumed to be non-isothermal in all sensitivity studies, however, the temperature variation of 329.8 K to 327.6 K for the Orkiszewski correlation and 329.9 K to 328.1 for the No Slip correlation, were considered negligible.

The flow patterns for the varying total mass flowrate in the outer annulus pipe can be seen in Figure 4.4.2.2, which for two-phase air-water flow in a 300 m wellbore, at a total mass flowrate of 1.151 kg/s at 0 m the flow was slug, from 0 m to 15 m the flow was *annular*, from 15 m to 150 m the flow was *transition* and from 150 m to 300 m the flow was s*lug*. While at a total mass flowrate of 2.303 kg/s at 0 m the flow was *slug*, from 0 m to 90 m the flow was *transition* and from 90 m to 300 m the flow was s*lug*. At the greater total mass flowrate of 4.606 kg/s at 0 m the flow was *slug* and from 0 m to 300 m the flow was *transition*. It is clear from Figure 4.4.2.2, that for increasing total mass flowrate using the Orkiszewski correlation, the earlier the formation and hence, the greater the presence of unstable flow patterns in the 300 m wellbore. For the 300 m vertical wellbore with a total mass flowrate of 1.151 kg/s through the outer annulus drill pipe, the Orkiszewski correlation predicts a change in liquid holdup from 0.6% to 8.9%, while the No Slip correlation predicts 0.6% to 2.8%. For a total mass flowrate of 2.303 kg/s, the Orkiszewski correlation predicts a change in liquid holdup from 1.0% to 8.7%, while the No Slip correlation predicts 1.3% to 5.5%. For the greatest total mass flowrate of 4.606 kg/s, the Orkiszewski correlation shows a liquid holdup variation from 1.4% to 1.5% and the No Slip correlation shows 2.7% to 10.6%.

Therefore, the relationship between total mass flowrate, liquid holdup and unstable flow pattern for the outer annulus pipe was determined, that for increasing total mass flowrate, the liquid holdup increased and the unstable, Slug flow pattern was developed. However, at very high mass flowrate *Transitional* flow is established in which no constant flow pattern is reached. This is due to the increased mean fluid velocity, resulting in increased two-phase air-water pressure drop (Figure 4.4.2.1), and the frequency of eddies and turbulent flow as previously explained.

4.4.3. Two-Phase Air-Water Flow Model Sensitivity Studies Evaluation

The method for selecting the PIPESIM vertical, multiphase flow correlations for the analysis of the outer annulus pipe was mainly qualitative, similar to that for the inner pipe. Therefore, correlation selection to obtain results of maximum accuracy would require extended knowledge on vertical, multiphase flow correlations and their quantitative boundary conditions. However, the literature available for the multiphase, vertical flow correlations had limited quantitative boundary condition data and its applicability for non-circular geometries, such as the outer annulus pipe. Based on these potential improvements identified, the project considered periods to further learn the capabilities and specific models of PIPESIM including which simulations correlation converge and obtain feasible data values and allow the completion simulation modelling tasks. The key learnings obtained from this aspect of research project are to ensure to simulate multiphase vertical flow in a complete RC drilling rig. These learnings include use of basic PIPESIM software functions for two-phase flow, familiarity with some vertical, multiphase flow correlations, and general understanding of expected pressure drop, liquid holdup and flow patterns for multiphase flow in the inner and outer annulus drill pipe flow. The simulation results obtained from two-phase air-water flow in the inner and outer drill pipes will be utilised for the operational regime chart simulations for validation. The PIPESIM simulation results obtained can be considered valid for continued utilisation, as the previous single phase compressible air, single phase water and two-phase air-water flow simulation data have been extensively validated and all two-phase air-water flow simulation data follows the expected heuristics.

4.5. Operating Regime Charts for RC Air Drilling

4.5.1. Two-Phase Air-Water Flow in RC Drill String Pipes Operating Regime Charts

The inner and outer drill pipes were simulated for two-phase air-water flow for a constant air mass flowrate of 0.426 kg/s and 0.853 kg/s, respectively, outer pipe inlet pressure of 50 bar(a) and inner pipe outlet pressure of 1.5 bar(a), based on a series of sensitivity studies with varying LGR. The drill string geometry, including the inner pipe diameter of 49 mm, outer annulus inner diameter of 60.3 mm and outer diameter of 89 mm, and depth of 90 m was kept constant as previously specified in Figure 3.2.11. The two-phase air-water flow composition were specified on a molar basis and the physical properties of air-water flow were specified by built in PIPESIM functions, for LGR of 0.11 kg/kg, 0.25 kg/kg, 0.43 kg/kg, 0.67 kg/kg, 1 kg/kg, 1.5 kg/kg, 2.33 kg/kg and 4 kg/kg. The selected LGR correspond to liquid water volumetric flowrates of 2.8 L/min, 6.4 L/min, 11.0 L/min, 17.0 L/min, 25.6 L/min, 38.3 L/min, 59.6 L/min and 102.2 L/min, respectively for the inner pipe and 5.7 L/min, 12.8 L/min, 21.9 L/min, 34.1 L/min, 51.2 L/min, 76.8 L/min, 119.4 L/min and 204.7 L/min, respectively for the outer annulus pipe. The overall pressure drop ratio of two-phase air-water flow to single-phase air flow and associated flow patterns of the vertical air-water flow for the inner drill pipe are presented in Figures 4.5.1.1 to 4.5.1.2, using the Ansari correlation and No Slip correlations, and for the outer annulus drill pipe presented in Figures 4.5.2.1 to 4.5.2.2, using the Orkiszewski correlation and No Slip correlations. As PIPESIM can only perform nodal analysis for a single point, Figure 4.5.1.2 was created through a series of individual simulations, as previously explained.

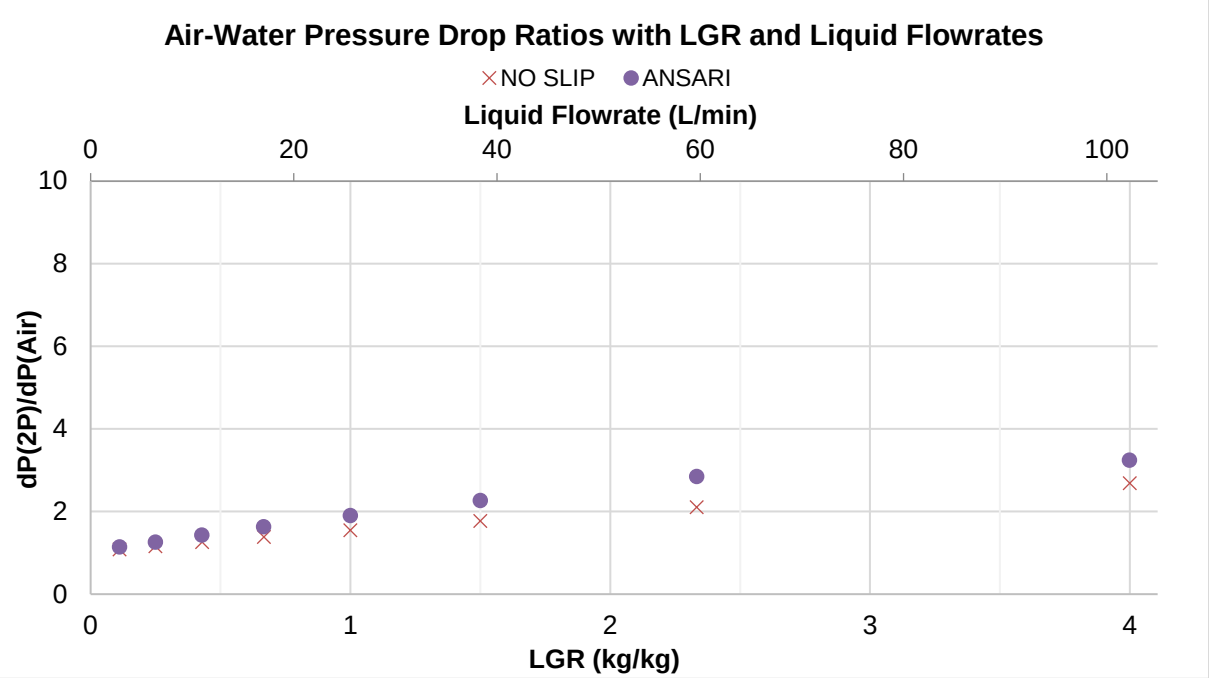

Figure 4.5.1.1: Two-phase air-water, inner pipe operating regime chart.

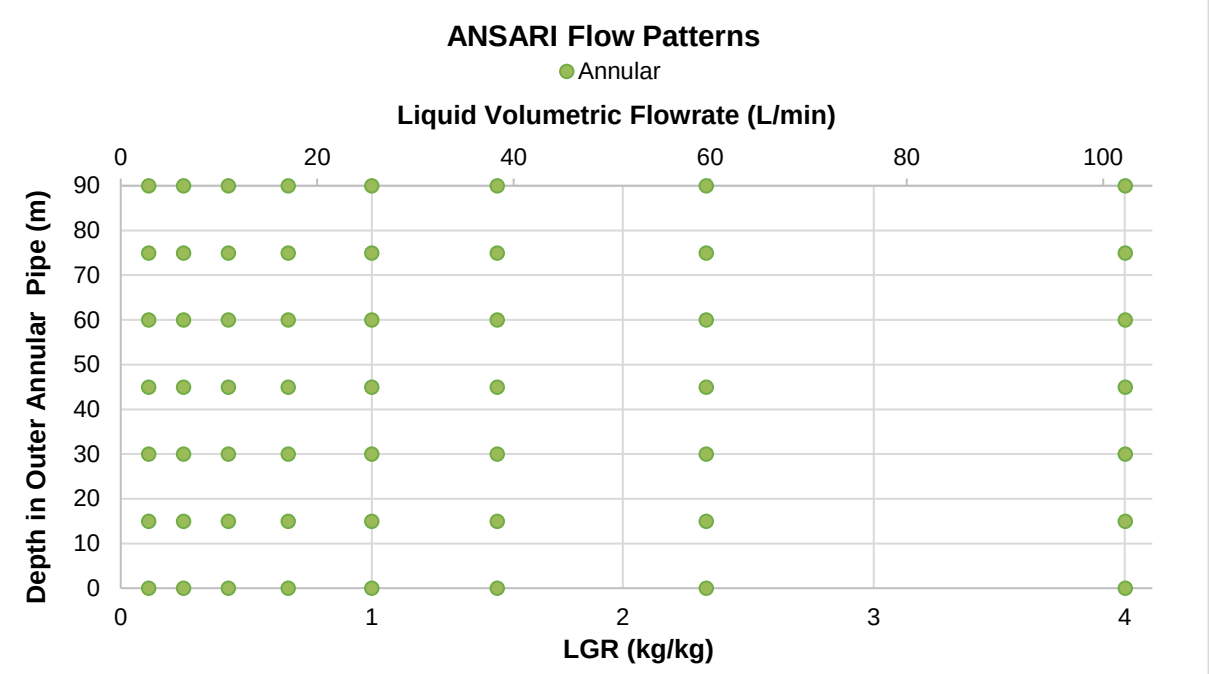

Figure 4.5.1.2: Two-phase air-water, inner pipe operating regime chart associated flow patterns.

The Ansari and No Slip correlations were once again utilised for the operating regime sensitivity studies with variation in the LGR to compare the results between homogeneous and non-homogeneous flow assumptions. The overall pressure drop ratios for two-phase air-water

flow in Figure 4.5.1.1, show for the Ansari correlation at a LGR of 0.11, a pressure drop ratio of 2.84 is observed, while at a LGR of 4, there is a pressure drop ratio of 3.24. For the No Slip correlation at a LGR of 0.11, a pressure drop ratio of 1.08 is observed and at a LGR of 4, there was pressure drop ratio of 2.68. It can be observed that the pressure drop ratios for the varying LGR are greater in the Ansari correlation compared to the No Slip correlation, which can be attributed to increased frictional pressure losses calculated in the heterogeneous Ansari correlation, as previously discussed. As the pressure drop ratio results for varying LGRs are greater than 1, indicating that the two-phase air-water pressure drop is greater than the single-phase air pressure drop of 3.93 bar(a), the Ansari correlation for the simulation of a RC drilling inner pipe can be considered valid, as results are as expected by literature heuristics. The mass flowrates of gas and liquid phases were specified under the fluid manager composition for the given LGR study. The friction factor correlation was specified by the IPR model as specified previously for two-phase air-water flow. This two-phase air-water flow was also assumed to be non-isothermal in all sensitivity studies, with temperature changes from 300 K for a LGR of 0.11 to 325.9 K and for a LGR of 4 to 329.8 using the Ansari and No Slip correlations, which appears to vary linearly with LGR.

The associated flow patterns for the varying LGR can be seen in Figure 4.5.1.2, which for two-phase air-water flow in a 90 m wellbore, at LGRs from 0.11 to 4 from 0 m to 90 m the flow patterns were a*nnular*. For the 90 m vertical wellbore through the inner drill pipe, the Ansari correlation predicts a liquid holdup of 0.18% at a LGR of 0.11 kg/kg, 0.28% at 0.25 kg/kg, 0.36% at 0.43 kg/kg, 0.44% at 0.67 kg/kg, 0.68% at 1 kg/kg, 0.89% at 1.5 kg/kg, 1.15% at 2.33 kg/kg and 1.76% at 4 kg/kg, while the No Slip correlation predicts 0.01%, 0.04%, 0.06%, 0.10%, 0.15%, 0.23%, 0.36% and 0.64%, respectively. The relationship between LGR, liquid holdup and flow pattern has been identified, as for increasing LGR, the liquid holdup increased and the flow pattern becomes less stable, approaching *transition* and *slug* flow. This is due to the increasing liquid water mass flowrate with LGR, resulting in increased two-phase air-water pressure drop, including hydrostatic and frictional pressure drops (Figure 4.4.1.1), and the frequency of eddies and turbulent flow with distance through the inner drill pipe. Therefore, it can be observed from Figures 4.5.1.1 and 4.5.1.2, that for all LGR values the flow pattern is *annular* and acceptable for RC drilling operations. However, for only the LGRs below 1 with a liquid water volumetric flowrate less than 25.6 L/min, the pressure drop in the inner drill pipe is considered viable at less than twice the pressure drop of single-phase air flow. Above a LGR value of 1 with a liquid water volumetric flowrate of 25.6 L/min, the cost of fuel for operating pumping equipment will be significantly increased and not economical for operation.

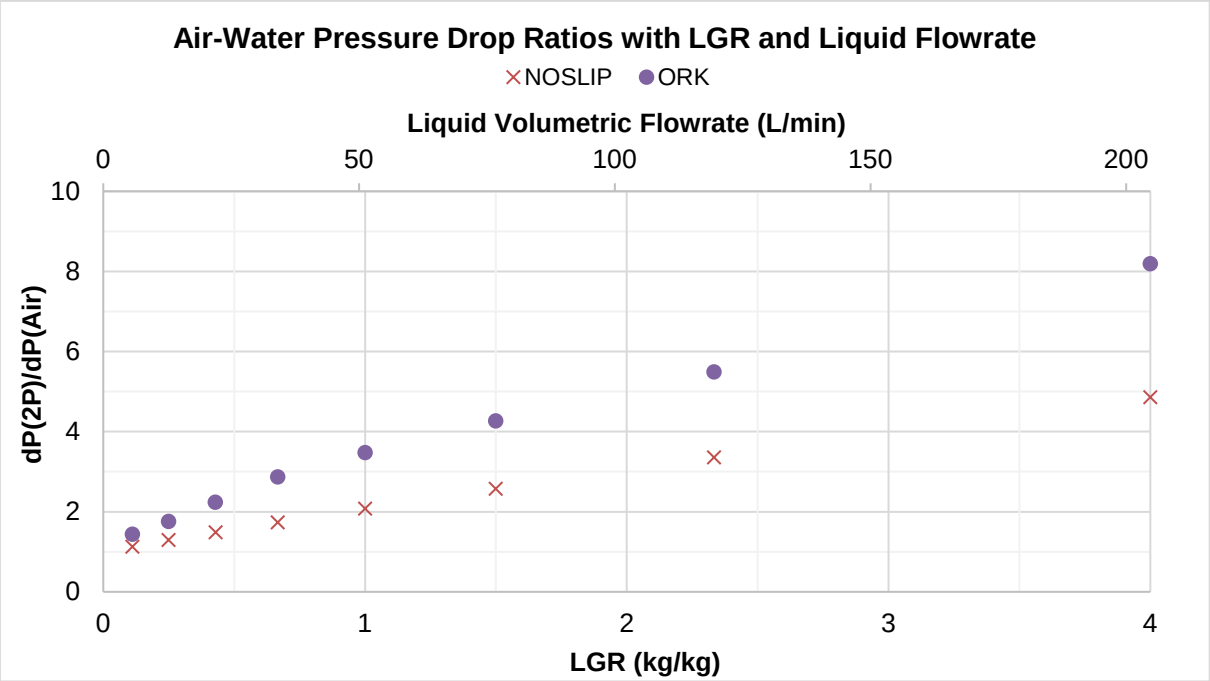

Figure 4.5.1.3: Two-phase air-water, outer annulus pipe operating regime chart.

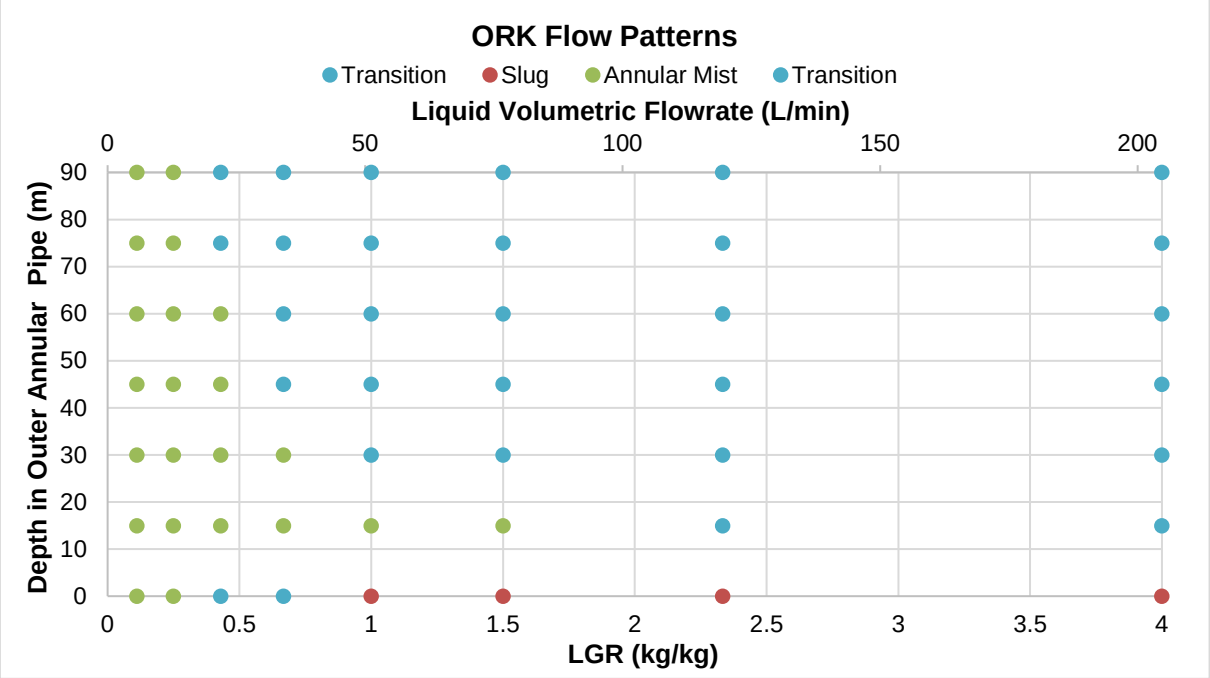

Figure 4.5.1.4: Two-phase air-water, outer annulus pipe operating regime chart associated flow patterns.

The Orkiszewski and No Slip correlations were once again utilised for the operating regime sensitivity studies with variation in the LGR to compare homogeneous and heterogenous flow assumption results. The overall pressure drop ratios for two-phase air-water flow in Figure

4.5.1.4, show for the Orkiszewski correlation at a LGR of 0.11 kg/kg, a pressure drop ratio of 1.44 is observed, while at a LGR of 4 kg/kg, there is a pressure drop ratio of 8.14. For the No Slip correlation at a LGR of 0.11 kg/kg, a pressure drop ratio of 1.13 is observed and at a LGR of 4 kg/kg, there was pressure drop ratio of 4.86. It can be observed that the pressure drop ratios for the varying LGR are greater in the Orkiszewski correlation compared to the No Slip correlation, as expected and previously discussed. As the pressure drop ratio results for varying LGRs are greater than 1, indicating that the two-phase air-water pressure drop in the outer annulus pope is greater than the single-phase air pressure drop of 2.60 bar(a) in the outer annulus pipe, the Orkiszewski correlation for the simulation of a RC drilling outer pipe can be considered valid, as results are as expected by literature heuristics. The mass flowrates of gas and liquid phases were specified under the fluid manager composition for the given LGR study, similar to the inner pipe LGR studies. The friction factor correlation was specified by the IPR model as specified previously for two-phase air-water flow. This two-phase air-water flow was assumed to be non-isothermal in all sensitivity studies, with temperature changes from 300 K for a LGR of 0.11 kg/kg to 325.4 K and for a LGR of 4 kg/kg to 329.8 using the Orkiszewski correlation, and from 300 K for a LGR of 0.11 kg/kg to 325.9 K and for a LGR of 4 kg/kg to 329.8 using the No Slip correlation, which both appear to vary linearly with LGR.

The associated flow patterns for the varying LGR can be seen in Figure 4.5.1.4, which for two-phase air-water flow in a 90 m wellbore, at LGRs from 0.11 kg/kg to 0.25 kg/kg from 0 m to 90 m, the flow patterns were *annular mist*. For LGRs from 0.43 kg/kg to 1.5 kg/kg the presence of *annular mist* flow decreases with the increasing s*lug* and *transition* flow, to which at LGRs of 2.33 kg/kg and 4 kg/kg, the flow changes between *slug* to *transition* flow only. For the 90 m vertical wellbore through the outer annulus drill pipe, the Orkiszewski correlation predicts a liquid holdup of 0.12% at a LGR of 0.11 kg/kg, 0.30% at 0.25 kg/kg, 1.44% at 0.43 kg/kg, 2.50% at 0.67 kg/kg, 3.20% at 1 kg/kg, 3.03% at 1.5 kg/kg, 1.80% at 2.33 kg/kg and 1.36% at 4 kg/kg, while the No Slip correlation predicts 0.12%, 0.30%, 0.56%, 0.95%, 1.55%, 2.59%, 4.59% and 9.34%, respectively. The relationship between LGR, liquid holdup and flow pattern has been identified, as for increasing LGR, the liquid holdup generally increased and the flow pattern becomes less stable, approaching *transition* and *slug* flow. This is due to the increasing liquid water mass flowrate with LGR, resulting in increased two-phase air-water pressure drop and the frequency of eddies and turbulent flow with distance through the inner drill pipe, as previously explained. However, for *transition* flow patterns the liquid holdup values appear relatively random due to the high level of turbulence and no constant flow pattern maintained. Therefore, as shown Figures 4.5.1.3 and 4.5.1.4, for LGR values including and below 0.25 kg/kg with a liquid water flowrate of 12.8 L/min, the flow pattern is *annular mist* with a pressure

drop in the outer drill pipe less than twice the pressure drop of single-phase air flow and hence, can be considered as acceptable for RC drilling operations. However, for the LGRs above 0.25 kg/kg with a liquid water volumetric flowrate greater than 12.8 L/min, the increasingly unstable flow patterns would result in increased pressure drop and fluid loss through the wellbore, increasing fuel costs for operating pumping equipment significantly and decreasing the economic viability of operations.

4.5.2. RC Air Drilling Operating Regime Charts Evaluation

The method for selecting the PIPESIM vertical, multiphase flow correlations for the sensitivity studies of the inner and outer annulus drill pipes were qualitative, as previously discussed for the two-phase air-water inner and outer drill pipe flow and varying total mass flowrate sensitivity studies. Therefore, correlation selection to obtain results of maximum accuracy would require extended knowledge on vertical, multiphase flow correlations and their quantitative boundary conditions. Based on these potential improvements identified, further study into determining quantitative boundaries of the inner and outer annulus drill pipes PIPESIM correlations, including the Ansari correlation and the Orkiszewski correlation, to validate the selection and utilisation for the two-phase air-water flow studies and ensure feasible data values. The key learnings obtained from this aspect of research project are to ensure to simulate multiphase vertical flow in a complete RC drilling rig. These learnings include use of basic PIPESIM software functions for two-phase flow, familiarity with the Ansari and Orkiszewski correlations for vertical, multiphase flow, and general understanding of expected pressure drop, liquid holdup and flow patterns for multiphase flow in the inner and outer annulus drill pipe flow with varying LGR. The PIPESIM simulation results obtained can be considered valid for continued utilisation, as the previous single phase compressible air, single phase water and two-phase air-water flow simulation data have been extensively validated and all two-phase air-water flow sensitivity study simulation data follows the expected heuristics.

5. CONCLUSIONS

Based on the overall project objectives: (1) to develop a software simulation for two-phase, compressible, steady state flow in vertical RC drilling to study the influence of hydrostatic pressure and major head losses on the overall drill string pressure drop, (2) to investigate the influence of RC drilling variables, including drilling depth, total mass flowrate and LGR, on pressure drop, liquid holdup and flow pattern through sensitivity studies, and (3) validate simulation results by comparison of analytical model data, all research objectives have been achieved. For objective 1, single-phase air and water vertical flow simulations using PIPESIM and ANSYS Fluent, and two-phase air-water vertical flow using PIPESIM in the inner and outer annulus drill pipes were developed and validated. For objective 2, several sensitivity studies for two-phase air-water flow with varying total flowrate and LGR values to obtain industry applicable operating regime charts for the inner and outer annulus drill pipe of a 90 m wellbore were conducted and feasible result obtained. For objective 3, the single-phase air and water flow in the inner and outer drill pipes and two-phase air-water flow simulations in the inner drill rod were validated against the DMG analytical model and DMG Simulink model, in which the two-phase air-water flow in the outer annulus pipe and two-phase air-water sensitivity studies were validated informally with literature heuristic values.

From this research project, the key learnings include:

- The validation of pressure drop and velocity profiles for single-phase air and water flow, in the inner and outer RC drill pipes, with the no-slip models, for up to 90 m drill depth.
- Cross-validation of ANSYS and PIEPSIM two-phase heterogenous flow models for air-water, for up to 90 m drill depth.
- For the specific models available and variable conditions, the Ansari and Orkiszewski correlations were considered to be highly applicable for the simulation of the inner and outer annulus drill pipes in RC drilling scenarios, with between 36.3% and 65.3% increase in pressure drop, compared to the No Slip models.
- The Gomez [Neotec], Gomez Enhanced [Neotec], Mukherjee & Brill [Baker Jardine], Mukherjee & Brill [Tulsa (Legacy 1989)], Aziz Govier Fogarasi [Neotec], Govier, Aziz & Fogarasi [Baker Jardine], Govier, Aziz [Tulsa (Legacy 1989)], Duns & Ros [Baker Jardine], Buns & Ros [Tulsa (Legacy 1989)], Hagedorn & Brown (Original) [Tulsa (Legacy 1989)], Hagedorn & Brown (Revised) [Baker Jardine], Hagedorn & Brown (Revised) with Duns & Ros map [Baker Jardine], Hagedorn & Brown (Revised) [Tulsa

(Legacy 1989)], TUFFP (v. 2011 2-Phase) [TUFFP Unified], Beggs & Brill Original [Baker Jardine], Beggs & Brill Revised [Baker Jardine] and Beggs & Brill Revised [Tulsa (Legacy 1989)] correlations were excluded from the simulation of the vertical drill pipes for multiphase compressible flow due to reduced applicability.

- The flow pattern for two-phase air-water flow in the inner drill pipe, at LGRs from 0.11 to 4 from 0 m to 90 m was *annular*. While the flow pattern for two-phase air-water flow in the outer annulus drill pipe, at LGRs from 0.11 kg/kg to 0.25 kg/kg from 0 m to 90 m was *annular mist*, at LGRs from 0.43 kg/kg to 1.5 kg/kg the presence of *annular mist* flow decreases with the increasing *Slug* and *Transition* flow, to which at LGRs of 2.33 kg/kg and 4 kg/kg, the flow changes between *Slug* and *Transition* flow only.
- Development of operating regime charts to establish the operational boundaries for minimising pressure drop and optimising flow pattern (i.e.: decreasing liquid holdup) with varying liquid water flowrate, expected to supersede the use of general heuristics which are currently used by RC drilling operators.

6. RECOMMENDATIONS

The future research studies conducted in line with this research project may be more accurate by spending time investigating all the capabilities of the PIPESIM and ANSYS Fluent software through self-study, guidance from experienced PIPESIM and/or ANSYS Fluent simulation researchers and structured online workshop tutorials. The key simulation understanding will allow for a more efficient research methodology, and future research studies and associated tasks, including which of the software will be utilised for a given task. Based on thorough investigation of the PIPESIM software, the possibility of modelling a complete drill string including loss of two-phase air-water to the wellbore and drill bit opening should be considered, due to PIPESIM's user friendly interface and increased time efficiency compared to ANSYS Fluent. The applications that have arisen based on the results analysis and validation, including using the simulations developed for single-phase air and water flow, and two-phase air-water flow in the inner and outer annulus drill pipes as the foundation for validation of related research studies for the expected pressure drops, temperatures, liquid holdup, and flow patterns. These results are also to be used for the foundation for simulating a complete drilling string geometry, with three-phase air-water-cuttings flow in the inner rod.

REFERENCES

Adaze, Ernest, H. M. Badr, and A. Al-Sarkhi. 2019. "CFD modeling of two-phase annular flow toward the onset of liquid film reversal in a vertical pipe." *Journal of Petroleum Science and Engineering* 175: 755-774. https://doi.org/https://doi.org/10.1016/j.petrol.2019.01.026. https://www.sciencedirect.com/science/article/pii/S0920410519300361.

ANSYS, Inc. 2021. "Ansys Fluent Fluid Simulation Software." https://www.ansys.com/products/fluids/ansys-fluent.

Aslani, Mohamad, and Jonathan D. Regele. 2018. "A localized artificial diffusivity method to simulate compressible multiphase flows using the stiffened gas equation of state." *International Journal for Numerical Methods in Fluids* 88 (9): 413-433. https://doi.org/https://doi.org/10.1002/fld.4668. https://onlinelibrary.wiley.com/doi/abs/10.1002/fld.4668.

Awad, M. M., and Y. S. Muzychka. 2008. "Effective property models for homogeneous two-phase flows." *Experimental Thermal and Fluid Science* 33 (1): 106-113. https://doi.org/https://doi.org/10.1016/j.expthermflusci.2008.07.006. https://www.sciencedirect.com/science/article/pii/S0894177708001027.

Beggs, D.H., and J.P. Brill. 1973. "A Study of Two-Phase Flow in Inclined Pipes." *Journal of Petroleum Technology* 25 (05): 607-617. https://doi.org/10.2118/4007-pa. https://doi.org/10.2118/4007-PA.

Ben Mahmud, Hisham. 2012. "Multiphase Transient Flow in Pipes." Thesis (PhD)--Curtin University., Curtin University, Department of Chemical Engineering.

Bustillo Revuelta, Manuel author. 2018. *Mineral Resources : From Exploration to Sustainability Assessment / by Manuel Bustillo Revuelta*. 1st ed. 2018.. ed.: Cham : Springer International Publishing : Imprint: Springer.

Caenn, Ryen, H. C. H. Darley, and George R. Gray. 2017. "1. Introduction to Drilling Fluids." In *Composition and Properties of Drilling and Completion Fluids (7th Edition)*. Elsevier.

Cao, Pinlu, Hongyu Cao, Jine Cao, Miaomiao Liu, and Baoyi Chen. 2019. "Studies on pneumatic transport of ice cores in reverse circulation air drilling." *Powder Technology* 356: 50-59. https://doi.org/https://doi.org/10.1016/j.powtec.2019.08.001. https://www.sciencedirect.com/science/article/pii/S003259101930600X.

Cao, Pinlu, Miaomiao Liu, Zhuo Chen, Baoyi Chen, and Qi Zhao. 2018. "Theory calculation and testing of air injection parameters in ice core drilling with air reverse circulation." *Polar Science* 17: 23-32. https://doi.org/https://doi.org/10.1016/j.polar.2018.06.005. https://www.sciencedirect.com/science/article/pii/S1873965218300197.

Crane. 2009. *Flow of Fluid Through Valves, Fittings, and Pipe*. Stamford, Connecticut: Crane Company.

Dando Drilling International. 2016. Reverse Circulation Drilling. Dando Drilling International.

DET CRC. 2014. "May 2014: Breakthrough Technology Will Cut Mineral exploration Drilling Costs By 85%." https://detcrc.com.au/2014/breakthrough-technology-will-cut-mineral-exploration-drilling-costs-by-85/.

Dong, Shun, Cong Zeng, Samuel T. Ariaratnam, Baosong Ma, Xuefeng Yan, Zhijie Li, and Xinjie Li. 2020. "Experimental and performance analysis of reverse circulation reaming in horizontal directional drilling." *Tunnelling and Underground Space Technology* 95: 103128. https://doi.org/https://doi.org/10.1016/j.tust.2019.103128. https://www.sciencedirect.com/science/article/pii/S0886779819304419.

Duns, H., Jr., and N.C.J. Ros. 1963. "Vertical flow of gas and liquid mixtures in wells." 6th World Petroleum Congress.

Eissa, M. Al-Safran, and P. Brill James. 2017. *Applied Multiphase Flow in Pipes and Flow Assurance : Oil and Gas Production*. Richardson, UNITED STATES: SPE.

Ellul, Ivor R., Geir Saether, and Mack E. Shippen. 2004. "The Modeling of Multiphase Systems Under Steady-State And Transient Conditions - A Tutorial." PSIG Annual Meeting.

Fetoui, I. 2017. "Multiphase Flow Correlations." *Production Technology*.

Ganat, Tarek A., Meftah Hrairi, Belladonna Maulianda, and Eghbal Motaei. 2019. "Analytical model for predicting frictional pressure drop in upward vertical two-phase flowing wells." *Heat and Mass Transfer* 55 (8): 2137-2151. https://doi.org/10.1007/s00231-019-02565-6. https://doi.org/10.1007/s00231-019-02565-6.

Ghorai, Subhashini, and K. D. P. Nigam. 2006. "CFD modeling of flow profiles and interfacial phenomena in two-phase flow in pipes." *Chemical Engineering and Processing: Process Intensification* 45 (1): 55-65. https://doi.org/https://doi.org/10.1016/j.cep.2005.05.006. https://www.sciencedirect.com/science/article/pii/S0255270105001145.

Hagedorn, Alton R., and Kermit E. Brown. 1965. "Experimental Study of Pressure Gradients Occurring During Continuous Two-Phase Flow in Small-Diameter Vertical Conduits." *Journal of Petroleum Technology* 17 (04): 475-484. https://doi.org/10.2118/940-pa. https://doi.org/10.2118/940-PA.

Han, Xiaoming, Peibo Li, and Jialiang Li. 2020. "CFD-DEM Simulation of Reverse Circulation Pneumatic Cuttings Removal during Coal Seam Drilling." *Mathematical Problems in Engineering* 2020. https://doi.org/http://dx.doi.org/10.1155/2020/3707864.

Han, Xiaoming, Songnan Song, and Jialiang Li. 2020. "Pressure drop characteristics of reverse circulation pneumatic cuttings removal during coal seam drilling." *Science Progress* 103 (2): 0036850420925235. https://doi.org/10.1177/0036850420925235. https://doi.org/10.1177/0036850420925235.

Houim, Ryan W., and Elaine S. Oran. 2016. "A multiphase model for compressible granular-gaseous flows: formulation and initial tests." *Journal of Fluid Mechanics* 789: 166-220. https://doi.org/http://dx.doi.org/10.1017/jfm.2015.728.

Krishna, Shwetank, Syahrir Ridha, Pandian Vasant, Suhaib Umer Ilyas, Sonny Irawan, and Raoof Gholami. 2020. "Explicit flow velocity modelling of yield power-law fluid in concentric annulus to predict surge and swab pressure gradient for petroleum drilling applications." *Journal of Petroleum Science and Engineering* 195: 107743. https://doi.org/https://doi.org/10.1016/j.petrol.2020.107743. https://www.sciencedirect.com/science/article/pii/S0920410520308068.

Le Métayer, O., J. Massoni, and R. Saurel. 2005. "Modelling evaporation fronts with reactive Riemann solvers." *Journal of computational physics* 205 (2): 567-610. https://doi.org/10.1016/j.jcp.2004.11.021.

López, Jorge, Hugo Pineda, David Bello, and Nicolás Ratkovich. 2016. "Study of liquid–gas two-phase flow in horizontal pipes using high speed filming and computational fluid dynamics." *Experimental Thermal and Fluid Science* 76: 126-134. https://doi.org/https://doi.org/10.1016/j.expthermflusci.2016.02.013. https://www.sciencedirect.com/science/article/pii/S0894177716300371.

Lyons, William C., Boyun Guo, Reuben L. Graham, and Greg D. Hawley. 2009. "Chapter 7 - Reverse Circulation Models." In *Air and Gas Drilling Manual (Third Edition)*, edited by William C. Lyons, Boyun Guo, Reuben L. Graham and Greg D. Hawley, 165-182. Burlington: Gulf Professional Publishing.

Marjoribanks, Roger. 2010. "Prospecting and the Exploration Process." In *Geological Methods in Mineral Exploration and Mining*, 1-12. Berlin, Heidelberg: Springer Berlin Heidelberg.

Moshfeghian, Mahmood 2008. "Two Phase Gas-Liquid Pipeline Simulation." Campbell, John M. . Last Modified 01/06/2008. http://www.jmcampbell.com/tip-of-the-month/2008/06/two-phase-gas-liquid-pipeline-simulation/#:~:text=Two%20Phase%20Gas-

Liquid%20Pipeline%20Simulation%20As%20gas%20moves,Joule-Thompson%20effect%2C%20and%20heat%20transfer%20from%20the%20surroundings.

Nguyen, Van-Tu, Thanh-Hoang Phan, Trong-Nguyen Duy, and Warn-Gyu Park. 2021. "Numerical modeling for compressible two-phase flows and application to near-field underwater explosions." *Computers & Fluids* 215: 104805. https://doi.org/https://doi.org/10.1016/j.compfluid.2020.104805. https://www.sciencedirect.com/science/article/pii/S0045793020303753.

Nguyen, Van-Tu, Thanh-Hoang Phan, and Warn-Gyu Park. 2021. "Numerical modeling of multiphase compressible flows with the presence of shock waves using an interface-sharpening five-equation model." *International Journal of Multiphase Flow* 135: 103542. https://doi.org/https://doi.org/10.1016/j.ijmultiphaseflow.2020.103542. https://www.sciencedirect.com/science/article/pii/S0301932220306534.

Pedrosa, Camilo, Arild Saasen, and Jan David Ytrehus. 2021. "Fundamentals and Physical Principles for Drilled Cuttings Transport—Cuttings Bed Sedimentation and Erosion." *Energies* 14 (3): 545. https://www.mdpi.com/1996-1073/14/3/545.

Ping, Li-qiu, Zhi-ming Wang, and Jian-guang Wei. 2006. "Pressure drop models for gas-liquid two-phase flow and its application in underbalanced drilling* *Supported by program for Changjiang Scholars and Innovative Research Team in University (IRT0411)." *Journal of Hydrodynamics, Ser. B* 18 (3, Supplement): 405-411. https://doi.org/https://doi.org/10.1016/S1001-6058(06)60086-3. https://www.sciencedirect.com/science/article/pii/S1001605806600863.

Quyn, D. 2020. *Modelling Pressure Drop in Reverse Circulation Air Drilling.* MinEx CRC.

Ros, N.C.J. 1961. "Simultaneous Flow of Gas and Liquid As Encountered in Well Tubing." *Journal of Petroleum Technology* 13 (10): 1037-1049. https://doi.org/10.2118/18-pa. https://doi.org/10.2118/18-PA.

Schlumberger. 2020. *PIPESIM 2019.*

Sookprasong, Prasart, James Brill, and Z. Schmidt. 1986. "Two-Phase Flow in Piping Components." *J. Energy Resour. Technol.* 108. https://doi.org/10.1115/1.3231264.

Taitel, Yehuda, Dvora Bornea, and A. E. Dukler. 1980. "Modelling flow pattern transitions for steady upward gas-liquid flow in vertical tubes." *AIChE journal* 26 (3): 345-354. https://doi.org/10.1002/aic.690260304.

Wang, Hao, Enyuan Wang, Zhonghui Li, Rongxi Shen, Xiaofei Liu, Qiming Zhang, and Bing Li. 2020. "Study and application of dynamic inversion model of coal seam gas pressure with drilling." *Fuel* 280: 118653. https://doi.org/https://doi.org/10.1016/j.fuel.2020.118653. https://www.sciencedirect.com/science/article/pii/S0016236120316495.

Xiao-ming, Han, Luo Chen-xu, Li Jia-liang, and Wang Han. 2017. "Drilling Cuttings Migration Characteristics during Gas Extraction Borehole in Soft Coal Seam." *Electronic Journal of Geotechnical Engineering* 22 (8): 3049.

Xiumin, Ma, Chen Yue, and Qi Luheng. 2014. "Research and Application of Gas-lift Reverse Circulation Drilling Technology to Geothermal Well Construction in Dalian Jiaoliu Island." *Procedia Engineering* 73: 252-257. https://doi.org/https://doi.org/10.1016/j.proeng.2014.06.195. https://www.sciencedirect.com/science/article/pii/S1877705814007115.

Zhang, Hongtu, Botao Li, Jian Zhang, and Jianping Wei. 2021. "Pressure drop characteristic of dilute negative pressure pneumatic conveying." *Particulate Science and Technology* 39 (1): 101-107. https://doi.org/10.1080/02726351.2019.1666949. https://doi.org/10.1080/02726351.2019.1666949.

Zhu, L. H., Y. Huang, R. H. Wang, and J. Y. Wang. 2015. "A mathematical model of the motion of cutting particles in reverse circulation air drilling." *Applied Mathematics and Computation* 256: 192-202. https://doi.org/https://doi.org/10.1016/j.amc.2014.12.153. https://www.sciencedirect.com/science/article/pii/S009630031500017X.

APPENDIX A – RESEARCH PROJECT GANTT CHART

Gantt Chart - Industry Research Project

Teaching Week	0	1	2	3	4	5		6	7	8	9	10
Starting Date	28-February-2021	01-March-2021	08-March-2021	15-March-2021	22-March-2021	29-March-2021	05-April-2021	12-April-2021	19-April-2021	26-April-2021	03-May-2021	10-May-2021
Semester 1, 2020												
Orientation Week												
Tutition Week												
Tutition-Free Week												
Study Week												
Exam Week												
Holidays												
ENGR4000: Industry Research Project 1												
• Conduct background reading on reverse circulation air drilling systems.	Reading											
• Conduct background reading on commercial software used to simulate drilling, in particular reverse circulation air	Reading											
• Conduct background reading on fluid mechanics principles.	Reading											
• Become familiar with how to use ANSYS Fluent and									Familarisation	Familarisation		
1. Project Proposal Report			Compiling & Writing		Editing	Due						
2. Literature Review Report: Perform a comprehensive literature review to critically interpret current reverse circulation air drilling software used.			Compiling	Compiling		Compiling & Writing			Editing	Due		
• Establish a clear research methodology.											Compiling & Writing	
• Establish and validate preliminary single-phase (i.e.: air, water) flow simulations for inner drill pipe and outer annular											Modelling	
• Establish and validate two-phase, air-water flow simulations for inner drill pipe in RC air drilling using PIPESIM.												M
• Conduct sensitivity studies to investigate the influence of drilling depth and LGR in two-phase flow on the pressure drop and velocity profile of the inner drilling pipe using PIPESIM.												Dat
3. Project Progress Report									Notes	Notes		Comp
ENGR4001: Industry Research Project 2												
1. Reflections Logbook												
• Establish and validate two-phase, air-water flow simulation for inner drill pipe in RC air drilling using ANSYS Fluent.												
• Investigate the capabilities of PIPESIM and ANSYS Fluent for three-phase, air-water-cutting flow simulation for the inner drill pipe in RC air drilling.												
• Investigate the capabilities of PIPESIM and ANSYS Fluent for two-phase, air-water flow simulation for the outer annular drill pipe in RC air drilling.												
• Establish and validate three-phase, air-water-cutting flow simulations for inner drill pipe in RC air drilling using PIPESIM and ANSYS Fluent.												
• Establish and validate two-phase, air-water flow simulations for outer drill pipe in RC air drilling using PIPESIM and ANSYS Fluent.												
• Establish and validate two-phase and three-phase flow simulations for a complete drill string in RC air drilling.												
• Study the influence of major and minor pressure losses on the overall drill string pressure drop.												
• Conduct sensitivity studies (SS) on the overall drill string pressure drop, and explore performance-based RC drilling variables (e.g.: carrying capacity).												
2. Final Project Report												
3. Oral Presentation												
Other Semester 1 Units:												
CHEN4001: Process Safety and Risk Management												
1. Mid Semester Test												
2. Case Study Project and Presentation												
3. Final Examination												
CHEN4012: Advanced Separation Processes												
1. Module 1 Test												
2. Module 2 Test												
3. Case Study Project												
CHEN4017: Bioprocess Engineering												
1. Mid Semester Test												
2. Group Project												
3. Final Examination												
Other Semester 2 Units:												
CHEN4015: Chemical Engineering Design Project												
1. Memos												
2. Group Presentation												
3. Final Design Project Report												
CHEN4010: Advanced Thermodynamics and Reaction Engineering												
1. Test 1												
2. Group Project												
3. Test 2												

Gantt Chart - Industry Research Project

Teaching Week		11	12	13	14	15						
Starting Date		17-May-2021	24-May-2021	31-May-2021	07-June-2021	14-June-2021	21-June-2021	28-June-2021	05-July-2021	12-July-2021	19-July-2021	26-July-2021
Semester 1, 2020												
Orientation Week												
Tutition Week												
Tutition-Free Week												
Study Week												
Exam Week												
Holidays												
ENGR4000: Industry Research Project 1												
• Conduct background reading on reverse circulation air drilling systems.												
• Conduct background reading on commercial software used to simulate drilling, in particular reverse circulation air												
• Conduct background reading on fluid mechanics principles.												
• Become familiar with how to use ANSYS Fluent and												
1. Project Proposal Report												
2. Literature Review Report: Perform a comprehensive literature review to critically interpret current reverse circulation air drilling software used.												
• Establish a clear research methodology.	Writing											
• Establish and validate preliminary single-phase (i.e.: air, water) flow simulations for inner drill pipe and outer annular		Finalise										
• Establish and validate two-phase, air-water flow simulations for inner drill pipe in RC air drilling using PIPESIM.	Modelling											
• Conduct sensitivity studies to investigate the influence of drilling depth and LGR in two-phase flow on the pressure drop and velocity profile of the inner drilling pipe using PIPESIM.	a Collection											
3. Project Progress Report	iling & Writing		Editing	Due								
ENGR4001: Industry Research Project 2												
1. Reflections Logbook												Writing
• Establish and validate two-phase, air-water flow simulation for inner drill pipe in RC air drilling using ANSYS Fluent.							Modelling	Data Collection	Extended Period: If all two-phase flow in inner pipe simulation data is not obtained.			
• Investigate the capabilities of PIPESIM and ANSYS Fluent for three-phase, air-water-cutting flow simulation for the inner drill pipe in RC air drilling.									Research and Preliminary Modellling	Extended Period: If a conclusion on three-phase flow simulation is not obtained.		
• Investigate the capabilities of PIPESIM and ANSYS Fluent for two-phase, air-water flow simulation for the outer annular drill pipe in RC air drilling.									Research and Preliminary Modellling	Extended Period: If a conclusion on annular flow simulation is not obtained.		
• Establish and validate three-phase, air-water-cutting flow simulations for inner drill pipe in RC air drilling using PIPESIM and ANSYS Fluent.										Extended Period: Modelling of three-phase flow in inner drill pipe may be modelled after reserch and preliminary modelling.	Modelling	Data Collection	Extended Period: If all three-phase flow in inner pipe simulation data is not obtained.
• Establish and validate two-phase, air-water flow simulations for outer drill pipe in RC air drilling using PIPESIM and ANSYS Fluent.												
• Establish and validate two-phase and three-phase flow simulations for a complete drill string in RC air drilling.												
• Study the influence of major and minor pressure losses on the overall drill string pressure drop.												
• Conduct sensitivity studies (SS) on the overall drill string pressure drop, and explore performance-based RC drilling variables (e.g.: carrying capacity).												
2. Final Project Report												
3. Oral Presentation												
Other Semester 1 Units:												
CHEN4001: Process Safety and Risk Management												
1. Mid Semester Test												
2. Case Study Project and Presentation												
3. Final Examination												
CHEN4012: Advanced Separation Processes												
1. Module 1 Test												
2. Module 2 Test												
3. Case Study Project												
CHEN4017: Bioprocess Engineering												
1. Mid Semester Test												
2. Group Project												
3. Final Examination												
Other Semester 2 Units:												
CHEN4015: Chemical Engineering Design Project												
1. Memos												
2. Group Presentation												
3. Final Design Project Report												
CHEN4010: Advanced Thermodynamics and Reaction Engine												
1. Test 1												
2. Group Project												
3. Test 2												

Gantt Chart - Industry Research Project

Teaching Week		1	2	3	4	5	6	7	8	9	10	11
Starting Date		02-August-2021	09-August-2021	16-August-2021	23-August-2021	30-August-2021	06-September-2021	13-September-2021	20-September-2021	27-September-2021	04-October-2021	11-October-2021
Semester 1, 2020												
Orientation Week												
Tutition Week												
Tutition-Free Week												
Study Week												
Exam Week												
Holidays												
ENGR4000: Industry Research Project 1												
• Conduct background reading on reverse circulation air drilling systems.												
• Conduct background reading on commercial software used to simulate drilling, in particular reverse circulation air												
• Conduct background reading on fluid mechanics principles.												
• Become familiar with how to use ANSYS Fluent and												
1. Project Proposal Report												
2. Literature Review Report: Perform a comprehensive literature review to critically interpret current reverse circulation air drilling software used.												
• Establish a clear research methodology.												
• Establish and validate preliminary single-phase (i.e.: air, water) flow simulations for inner drill pipe and outer annular												
• Establish and validate two-phase, air-water flow simulations for inner drill pipe in RC air drilling using PIPESIM.												
• Conduct sensitivity studies to investigate the influence of drilling depth and LGR in two-phase flow on the pressure drop and velocity profile of the inner drilling pipe using PIPESIM.												
3. Project Progress Report												
ENGR4001: Industry Research Project 2												
1. Reflections Logbook		Writing	Writing	Writing	Writing	Writing	Writing	Writing	Writing	Writing	Writing	Writing
• Establish and validate two-phase, air-water flow simulation for inner drill pipe in RC air drilling using ANSYS Fluent.												
• Investigate the capabilities of PIPESIM and ANSYS Fluent for three-phase, air-water-cutting flow simulation for the inner drill pipe in RC air drilling.												
• Investigate the capabilities of PIPESIM and ANSYS Fluent for two-phase, air-water flow simulation for the outer annular drill pipe in RC air drilling.												
• Establish and validate three-phase, air-water-cutting flow simulations for inner drill pipe in RC air drilling using PIPESIM and ANSYS Fluent.												
• Establish and validate two-phase, air-water flow simulations for outer drill pipe in RC air drilling using PIPESIM and ANSYS Fluent.		Modelling	Data Collection	Extended Period: If all two-phase annular flow simulation data is not obtained.								
• Establish and validate two-phase and three-phase flow simulations for a complete drill string in RC air drilling.				Modelling			Data Collection		Extended Period: If all two-phase annular flow and three-phase inner pipe flow with 50% mass loss simulation data is not obtained.			
• Study the influence of major and minor pressure losses on the overall drill string pressure drop.									Data Collection	Extended Period: If all pressure drop data for complete RC air drilling is not obtained.		
• Conduct sensitivity studies (SS) on the overall drill string pressure drop, and explore performance-based RC drilling variables (e.g.: carrying capacity).										Data Collection	Extended Period: If all SS and performance-base data is not obtained.	
2. Final Project Report												
3. Oral Presentation												
Other Semester 1 Units:												
CHEN4001: Process Safety and Risk Management												
1. Mid Semester Test												
2. Case Study Project and Presentation												
3. Final Examination												
CHEN4012: Advanced Separation Processes												
1. Module 1 Test												
2. Module 2 Test												
3. Case Study Project												
CHEN4017: Bioprocess Engineering												
1. Mid Semester Test												
2. Group Project												
3. Final Examination												
Other Semester 2 Units:												
CHEN4015: Chemical Engineering Design Project												
1. Memos												
2. Group Presentation												
3. Final Design Project Report												
CHEN4010: Advanced Thermodynamics and Reaction Engine												
1. Test 1												
2. Group Project												
3. Test 2												

Compilation & Writing

Gantt Chart - Industry Research Project

Teaching Week					
Starting Date		18-October-2021	25-October-2021	01-November-2021	08-November-2021
Semester 1, 2020					
Orientation Week					
Tutition Week					
Tutition-Free Week					
Study Week					
Exam Week					
Holidays					
ENGR4000: Industry Research Project 1					
• Conduct background reading on reverse circulation air drilling systems.					
• Conduct background reading on commercial software used to simulate drilling, in particular reverse circulation air					
• Conduct background reading on fluid mechanics principles.					
• Become familiar with how to use ANSYS Fluent and					
1. Project Proposal Report					
2. Literature Review Report: Perform a comprehensive literature review to critically interpret current reverse circulation air drilling software used.					
• Establish a clear research methodology.					
• Establish and validate preliminary single-phase (i.e.: air, water) flow simulations for inner drill pipe and outer annular					
• Establish and validate two-phase, air-water flow simulations for inner drill pipe in RC air drilling using PIPESIM.					
• Conduct sensitivity studies to investigate the influence of drilling depth and LGR in two-phase flow on the pressure drop and velocity profile of the inner drilling pipe using PIPESIM.					
3. Project Progress Report					
ENGR4001: Industry Research Project 2					
1. Reflections Logbook		Writing	Writing and Editing	Due	
• Establish and validate two-phase, air-water flow simulation for inner drill pipe in RC air drilling using ANSYS Fluent.					
• Investigate the capabilities of PIPESIM and ANSYS Fluent for three-phase, air-water-cutting flow simulation for the inner drill pipe in RC air drilling.					
• Investigate the capabilities of PIPESIM and ANSYS Fluent for two-phase, air-water flow simulation for the outer annular drill pipe in RC air drilling.					
• Establish and validate three-phase, air-water-cutting flow simulations for inner drill pipe in RC air drilling using PIPESIM and ANSYS Fluent.					
• Establish and validate two-phase, air-water flow simulations for outer drill pipe in RC air drilling using PIPESIM and ANSYS Fluent.					
• Establish and validate two-phase and three-phase flow simulations for a complete drill string in RC air drilling.					
• Study the influence of major and minor pressure losses on the overall drill string pressure drop.					
• Conduct sensitivity studies (SS) on the overall drill string pressure drop, and explore performance-based RC drilling variables (e.g.: carrying capacity).					
2. Final Project Report		Editing	Extended Period: If additional data, compilation, writing and/or editing is required.	Due	
3. Oral Presentation			Compilation & Writing	Extended Period: If further compilation, writing and/or editing is required, and for speech memorisation.	Due
Other Semester 1 Units:					
CHEN4001: Process Safety and Risk Management					
1. Mid Semester Test					
2. Case Study Project and Presentation					
3. Final Examination					
CHEN4012: Advanced Separation Processes					
1. Module 1 Test					
2. Module 2 Test					
3. Case Study Project					
CHEN4017: Bioprocess Engineering					
1. Mid Semester Test					
2. Group Project					
3. Final Examination					
Other Semester 2 Units:					
CHEN4015: Chemical Engineering Design Project					
1. Memos					
2. Group Presentation					
3. Final Design Project Report					
CHEN4010: Advanced Thermodynamics and Reaction Engine					
1. Test 1					
2. Group Project					
3. Test 2					

Research Data Management Plan

Software Simulation of Reverse Circulation Air Drilling

Supervisor	Dimple Quyn
Data Management Plan Edited by	Chloe Thiel
Modified Date	31/03/2021
Data Management Plan ID	QUYN0D-SE09167
Faculty	Science and Engineering

1 Research Project Details

1.1 Research project title

Software Simulation of Reverse Circulation Air Drilling

1.2 Research project summary

This research project aims to simulate two-phase gas-liquid (i.e.: air-water), compressible, steady state flow in vertical reverse circulation air drilling of minerals through software. This will allow the determination of wellbore flow pattern, liquid holdup, velocity profile and pressure drop. The ability to model three-phase gas-liquid-solid (i.e.: air-water-mineral cuttings) flow is to be explored based on the software capabilities, for improved simulation accuracy, and if applicable, the simulation is to be extended to include the third solid particle phase. The simulation will be used to study the influence of major pressure loss due to friction and minor pressure loss due to changes in pipe geometry and pipe restrictions on the pressure drop of a specified drilling pipe. The influence of other variables, including drilling depth on the velocity profile, liquid holdup and pressure drop is also to be thoroughly investigated through a series of extensive sensitivity studies. Exploration into other key performance related variables in reverse circulation drilling, including carrying capacity of drilling fluid, is to be conducted for a complete analysis of the drilling simulation. The software simulation will be validated using theoretical and/or experimental data from unpublished university research studies. This simulation of reverse circulation air drilling will satisfy the modelling requirements for use in industry optimisation.

1.3 Keywords

Reverse circulation drilling, mineral drilling, air drilling, software, multiphase flow

2 Research Project Data Details

2.1 Research project data summary

This project involves the following data generated using PipeSIm/ANSYS Fluent Software: 1. # two-phase flow software simulation files 2. # three-phase flow software simulation files. 3. # major and minor pressure loss software simulation analysis files. 4. # major and minor pressure loss analysis files exported to Microsoft Excel. 5. # pressure drop sensitivity studies/analysis software files. 6. # pressure drop sensitivity studies/analysis files exported to Microsoft Excel. 7. # performance related analysis software files and exported Microsoft Excel files. 8. # performance related analysis files exported Microsoft Excel.

2.2 Will the data be identifiable

- Not applicable — no human data used

2.3 Will biospecimens or human participant information be sent overseas?

No

2.4 Will novel information about controlled goods or technologies on the Defence and Strategic Goods List (DSGL) be sent overseas?

No

2.5 Data organisation and structure

Digital simulation files will be organised within a "Industry Research Project" folder, under "Simulations and Data Collection" containing the folders "Simulations" and "Data Collection."

The simulation software and Microsoft Excel files will be named according to version type (i.e.: draft, final), name, version number and date, for example:

Draft*Two-Phase*Simulation*v1*31/03/2021

The "Simulation and Data Collection" file will be connected to a Microsoft OneDrive which can be shared with other researches, to gain access to software simulation and Microsoft Excel files at anytime.

3 Research Project Data Storage, Retention and Dissemination Details

3.1 Storage arrangements

For the duration of the project, digital data will be stored on the primary research's laptop, which is automatically backed up to a OneDrive account and will be backed up to an external USB hard drive on a daily basis.

Upon returning to Curtin University, all digital data will also be transferred to Curtin's R Drive.

3.2 Estimated data storage volume

Physical Data: None.

Digital Data: During the project, up to 500 GB of data storage may be required, subject to the number of draft simulations and data analysis' required. After the project is completed, the draft data may be deleted.

3.3 Safeguarding measures

For the duration of the project, all copies of software simulations and data analysis will be kept on a password-protected laptop, password-protected OneDrive, and a USB hard drive. Backups will be performed on a daily basis after the data is no longer to be changed.

When a simulation or analysis is complete, the files will be transferred to the Curtin R drive, which is set up according to standard Curtin Information Technology Services security and safeguarding protocols.

Snapshots of the data analysis files will also be made weekly and stored on Curtin's R drive.

3.4 Retention requirements

7 years (All other research with outcomes that are classed as Minor)

3.5 Collaboration

This project is conducted as part of the research by Curtin University's Drilling Mechanics Group at Technology Park (Building 619).

Curtin Staff: Dimple Quyn (Primary Supervisor) Masood Mostofi (Supervisor) Chloe Thiel (Research Student)

3.6 Data dissemination

The data collection will be deposited to the Curtin Research Data Collection.

3.7 Embargo period

Not applicable.

APPENDIX C – ANSYS FLUENT SIMULATION MODELLING

Figure C.1: ANSYS Fluent simulation Realized k-epsilon viscous model and constraints.

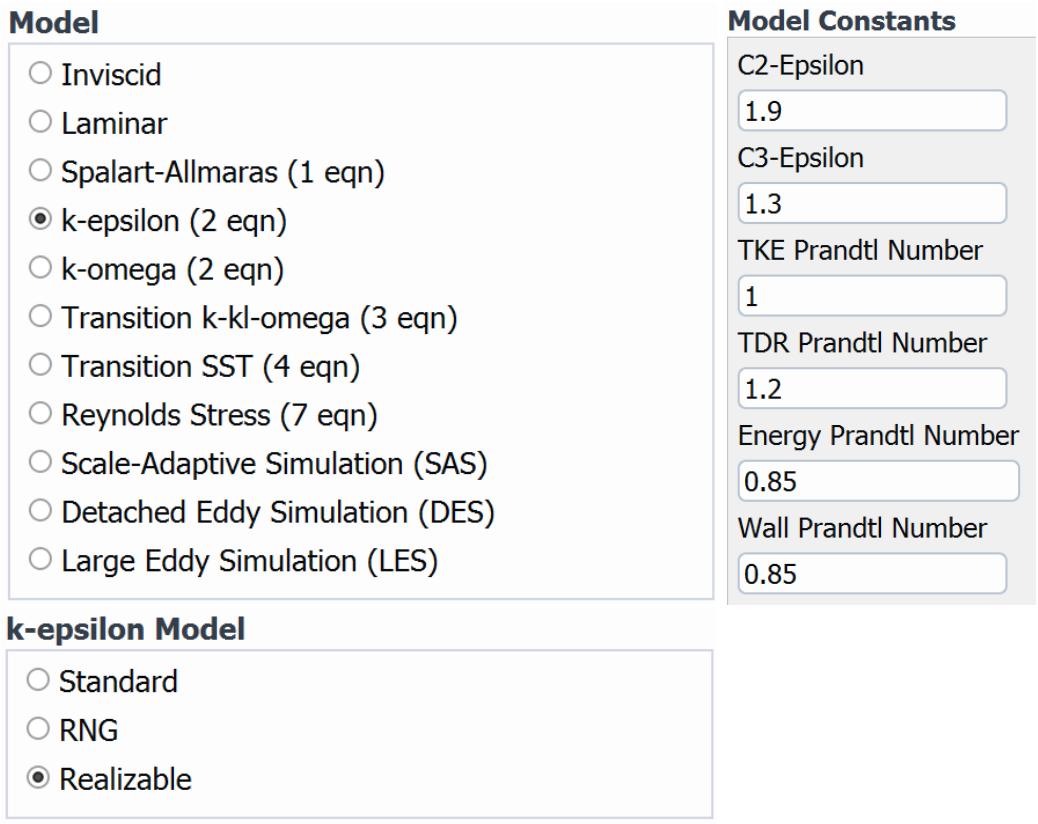

Figure C.2: ANSYS Fluent simulation Realized k-epsilon viscous model with Enhanced Wall Treatment.

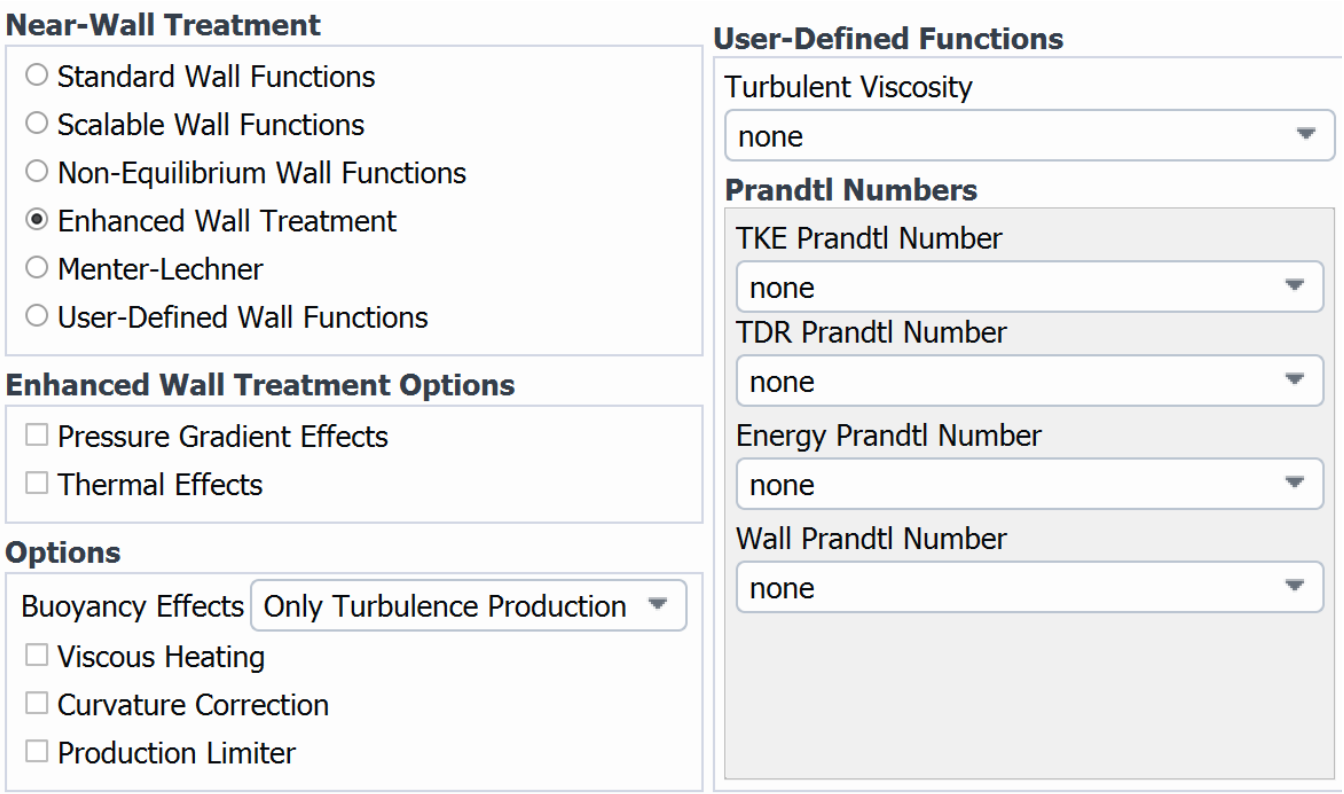

A Comprehensive Mechanistic Model for Upward Two-Phase Flow in Wellbores

A.M. Ansari, Pakistan Petroleum Ltd.; **N.D. Sylvester,** U. of Akron; and **C. Sarica, O. Shoham,** and **J.P. Brill,** U. of Tulsa

Summary. A comprehensive model is formulated to predict the flow behavior for upward two-phase flow. This model is composed of a model for flow-pattern prediction and a set of independent mechanistic models for predicting such flow characteristics as holdup and pressure drop in bubble, slug, and annular flow. The comprehensive model is evaluated by using a well data bank made up of 1,712 well cases covering a wide variety of field data. Model performance is also compared with six commonly used empirical correlations and the Hasan-Kabir mechanistic model. Overall model performance is in good agreement with the data. In comparison with other methods, the comprehensive model performed the best.

Introduction

Two-phase flow is commonly encountered in the petroleum, chemical, and nuclear industries. This frequent occurrence presents the challenge of understanding, analyzing, and designing two-phase systems.

Because of the complex nature of two-phase flow, the problem was first approached through empirical methods. The trend has shifted recently to the modeling approach. The fundamental postulate of the modeling approach is the existence of flow patterns or flow configurations. Various theories have been developed to predict flow patterns. Separate models were developed for each flow pattern to predict flow characteristics like holdup and pressure drop. By considering basic fluid mechanics, the resulting models can be applied with more confidence to flow conditions other than those used for their development.

Only Ozon *et al.*[1] and Hasan and Kabir[2] published studies on comprehensive mechanistic modeling of two-phase flow in vertical pipes. More work is needed to develop models that describe the physical phenomena more rigorously.

The purpose of this study is to formulate a detailed comprehensive mechanistic model for upward two-phase flow. The comprehensive model first predicts the existing flow pattern and then calculates the flow variables by taking into account the actual mechanisms of the predicted flow pattern. The model is evaluated against a wide range of experimental and field data available in the updated Tulsa U. Fluid Flow Projects (TUFFP) well data bank. The performance of the model is also compared with six empirical correlations and one mechanistic model used in the field.

Flow-Pattern Prediction

Taitel *et al.*[3] presented the basic work on mechanistic modeling of flow-pattern transitions for upward two-phase flow. They identified four distinct flow patterns (bubble, slug, churn, and annular flow) and formulated and evaluated the transition boundaries among them (**Fig. 1**). Barnea *et al.*[4] later modified the transitions to extend the applicability of the model to inclined flows. Barnea[5] then combined flow-pattern prediction models applicable to different inclination angle ranges into one unified model. Based on these different works, flow pattern can be predicted by defining transition boundaries among bubble, slug, and annular flows.

Bubble/Slug Transition. Taitel *et al.*[3] gave the minimum diameter at which bubble flow occurs as

$$d_{\min} = 19.01\left[\frac{(\rho_L-\rho_G)\sigma_L}{\rho_L^2 g}\right]^{1/2} \quad \ldots\ldots\ldots\ldots (1)$$

For pipes larger than this, the basic transition mechanism for bubble to slug flow is coalescence of small gas bubbles into large Taylor bubbles. This was found experimentally to occur at a void fraction of about 0.25. Using this value of void fraction, we can express the transition in terms of superficial and slip velocities:

$$v_{Sg} = 0.25v_s + 0.333v_{SL}, \quad \ldots\ldots\ldots\ldots (2)$$

where v_s is the slip or bubble-rise velocity given by[6]

$$v_s = 1.53\left[\frac{g\sigma_L(\rho_L-\rho_G)}{\rho_L^2}\right]^{1/4} \quad \ldots\ldots\ldots\ldots (3)$$

This is shown as Transition A in **Fig. 2**.

Dispersed Bubble Transition. At high liquid rates, turbulent forces break large gas bubbles down into small ones, even at void fractions exceeding 0.25. This yields the transition to dispersed bubble flow[5]:

$$2\left[\frac{0.4\sigma_L}{(\rho_L-\rho_G)g}\right]^{1/2}\left(\frac{\rho_L}{\sigma_L}\right)^{3/5}\left[\frac{f}{2d}\right]^{2/5}(v_{SL}+v_{Sg})^{1.2}$$

$$= 0.725 + 4.15\left(\frac{v_{Sg}}{v_{Sg}+v_{SL}}\right)^{0.5} \quad \ldots\ldots\ldots\ldots (4)$$

This is shown as Transition B in Fig. 2.

At high gas velocities, this transition is governed by the maximum packing of bubbles to give coalescence. Scott and Kouba[7] concluded that this occurs at a void fraction of 0.76, giving the transition for no-slip dispersed bubble flow as

$$v_{Sg} = 3.17v_{SL}. \quad \ldots\ldots\ldots\ldots (5)$$

This is shown as Transition C in Fig. 2.

Transition to Annular Flow. The transition criterion for annular flow is based on the gas-phase velocity required to prevent the entrained liquid droplets from falling back into the gas stream. This gives the transition as

$$v_{Sg} = 3.1\left[\frac{g\sigma_L(\rho_L-\rho_G)}{\rho_G^2}\right]^{1/4}, \quad \ldots\ldots\ldots\ldots (6)$$

shown as Transition D in Fig. 2.

Barnea[5] modified the same transition by considering the effects of film thickness on the transition. One effect is that a thick liquid film bridged the gas core at high liquid rates. The other effect is instability of the liquid film, which causes downward flow of the film at low liquid rates. The bridging mechanism is governed by the minimum liquid holdup required to form a liquid slug:

$$H_{LF} > 0.12, \quad \ldots\ldots\ldots\ldots (7)$$

where H_{LF} is the fraction of pipe cross section occupied by the liquid film, assuming no entrainment in the core. The mechanism of film instability can be expressed in terms of the modified Lockhart and Martinelli parameters, X_M and Y_M,

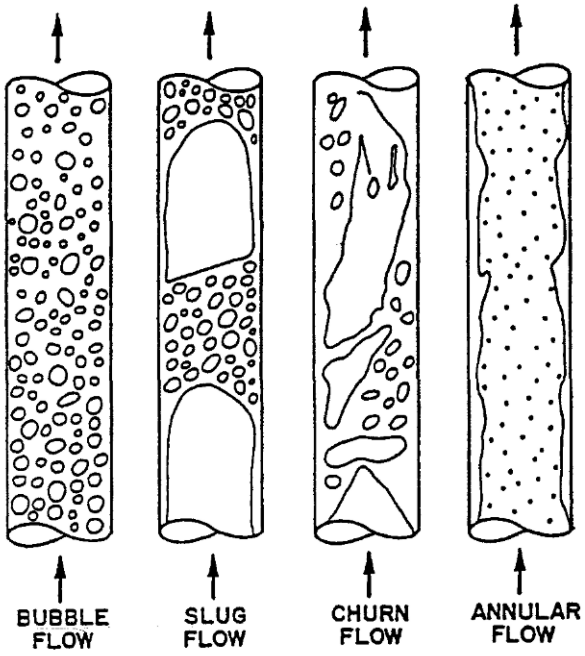

Fig. 1—Flow patterns in upward two-phase flow.

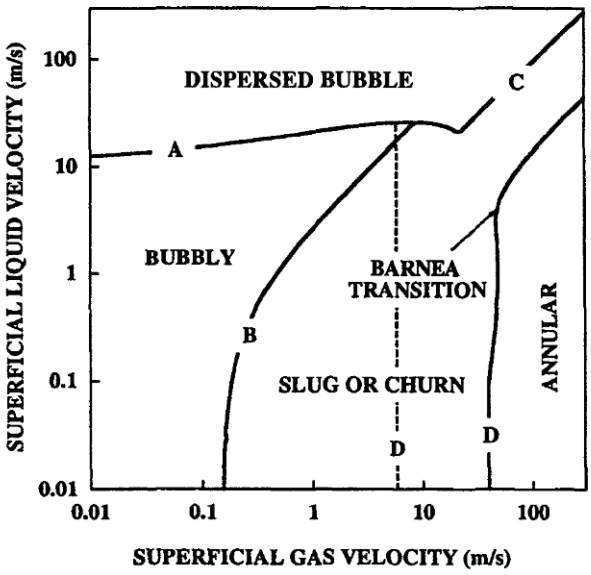

Fig. 2—Typical flow-pattern map for wellbores.

$$Y_M = \frac{2-1.5H_{LF}}{H_{LF}^3(1-1.5H_{LF})}X_M^2, \quad \ldots\ldots (8)$$

$$\text{where } X_M = \sqrt{B\frac{\left(\frac{dp}{dL}\right)_{SL}}{\left(\frac{dp}{dL}\right)_{SC}}}, \quad \ldots\ldots (9)$$

$$Y_M = \frac{g \sin\theta(\rho_L-\rho_C)}{\left(\frac{dp}{dL}\right)_{SC}}, \quad \ldots\ldots (10)$$

and $B=(1-F_E)^2(f_F/f_{SL})$. From geometric considerations, H_{LF} can be expressed in terms of minimum dimensionless film thickness, $\underline{\delta}_{\min}$, as

$$H_{LF} = 4\underline{\delta}_{\min}(1-\underline{\delta}_{\min}). \quad \ldots\ldots (11)$$

To account for the effect of the liquid entrainment in the gas core, Eq. 7 is modified here as

$$\left(H_{LF} + \lambda_{LC}\frac{A_C}{A_p}\right) > 0.12. \quad \ldots\ldots (12)$$

Annular flow exists if v_{Sg} is greater than that at the transition given by Eq. 6 and if the two Barnea criteria are satisfied. To satisfy the Barnea criteria, Eq. 8 must first be solved implicitly for $\underline{\delta}_{\min}$. H_{LF} is then calculated from Eq. 11; if Eq. 12 is not satisfied, annular flow exists. Eq. 8 can usually be solved for $\underline{\delta}_{\min}$ by using a second-order Newton-Raphson approach. Thus, Eq. 8 can be expressed as

$$F(\underline{\delta}_{\min}) = Y_M - \frac{2-1.5H_{LF}}{H_{LF}^3(1-1.5H_{LF})}X_M^2 \quad \ldots\ldots (13)$$

and

$$F'(\underline{\delta}_{\min}) = \frac{1.5H'_{LF}X_M^2}{H_{LF}^3(1-1.5H_{LF})}$$

$$+\frac{(2-1.5H_{LF})X_M^2H'_{LF}(3-5.5H_{LF})}{H_{LF}^3(1-1.5H_{LF})^2}. \quad \ldots\ldots (14)$$

The minimum dimensionless film thickness is then determined iteratively from

$$\underline{\delta}_{\min_{j+1}} = \underline{\delta}_{\min_j} - \frac{F(\underline{\delta}_{\min_j})}{F'(\underline{\delta}_{\min_j})}. \quad \ldots\ldots (15)$$

A good initial guess is $\underline{\delta}_{\min}=0.25$.

Flow-Behavior Prediction

After the flow patterns are predicted, the next step is to develop physical models for the flow behavior in each flow pattern. This step resulted in separate models for bubble, slug, and annular flow. Churn flow has not yet been modeled because of its complexity and is treated as part of slug flow. The models developed for other flow patterns are discussed below.

Bubble Flow Model. The bubble flow model is based on Caetano's[8] work for flow in an annulus. The bubble flow and dispersed bubble flow regimes are considered separately in developing the model for the bubble flow pattern.

Because of the uniform distribution of gas bubbles in the liquid and no slippage between the two phases, dispersed bubble flow can be approximated as a pseudosingle phase. With this simplification, the two-phase parameters can be expressed as

$$\rho_{TP} = \rho_L\lambda_L + \rho_g(1-\lambda_L), \quad \ldots\ldots (16)$$

$$\mu_{TP} = \mu_L\lambda_L + \mu_g(1-\lambda_L), \quad \ldots\ldots (17)$$

$$\text{and } v_{TP} = v_M v_{SL} + v_{Sg}, \quad \ldots\ldots (18)$$

$$\text{where } \lambda_L = v_{SL}/v_m. \quad \ldots\ldots (19)$$

For bubble flow, the slippage is considered by taking into account the bubble-rise velocity relative to the mixture velocity. By assuming a turbulent velocity profile for the mixture with the rising bubble concentrated more at the center than along the pipe wall, we can express the slippage velocity as

$$v_S = v_g - 1.2v_m. \quad \ldots\ldots (20)$$

Harmathy[6] gave an expression for bubble-rise velocity (Eq. 3). To account for the effect of bubble swarm, Zuber and Hench[9] modified this expression:

$$v_S = 1.53\left[\frac{g\sigma_L(\rho_L-\rho_g)}{\rho_L^2}\right]^{1/4}H_L^{n'}, \quad \ldots\ldots (21)$$

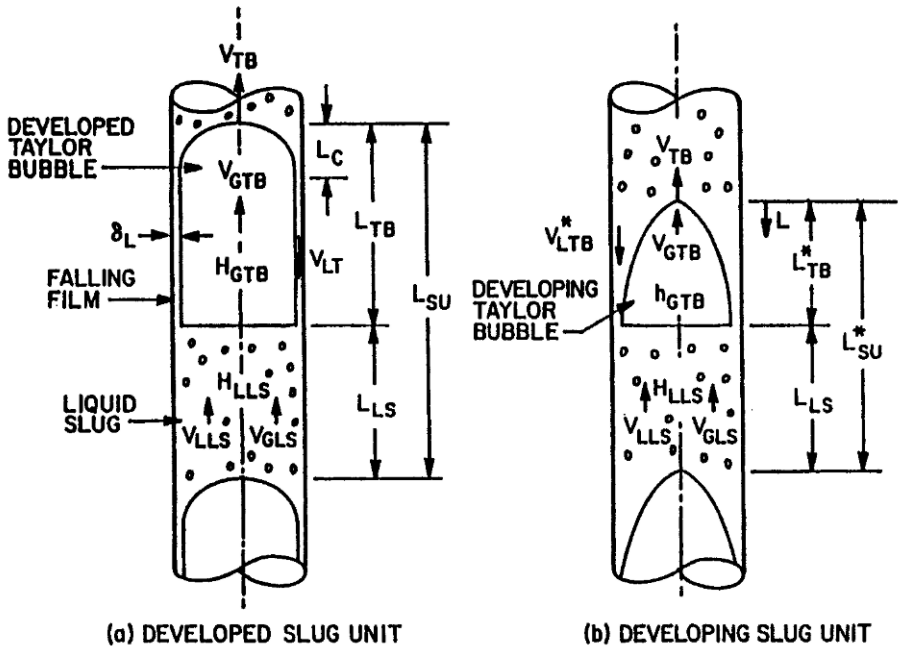

Fig. 3—Schematic of slug flow.

where the value of n' varies from one study to another. In the present study, n'=0.5 was used to give the best results. Thus, Eq. 20 yields

$$1.53\left[\frac{g\sigma_L(\rho_L-\rho_g)}{\rho_L^2}\right]^{1/4} H_L^{0.5} = \frac{v_{Sg}}{1-H_L} - 1.2v_M. \quad \ldots\ldots\ldots\ldots (22)$$

This gives an implicit equation for the actual holdup for bubble flow. The two-phase flow parameters can now be calculated from

$$\rho_{TP} = \rho_L H_L + \rho_g(1-H_L) \quad \ldots\ldots\ldots\ldots (23)$$

and $$\mu_{TP} = \mu_L H_L + \mu_g(1-H_L). \quad \ldots\ldots\ldots\ldots (24)$$

The two-phase pressure gradient is made up of three components. Thus,

$$\left(\frac{dp}{dL}\right) = \left(\frac{dp}{dL}\right)_e + \left(\frac{dp}{dL}\right)_f + \left(\frac{dp}{dL}\right)_a \quad \ldots\ldots\ldots\ldots (25)$$

The elevation pressure gradient is given by

$$\left(\frac{dp}{dL}\right)_e = \rho_{TP} g \sin\theta. \quad \ldots\ldots\ldots\ldots (26)$$

The friction component is given by

$$\left(\frac{dp}{dL}\right)_f = \frac{f_{TP}\rho_{TP}v_{TP}^2}{2d}, \quad \ldots\ldots\ldots\ldots (27)$$

where f_{TP} is obtained from a Moody diagram for a Reynolds number defined by

$$N_{\mathrm{Re}_{TP}} \frac{\rho_{TP}v_{TP}d}{\mu_{TP}}. \quad \ldots\ldots\ldots\ldots (28)$$

Because bubble flow is dominated by a relatively incompressible liquid phase, there is no significant change in the density of the flowing fluids. This keeps the fluid velocity nearly constant, resulting in essentially no pressure drop owing to acceleration. Therefore, the acceleration pressure drop is safely neglected, compared with the other pressure drop components.

Slug Flow Model. Fernandes *et al.*[10] developed the first thorough physical model for slug flow. Sylvester[11] presented a simplified version of this model. The basic simplification was the use of a correlation for slug void fraction. These models used an important assumption of fully developed slug flow. McQuillan and Whalley[12] introduced the concept of developing flow during their study of flow-pattern transitions. Because of the basic difference in flow geometry, the model treats fully developed and developing flow separately.

For a fully developed slug unit (**Fig. 3a**), the overall gas and liquid mass balances give

$$v_{Sg} = \beta v_{gTB}(1-H_{LTB}) + (1-\beta)v_{gLS}(1-H_{LLS}) \quad \ldots\ldots\ldots\ldots (29)$$

and $$v_{SL} = (1-\beta)v_{LLS}H_{LLS} - \beta V_{LTB}H_{LTB}, \quad \ldots\ldots\ldots\ldots (30)$$

respectively, where

$$\beta = L_{TB}/L_{SU}. \quad \ldots\ldots\ldots\ldots (31)$$

Mass balances for liquid and gas from liquid slug to Taylor bubble give

$$(v_{TB}\,cc-v_{LLS})H_{LLS} = [v_{TB}-(-V_{LTB})]H_{LTB} \quad \ldots\ldots\ldots\ldots (32)$$

and $$(v_{TB}-v_{gLS})(1-H_{LLS}) = (v_{TB}-v_{gTB})(1-H_{LTB}). \quad \ldots\ldots\ldots\ldots (33)$$

The Taylor bubble-rise velocity is equal to the centerline velocity plus the Taylor bubble-rise velocity in a stagnant liquid column; i.e.,

$$v_{TB} = 1.2v_m + 0.35\left[\frac{gd(\rho_L-\rho_g)}{\rho_L}\right]^{1/2}. \quad \ldots\ldots\ldots\ldots (34)$$

Similarly, the velocity of the gas bubbles in the liquid slug is

$$v_{gLS} = 1.2v_m + 1.53\left[\frac{g\sigma_L(\rho_L-\rho_g)}{\rho_L^2}\right]^{1/4} H_{LLS}^{0.5}, \quad \ldots\ldots\ldots\ldots (35)$$

where the second term on the right side represents the bubble-rise velocity defined in Eq. 21.

The velocity of the falling film can be correlated with the film thickness with the Brotz[13] expression,

$$v_{LTB} = \sqrt{196.7g\delta_L}, \quad \ldots\ldots\ldots\ldots (36)$$

where δ_L, the constant film thickness for developed flow, can be expressed in terms of Taylor bubble void fraction to give

$$v_{LTB} = 9.916\left[gd\left(1-\sqrt{H_{gTB}}\right)\right]^{1/2}. \quad \ldots\ldots\ldots\ldots (37)$$

The liquid slug void fraction can be obtained by Sylvester's[11] correlation and from Fernandes *et al.*'s[10] and Schmidt's[14] data,

$$H_{gLS} = \frac{v_{Sg}}{0.425 + 2.65v_m}. \quad \ldots\ldots\ldots\ldots\ldots\ldots\ldots\ldots (38)$$

Eqs. 29 or 30, 31 through 35, 37, and 38 can be solved iteratively to obtain the following eight unknowns that define the slug flow model: β, H_{LTB}, H_{gLS}, v_{gTB}, v_{LTB}, v_{gLS}, v_{LLS}, and v_{TB}. Vo and Shoham[15] showed that these eight equations can be combined algebraically to give

$$\left(9.916\sqrt{gd}\right)\left(1-\sqrt{1-H_{LTB}}\right)^{0.5} H_{LTB}-v_{TB}(1-H_{LTB}) + \tilde{A} = 0, \quad \ldots\ldots\ldots\ldots\ldots\ldots (39)$$

where $\tilde{A} = H_{gLS}v_{TB} + (1-H_{gLS})$

$$\times \left[v_m - H_{gLS} \left\{ 1.53 \left[\frac{\sigma_L g(\rho_L-\rho_g)}{\rho_L^2} \right]^{0.25} (1-H_{gLS})^{0.5} \right\} \right]. \quad \ldots\ldots\ldots\ldots\ldots\ldots (40)$$

With v_{TB} and H_{gLS} given by Eqs. 34 and 38, respectively, $\tilde{A}$ can be readily determined from Eq. 40. Eq. 39 is then used to find H_{LTB} with an iterative solution method. Defining the left side of Eq. 39 as $F(H_{LTB})$, then

$$F(H_{LTB}) = \left(9.916\sqrt{gd}\right)\left(1-\sqrt{1-H_{LTB}}\right)^{0.5} H_{LTB}-v_{TB}(1-H_{LTB}) + \tilde{A}. \quad \ldots\ldots\ldots\ldots\ldots\ldots (41)$$

Taking the derivative of Eq. 41 with respect to H_{LTB} yields

$$F'(H_{LTB}) = v_{TB} + \left(9.916\sqrt{gd}\right) \times \left[\left(1-\sqrt{1-H_{LTB}}\right)^{0.5} + \frac{H_{LTB}}{4\sqrt{(1-H_{LTB})\left(1-\sqrt{1-H_{LTB}}\right)}} \right]. \quad \ldots\ldots\ldots\ldots\ldots\ldots (42)$$

H_{LTB}, the root of Eq. 39, is then determined iteratively from

$$H_{LTB_{j+1}} = H_{LTB_j} - \frac{F(H_{LTB_j})}{F'(H_{LTB_j})}. \quad \ldots\ldots\ldots\ldots\ldots\ldots\ldots\ldots (43)$$

The step-by-step procedure for determining all slug flow variables is as follows.

1. Calculate v_{TB} and H_{gLS} from Eqs. 34 and 38.
2. Using Eqs. 40 through 43, determine H_{LTB}. A good initial guess is H_{LTB}=0.15.
3. Solve Eq. 37 for v_{LTB}. Note that H_{gTB}=1–H_{LTB}.
4. Solve Eq. 32 for v_{LLS}. Note that H_{LLS}=1–H_{gLS}.
5. Solve Eq. 35 for v_{gLS}.
6. Solve Eq. 33 for v_{gTB}.
7. Solve Eq. 29 or 30 for β.
8. Assuming that L_{LS}=30d, calculate L_{SU} and L_{TB} from the definition of β.

To model developing slug flow, as in **Fig. 3b**, we must determine the existence of such flow. This requires calculating and comparing the cap length with the total length of a developed Taylor bubble. The expression for the cap length is[12]

$$L_c = \frac{1}{2g}\left[v_{TB} + \frac{v_{NgTB}}{H_{NLTB}}(1-H_{NLTB}) - \frac{v_m}{H_{NLTB}} \right]^2, \quad \ldots\ldots\ldots (44)$$

where v_{NgTB} and H_{NLTB} are calculated at the terminal film thickness (called Nusselt film thickness) given by

$$\delta_N = \left[\frac{3}{4} d \frac{v_{NLTB}\mu_L(1-H_{NLTB})}{g(\rho_L-\rho_g)} \right]^{1/3}. \quad \ldots\ldots\ldots\ldots\ldots (45)$$

The geometry of the film flow gives H_{NLTB} in terms of δ_N as

$$H_{NLTB} = 1-\left(1-\frac{2\delta_N}{d}\right)^2. \quad \ldots\ldots\ldots\ldots\ldots\ldots\ldots (46)$$

To determine v_{NgTB}, the net flow rate of δ_N can be used to obtain

$$v_{NgTB} = v_{TB} - (v_{TB} - v_{gLS})\frac{(1-H_{LLS})}{(1-H_{NLTB})}. \quad \ldots\ldots\ldots\ldots\ldots (47)$$

The length of the liquid slug can be calculated empirically from

$$L_{LS} = C'd, \quad \ldots\ldots\ldots\ldots\ldots\ldots\ldots\ldots\ldots (48)$$

where C' was found[16] to vary from 16 to 45. We use C'=30 in this study. This gives the Taylor bubble length as

$$L_{TB} = [L_{LS}/(1-\beta)]\beta. \quad \ldots\ldots\ldots\ldots\ldots\ldots\ldots (49)$$

From the comparison of L_c and L_{TB}, if $L_c \geq L_{TB}$, the flow is developing slug flow. This requires new values for L^*_{TB}, H^*_{LTB}, and v^*_{LTB} calculated earlier for developed flow.

For L^*_{TB}, Taylor bubble volume can be used:

$$V^*_{gTB} = \int_o^{L^*_{TB}} A^*_{TB}(L)\mathrm{d}L, \quad \ldots\ldots\ldots\ldots\ldots\ldots\ldots (50)$$

where A^*_{TB} can be expressed in terms of local holdup $h_{LTB}(L)$, which in turn can be expressed in terms of velocities by using Eq. 32. This gives

$$A^*_{TB}(L) = \left[1-\frac{(v_{TB}-v_{LLS})H_{LLS}}{\sqrt{2gL}} \right] A_p. \quad \ldots\ldots\ldots\ldots\ldots (51)$$

The volume can be expressed in terms of flow geometry as

$$V^*_{gTB} = v_{Sg}A_p\left(\frac{L^*_{TB}+L_{LS}}{v_{TB}}\right) - v_{gLS}A_p(1-H_{LLS})\frac{L_{LS}}{v_{TB}}. \quad \ldots\ldots (52)$$

Substitution of Eqs. 51 and 52 into Eq. 50 gives

$$v_{Sg}\left(\frac{L^*_{TB}+L_{LS}}{v_{TB}}\right) - v_{gLS}(1-H_{LLS})\frac{L_{LS}}{v_{TB}} = \int_o^{L^*_{TB}} \left[1-\frac{(v_{TB}-v_{LLS})H_{LLS}}{\sqrt{2gL}} \right]\mathrm{d}L \quad \ldots\ldots\ldots\ldots\ldots\ldots (53)$$

Eq. 53 can be integrated and then simplified to give

$$L^{*2}_{TB} + \left(\frac{-2ab-4c^2}{a^2}\right)L^*_{TB} + \frac{b^2}{a^2} = 0, \quad \ldots\ldots\ldots\ldots\ldots\ldots (54)$$

where a=1–v_{Sg}/v_{TB}, $\ldots\ldots\ldots\ldots\ldots\ldots\ldots\ldots\ldots\ldots (55)$

$$b = \frac{v_{Sg}-v_{gLS}(2-H_{LLS})}{v_{TB}}L_{LS}, \quad \ldots\ldots\ldots\ldots\ldots\ldots\ldots (56)$$

and $c = \frac{v_{TB}-v_{LLS}}{\sqrt{2g}}H_{LLS}$. $\ldots\ldots\ldots\ldots\ldots\ldots\ldots\ldots (57)$

After calculating L^*_{TB}, the other local parameters can be calculated from

$$v^*_{LTB}(L) = \sqrt{2gL} - v_{TB} \quad \ldots\ldots\ldots\ldots\ldots\ldots\ldots\ldots (58)$$

and $h^*_{LTB}(L) = \frac{(v_{TB}-v_{LLS})H_{LLS}}{\sqrt{2gL}}$. $\ldots\ldots\ldots\ldots\ldots\ldots (59)$

In calculating pressure gradients, we consider the effect of varying film thickness and neglect the effect of friction along the Taylor bubble.

For developed flow, the elevation component occurring across a slug unit is given by

$$\left(\frac{dp}{dL}\right)_e = [(1-\beta)\rho_{LS} + \beta\rho_g]g \sin\theta, \quad \ldots\ldots\ldots\ldots\ldots (60)$$

where $\rho_{LS} = \rho_L H_{LLS} + \rho_g(1-H_{LLS})$. $\ldots\ldots\ldots\ldots\ldots (61)$

The elevation component for developing slug flow is given by

$$\left(\frac{dp}{dL}\right)_e = [(1-\beta^*)\rho_{LS} + \beta^* \rho_{TBA}]g \sin\theta, \quad \ldots\ldots\ldots\ldots (62)$$

where ρ_{TBA} is based on average void fraction in the Taylor bubble section with varying film thickness. It is given by

$$\rho_{TBA} = \rho_L H_{LTBA} + \rho_g(1-H_{LTBA}), \quad \ldots\ldots\ldots\ldots\ldots (63)$$

where H_{LTBA} is obtained by integrating Eq. 59 and dividing by L^*_{TB}, giving

$$H_{LTBA} = \frac{2(v_{TB}-v_{LLS})H_{LLS}}{\sqrt{2gL^*_{TB}}} \quad \ldots\ldots\ldots\ldots\ldots\ldots (64)$$

The friction component is the same for both the developed and developing slug flows because it occurs only across the liquid slug. This is given as

$$\left(\frac{dp}{dL}\right)_f = \frac{f_{LS}\rho_{LS}v_m^2}{2d}(1-\beta), \quad \ldots\ldots\ldots\ldots\ldots\ldots (65)$$

where β should be replaced by β^* for developing flow. f_{LS} can be calculated by using

$$N_{Re_{LS}} = \rho_{LS}v_m d/\mu_{LS}. \quad \ldots\ldots\ldots\ldots\ldots\ldots (66)$$

For the pressure gradient due to acceleration, the velocity in the film must be considered. The liquid in the slug experiences deceleration as its upward velocity of v_{LLS} changes to a downward velocity of v_{LTB}. The same liquid also experiences acceleration when it exits from the film with a velocity v_{LTB} into an upward moving liquid slug of velocity v_{LLS}. If the two changes in the liquid velocity occur within the same slug unit, then no net pressure drop due to acceleration exists over that slug unit. This happens when the slug flow is stable. The correlation used for slug length is based on its stable length, so the possibility of a net pressure drop due to acceleration does not exist. Therefore, no acceleration component of pressure gradient is considered over a slug unit.

Annular Flow Model. A discussion on the hydrodynamics of annular flow was presented by Wallis.[17] Along with this, Wallis also presented the classic correlations for entrainment and interfacial friction as a function of film thickness. Later, Hewitt and Hall-Taylor[18] gave a detailed analysis of the mechanisms involved in an annular flow. All the models that followed later are based on this approach.

A fully developed annular flow is shown in **Fig 4**. The conservation of momentum applied separately to the core and the film yields

$$A_c\left(\frac{dp}{dL}\right)_c - \tau_i S_i - \rho_c A_c g \sin\theta = 0 \quad \ldots\ldots\ldots\ldots\ldots (67)$$

and $A_F\left(\frac{dp}{dL}\right)_F + \tau_i S_i - \tau_F S_F - \rho_L A_F g \sin\theta = 0. \quad \ldots\ldots\ldots (68)$

The core density, ρ_c, is a no-slip density because the core is considered a homogeneous mixture of gas and entrained liquid droplets flowing at the same velocity. Thus,

$$\rho_c = \rho_L\lambda_{LC} + \rho_g(1-\lambda_{LC}), \quad \ldots\ldots\ldots\ldots\ldots\ldots (69)$$

where $\lambda_{LC} = \frac{F_E v_{SL}}{v_{Sg} + F_E v_{SL}}$. $\ldots\ldots\ldots\ldots\ldots\ldots (70)$

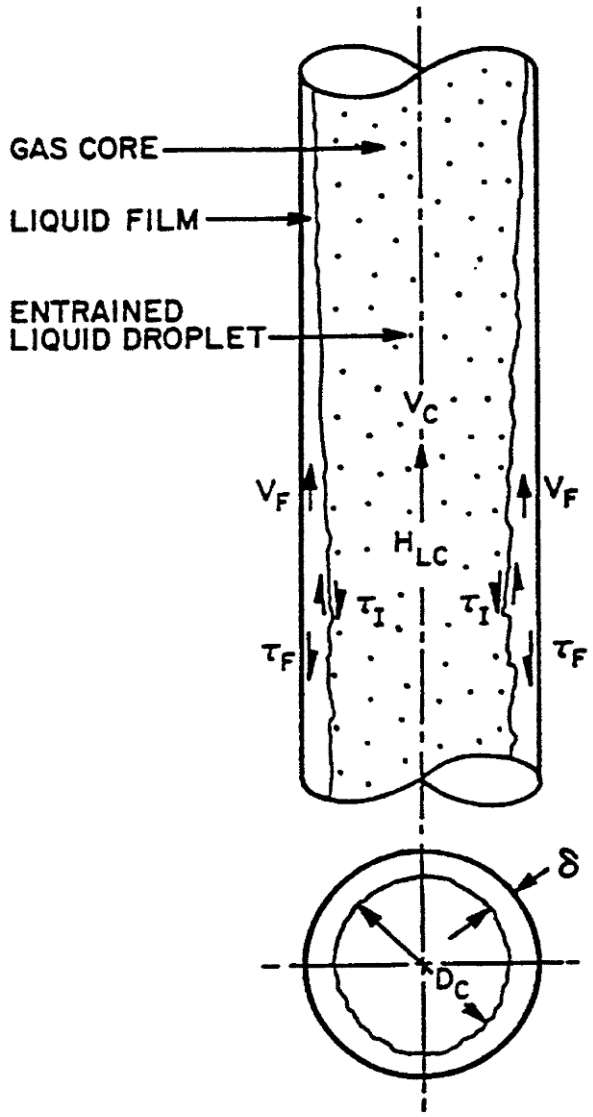

Fig. 4—Schematic of annular flow.

F_E is the fraction of the total liquid entrained in the core, given by Wallis as

$$F_E = 1-\exp[-0.125(v_{crit}-1.5)], \quad \ldots\ldots\ldots\ldots\ldots (71)$$

where $v_{crit} = 10,000\frac{v_{Sg}\mu_g}{\sigma_L}\left(\frac{\rho_g}{\rho_L}\right)^{1/2}$. $\ldots\ldots\ldots\ldots\ldots (72)$

The shear stress in the film can be expressed as

$$\tau_F = f_F\rho_L\frac{v_F^2}{8}, \quad \ldots\ldots\ldots\ldots\ldots\ldots (73)$$

where f_F is obtained from a Moody diagram for a Reynolds number defined by

$$N_{Re_F} = \frac{\rho_L v_F d_{HF}}{\mu_L}, \quad \ldots\ldots\ldots\ldots\ldots\ldots (74)$$

where $v_F = \frac{q_L(1-F_E)}{A_F} = \frac{v_{SL}(1-F_E)}{4\underline{\delta}(1-\underline{\delta})}$ $\ldots\ldots\ldots\ldots\ldots (75)$

and $d_{HF} = 4\underline{\delta}(1-\underline{\delta})d$. $\ldots\ldots\ldots\ldots\ldots\ldots (76)$

This gives

$$\tau_F = \frac{f_F}{8}(1-F_E)^2\rho_L\left[\frac{v_{SL}}{4\underline{\delta}(1-\underline{\delta})}\right]^2. \quad \ldots\ldots\ldots\ldots\ldots (77)$$

Eq. 77 reduces to

$$\tau_F = \frac{d}{4}\frac{(1-F_E)^2}{[4\underline{\delta}(1-\underline{\delta})]^2}\frac{f_F}{f_{SL}}\left(\frac{dp}{dL}\right)_{SL}, \quad \ldots\ldots (78)$$

where the superficial liquid friction pressure gradient is given by

$$\left(\frac{dp}{dL}\right)_{SL} = \frac{f_{SL}\rho_L v_{SL}^2}{2d}. \quad \ldots\ldots (79)$$

f_{SL} is the friction factor for superficial liquid velocity and can be obtained from a Moody diagram for a Reynolds number defined by

$$N_{Re_{SL}} = \rho_L v_{SL} d/\mu_L. \quad \ldots\ldots (80)$$

For the shear stress at the interface,

$$\tau_i = f_i\, \rho_C v_C^2/8, \quad \ldots\ldots (81)$$

where $v_c = v_{SC}/(1-2\underline{\delta})^2$ ..... (82)

and $f_i = f_{SC} Z$, ... (83)

where Z is a correlating factor for interfacial friction and the film thickness. Based on the performance of the model, the Wallis expression for Z works well for thin films or high entrainments, whereas the Whalley and Hewitt[19] expression is good for thick films or low entrainments. Thus,

$$Z = 1+300\underline{\delta} \quad \text{for } F_E > 0.9 \quad \ldots\ldots (84)$$

and $Z = 1 + 24\left(\frac{\rho_g}{\rho_g}\right)^{1/3}\underline{\delta}$ for $F_E < 0.9$. ..... (85)

Combining Eqs. 81 through 83 yields

$$\tau_i = \frac{d}{4}\frac{Z}{(1-2\underline{\delta})^4}\left(\frac{dp}{dL}\right)_{SC}. \quad \ldots\ldots (86)$$

The superficial friction pressure gradient in the core is given by

$$\left(\frac{dp}{dL}\right)_{SC} = \frac{f_{SC}\rho_C v_{SC}^2}{2d}, \quad \ldots\ldots (87)$$

where f_{SC} is obtained from a Moody diagram for a Reynolds number defined by

$$N_{Re_{SC}} = \rho_c v_{sc} d/\mu_{sc}, \quad \ldots\ldots (88)$$

$$v_{SC} = F_E v_{SL} + v_{Sg}, \quad \ldots\ldots (89)$$

and $\mu_C = \mu_L \lambda_{LC} + \mu_g(1-\lambda_{LC})$. ..... (90)

The pressure gradient for annular flow can be calculated by substituting the above equations into Eqs. 67 and 68. Thus,

$$\left(\frac{dp}{dL}\right)_C = \frac{Z}{(1-2\underline{\delta})^5}\left(\frac{dp}{dL}\right)_{SC} + \rho_C g \sin\theta \quad \ldots\ldots (91)$$

and $\left(\frac{dp}{dL}\right)_F = \frac{(1-F_E)^2}{64\underline{\delta}^3(1-\underline{\delta})^3}\left(\frac{f_F}{f_{SL}}\right)\left(\frac{dp}{dL}\right)_{SL}$

$$-\frac{Z}{4\underline{\delta}(1-\underline{\delta})(1-2\underline{\delta})^3}\left(\frac{dp}{dL}\right)_{SC} + \rho_L g \sin\theta. \quad \ldots\ldots (92)$$

The basic unknown in the above equations is the dimensionless film thickness, $\underline{\delta}$. An implicit equation for $\underline{\delta}$ can be obtained by equating Eqs. 91 and 92. This gives

$$\frac{Z}{4\underline{\delta}(1-\underline{\delta})(1-2\underline{\delta})^5}\left(\frac{dp}{dL}\right)_{SC} - (\rho_L-\rho_C)g \sin\theta$$

$$-\frac{(1-FE)^2}{64\underline{\delta}^3(1-\underline{\delta})^3}\frac{f_F}{f_{SL}}\left(\frac{dp}{dL}\right)_{SL} = 0. \quad \ldots\ldots (93)$$

To simplify this equation, the dimensionless approach developed by Alves *et al.*[20] is used. This approach defines the following dimensionless groups in addition to previously defined modified Lockhart Martinelli parameters, X_M and Y_M.

$$\phi_C^2 = \frac{(dp/dL)_C - g\rho_C \sin\theta}{(dp/dL)_{SC}}. \quad \ldots\ldots (94)$$

and $\phi_F^2 = \frac{(dp/dL)_F - g\rho_L \sin\theta}{(dp/dL)_{SL}}$. ..... (95)

By using the modified Lockhart Martinelli parameters, Eq. 93 reduces to

$$Y_M - \frac{Z}{4\underline{\delta}(1-\underline{\delta})[1-4\underline{\delta}(1-\underline{\delta})]^{2.5}} + \frac{X_M^2}{[4\underline{\delta}(1-\underline{\delta})]^3} = 0. \quad \ldots\ldots (96)$$

The above equations can be solved iteratively to obtain $\underline{\delta}$. If Eq. 96 is $F(\underline{\delta})$, then taking the derivative of Eq. 96 with respect to $\underline{\delta}$ yields

$$F'(\underline{\delta}) = \frac{Z[4(1-2\underline{\delta})]}{[4\underline{\delta}(1-\underline{\delta})]^2[1-4\underline{\delta}(1-\underline{\delta})]^{2.5}}$$

$$-\frac{Z'}{4\underline{\delta}(1-\underline{\delta})[1-4\underline{\delta}(1-\underline{\delta})]^{2.5}}$$

$$-\frac{2.5Z[4(1-2\underline{\delta})]}{4\underline{\delta}(1-\underline{\delta})[1-4\underline{\delta}(1-\underline{\delta})]^{3.5}} - \frac{3X_M^2[4(1-2\underline{\delta})]}{[4\underline{\delta}(1-\underline{\delta})]^4}. \quad \ldots\ldots (97)$$

The Newton-Raphson method can be incorporated to determine $\underline{\delta}$, the root of Eq. 96. Thus,

$$\underline{\delta}_{j+1} = \underline{\delta}_j - \frac{F(\underline{\delta}_j)}{F'(\underline{\delta}_j)}. \quad \ldots\ldots (98)$$

Once $\underline{\delta}$ is known, the dimensionless groups ϕ_F and ϕ_C can be obtained from the following form of Eqs. 91 and 92

$$\phi_C^2 = \frac{Z}{(1-2\underline{\delta})^5} \quad \ldots\ldots (99)$$

and $\phi_F^2 = \frac{(1-FE)^2}{[1-(1-2\underline{\delta})^2]^2}\frac{f_F}{f_{SL}}x$

$$\left\{\frac{\frac{Z}{(1-2\underline{\delta})^5} - Y_M}{\frac{Z}{(1-2\underline{\delta})^5} - Y_M[1-(1-2\underline{\delta})^2]^2}\right\}. \quad \ldots\ldots (100)$$

Alves[20] stated that Eq. 100 can be expressed as

$$\phi_F^2 = \frac{\phi_C^2 - Y_M}{X_M^2}. \quad \ldots\ldots (101)$$

The total pressure gradient can then be obtained from either Eq. 94 or 95 because the pressure gradient in the film and core must be the same. Thus,

$$\left(\frac{dp}{dL}\right)_T = \left(\frac{dp}{dL}\right)_C = \phi_C^2\left(\frac{dp}{dL}\right)_{SC} + g\rho_C \sin\theta \quad \ldots\ldots (102)$$

or $\left(\frac{dp}{dL}\right)_T = \left(\frac{dp}{dL}\right)_F = \phi_F^2\left(\frac{dp}{dL}\right)_{SL} + g\rho_L \sin\theta$. ..... (103)

Note that the above total pressure gradient equations do not include accelerational pressure gradient. This is based on results found by Lopes and Dukler[21] indicating that, except for a limited range of high liquid flow rates, the accelerational component result-

TABLE 1—RANGE OF WELL DATA

Source	Nominal Diameter (in.)	Oil Rate (STB/D)	Gas Rate (MSCF/D)	Oil Gravity (°API)
Old TUFFP* Data Bank	1 to 8	0 to 10,150	1.5 to 10,567	9.5 to 70.5
Govier and Fogarasi[22]	2 to 4	8 to 1,600	114 to 27,400	17 to 112
Asheim[23]	$2^7/_8$ to 6	720 to 27,000	740 to 55,700	35 to 86
Chierici *et al.*[24]	$2^7/_8$ to 5	0.3 to 69	6 to 27,914	8.3 to 46
Prudhoe Bay	5½ to 7	600 to 23,000	200 to 110,000	24 to 86

*Includes data from Poettmann and Carpenter,[25] Fancher and Brown,[26] Hagedorn,[27] Baxendell and Thomas,[28] Orkiszewski,[29] Espanol,[30] Messulam,[31] Camacho,[32] and field data from several oil companies.

ing from the exchange of liquid droplets between the core and the film is negligible.

Evaluation

The evaluation of the comprehensive model is carried out by comparing the pressure drop from the model with the measured data in the updated TUFFP well data bank that comprises 1,712 well cases with a wide range of data, as given in **Table 1**. The performance of the model is also compared with that of six correlations and another mechanistic model that are commonly used in the petroleum industry.

Criteria for Comparison with Data

The evaluation of the model using the data bank is based on the following statistical parameters.

Average percent error:

$$E_1 = \left(\frac{1}{n}\sum_{i=1}^{n} e_{ri}\right)\text{x}100, \quad \ldots\ldots (104)$$

where $e_{ri} = \dfrac{\Delta p_{icalc} - \Delta p_{imeas}}{\Delta p_{imeas}}$. $\ldots\ldots (105)$

E_1 indicates the overall trend of the performance, relative to the measured pressure drop.

Absolute average percentage error:

$$E_2 = \left(\frac{1}{n}\sum_{i=1}^{n} |e_{ri}|\right)\text{x}100. \quad \ldots\ldots (106)$$

E_2 indicates how large the errors are on the average.

Percent standard deviation:

$$E_3 = \sum_{i=1}^{n}\sqrt{\frac{(e_{ri}-E_1)^2}{n-1}}. \quad \ldots\ldots (107)$$

E_3 indicates the degree of scattering of the errors about their average value.

Average error:

$$E_4 = \left(\frac{1}{n}\sum_{i=1}^{n} e_i\right), \quad \ldots\ldots (108)$$

where $e_i = \Delta p_{icalc} - \Delta p_{imeas}$. $\ldots\ldots (109)$

E_4 indicates the overall trend independent of the measured pressure drop.

Absolute average error:

$$E_5 = \left(\frac{1}{n}\sum_{i=1}^{n} |e_i|\right). \quad \ldots\ldots (110)$$

E_5 is also independent of the measured pressure drop and indicates the magnitude of the average error.

Standard deviation:

$$E_6 = \sum_{i=1}^{n}\sqrt{\frac{(e_i-E_4)^2}{n-1}}. \quad \ldots\ldots (111)$$

E_6 indicates the scattering of the results, independent of the measured pressure drop.

Criteria for Comparison With Other Correlations and Models

The correlations and models used for the comparison are a modified Hagedorn and Brown,[27] Duns and Ros,[33] Orkiszewski[29] with Triggia correction,[34] Beggs and Brill[35] with Palmer correction,[36] Mukherjee and Brill,[37] Aziz *et al.*,[38] and Hasan and Kabir.[2,39] The comparison is accomplished by comparing the statistical parameters. The comparison involves the use of a relative performance factor defined by

$$F_{rp} = \frac{|E_1| - |E_{1_{min}}|}{|E_{1_{max}}| - |E_{1_{min}}|} + \frac{E_2 - E_{2_{min}}}{E_{2_{max}} - E_{2_{min}}}$$

TABLE 2—RELATIVE PERFORMANCE FACTORS

	EDB	VW	DW	VNH	ANH	AB	AS	VS	SNH	VSNH	AAN
n	1712	1086	626	755	1381	29	1052	654	745	387	70
MODEL	0.700	1.121	1.378	**0.081**	**0.000**	0.143	1.295	1.461	**0.112**	**0.142**	**0.000**
HAGBR	**0.585**	**0.600**	**0.919**	0.876	0.774	2.029	**0.386**	**0.485**	0.457	0.939	0.546
AZIZ	1.312	1.108	2.085	0.803	1.062	0.262	1.798	1.764	1.314	1.486	0.214
DUNRS	1.719	1.678	1.678	1.711	1.792	1.128	2.056	2.028	1.852	2.296	1.213
HASKA	1.940	2.005	2.201	1.836	1.780	**0.009**	2.575	2.590	2.044	1.998	1.043
BEGBR	2.982	2.908	3.445	3.321	3.414	2.828	2.883	2.595	3.261	3.282	1.972
ORKIS	4.284	5.273	2.322	5.838	4.688	1.226	3.128	3.318	3.551	4.403	6.000
MUKBR	4.883	4.647	6.000	3.909	4.601	4.463	5.343	5.140	4.977	4.683	1.516

EBD=entire databank; VW=vertical well cases; DW=deviated well cases; VNH=vertical well cases without Hagedorn and Brown data; ANH=all well cases without Hagedorn and Brown data; AB=all well cases with 75% bubble flow; AS=all well cases with 100% slug flow; VS=vertical well cases with 100% slug flow; SNH=all well cases with 100% slug flow without Hagedorn and Brown data; VSNH=vertical well cases with 100% slug flow without Hagedorn and Brown data; AAN=all well cases with 100% annular flow; HAGBR=Hagedorn and Brown correlation; AZIZ=Aziz *et al.* correlation; DUNRS=Duns and Ros correlation; HASKA=Hasan and Kabir mechanistic model; BEGBR=Beggs and Brill correlation; ORKIS=Orkiszewski correlation; MUKBR=Mukherjee and Brill correlation.

$$+\frac{E_3-E_{3_{min}}}{E_{3_{max}}-E_{3_{min}}}+\frac{|E_4|-|E_{4_{min}}|}{|E_{4_{max}}|-|E_{4_{min}}|}$$

$$+\frac{E_5-E_{5_{min}}}{E_{5_{max}}-E_{5_{min}}}+\frac{E_6-E_{6_{min}}}{E_{6_{max}}-E_{6_{min}}}. \quad \ldots\ldots\ldots\ldots\ldots\ldots (112)$$

The minimum and maximum possible values for F_{rp} are 0 and 6, indicating the best and worst performances, respectively.

The evaluation of the model in terms of F_{rp} is given in **Table 2,** with the best value for each column being boldfaced.

Overall Evaluation. The overall evaluation involves the entire comprehensive model so as to study the combined performance of all the independent flow pattern behavior models together. The evaluation is first performed by using the entire data bank, resulting in Col. 1 of Table 2. Model performance is also checked for vertical well cases only, resulting in Col. 2 of Table 2, and for deviated well cases only, resulting in Col. 3 of Table 2. To make the comparison unbiased with respect to the correlations, a second database was created that excluded 331 sets of data from the Hagedorn and Brown study. For this reduced data bank, the results for all vertical well cases are shown in Col. 4 of Table 2, and the results for combined vertical and deviated well cases are shown in Col. 5 of Table 2.

Evaluation of Individual Flow Pattern Models. The performance of individual flow pattern models is based on sets of data that are dominant in one particular flow pattern, as predicted by the transitions described earlier. For the bubble flow model, well cases with bubble flow existing for more than 75% of the well length are considered in order to have an adequate number of cases. These results are shown in Col. 6 of Table 2. Cols. 7 through 10 of Table 2 give results for well cases predicted to have slug flow exist for 100% of the well length. The cases used for Col. 7 and 8 were selected from the entire data bank, whereas the cases used for Cols. 9 and 10 and 11 were selected from the reduced data bank that eliminated the Hagedorn and Brown data, which is one-third of all the vertical well cases. Finally, Col. 11 of Table 2 gives results for those cases in the total data bank that were predicted to be in annular flow for 100% of the well length.

Complete performance results of each model or correlation against individual statistical parameters (E_1, E_6) are given in the supplement to this paper.[40]

Conclusions

From Cols. 1 through 11 of Table 2, the performance of the model and other empirical correlations indicates the following.

1. The overall performance of the comprehensive model is superior to all other methods considered. However, the overall performances of the Hagedorn and Brown, Aziz *et al.*, Duns and Ros, and Hasan and Kabir models are comparable to that of the model. For the last three, this can be attributed to the use of flow mechanisms in these methods. The excellent performance of the Hagedorn and Brown correlation can be explained only by the extensive data used in its development and modifications made to the correlation. In fact, when the data without Hagedorn and Brown well cases are considered, the model performed the best (Cols. 4 and 5).

2. Although the Hagedorn and Brown correlation performed better than the other correlations and models for deviated wells, none of the methods gave satisfactory results (Col. 3).

3. Only 29 well cases were found with over 75% of the well length predicted to be in bubble flow. The model performed second best to the Hasan and Kabir mechanistic model for bubble flow (Col. 6).

4. The performance of the slug flow model is exceeded by the Hagedorn and Brown correlation when the Hagedorn and Brown data are included in the data bank (Cols. 7 and 8). The model performed best when Hagedorn and Brown data are not included for all well cases and all vertical well cases (Cols. 9 and 10).

5. The performance of the annular flow models is significantly better than all other methods (Col. 11).

6. Several variables in the mechanistic model, such as bubble rise velocities and film thickness, are dependent on pipe inclination angle. Modifications to include inclination angle effects on these variables should further improve model performance.

Acknowledgments

We thank the TUFFP member companies whose membership fees were used to fund part of this research project, and Pakistan Petroleum Ltd. for the financial support provided A.M. Ansari.

References

1. Ozon, P.M., Ferschneider, G., and Chwetzoff, A.: "A New Multiphase Flow Model Predicts Pressure and Temperature Profiles," paper SPE 16535 presented at the 1987 SPE Offshore Europe Conference, Aberdeen, Sept. 8–11, 1987.
2. Hasan, A.R. and Kabir, C.S.: "A Study of Multiphase Flow Behavior in Vertical Wells," *SPEPE* (May 1988) 263.
3. Taitel, Y., Barnea, D., and Dukler, A.E.: "Modelling Flow Pattern Transitions for Steady Upward Gas-Liquid Flow in Vertical Tubes," *AIChE J.* (1980) **26,** 345.
4. Barnea, D., Shoham, O., and Taitel, Y.: "Flow Pattern Transition for Vertical Downward Two-Phase Flow," *Chem. Eng. Sci.* (1982) **37,** 741.
5. Barnea, D.: "A Unified Model for Predicting Flow-Pattern Transition for the Whole Range of Pipe Inclinations," *Intl. J. Multiphase Flow* (1987) **13,** 1.
6. Harmathy, T.Z.: "Velocity of Large Drops and Bubbles in Media of Infinite or Restricted Extent," *AIChE J.* (1960) **6,** 281.
7. Scott, S.L. and Kouba, G.E.: "Advances in Slug Flow Characterization for Horizontal and Slightly Inclined Pipelines," paper SPE 20628 presented at the 1990 SPE Annual Technical Conference and Exhibition, New Orleans, Sept. 23–26.
8. Caetano, E.F.: "Upward Vertical Two-Phase Flow Through an Annulus," PhD dissertation, U. of Tulsa, Tulsa, OK (1985).
9. Zuber, N. and Hench, J.: "Steady State and Transient Void Fraction of Bubbling Systems and Their Operating Limits. Part 1: Steady State Operation," General Electric Report 62GL100 (1962).
10. Fernandes, R.C., Semait, T., and Dukler, A.E.: "Hydrodynamic Model for Gas-Liquid Slug Flow in Vertical Tubes," *AIChE J.* (1986) **29,** 981.
11. Sylvester, N.D.: "A Mechanistic Model for Two-Phase Vertical Slug Flow in Pipes," *ASME J. Energy Resources Tech.* (1987) **109,** 206.
12. McQuillan, K.W. and Whalley, P.B.: "Flow Patterns in Vertical Two-Phase Flow," *Intl. J. Multiphase Flow* (1985) **11,** 161.
13. Brotz, W.: "Uber die Vorausberechnung der Absorptionsgesch-windigkeit von Gasen in Stromenden Flussigkeitsschichten," *Chem. Ing. Tech.* (1954) **26,** 470.
14. Schmidt, Z.: *Experimental Study of Gas-Liquid Flow in a Pipeline-Riser System,* MS thesis, U. of Tulsa, Tulsa (1976).
15. Vo, D.T. and Shoham, O.: "A Note on the Existence of a Solution for Two-Phase Slug Flow in Vertical Pipes," *ASME J. Energy Resources Tech.* (1989) **111,** 64.
16. Dukler, A.E., Maron, D.M., and Brauner, N.: "A Physical Model for Predicting the Minimum Stable Slug Length," *Chem. Eng. Sci.* (1985) 1379.
17. Wallis, G.B.: *One-Dimensional Two-Phase Flow,* McGraw-Hill Book Co. Inc., New York City (1969).
18. Hewitt, G.F. and Hall-Taylor, N.S.: *Annular Two-Phase Flow,* Pergamon Press, Houston (1970).
19. Whalley, P.B. and Hewitt, G.F.: "The Correlation of Liquid Entrainment Fraction and Entrainment Rate in Annular Two-Phase Flow," UKAEA Report AERE-R9187, Harwell (1978).
20. Alves, I.N. *et al.*: "Modeling Annular Flow Behavior for Gas Wells," paper presented at the 1988 Winter Annual Meeting of ASME, Chicago, Nov. 27–Dec. 2.
21. Lopes, J.C.B. and Dukler, A.E.: "Droplet Entrainment in Vertical Annular Flow and Its Contribution to Momentum Transfer," *AIChE J.* (1986) 1500.
22. Govier, G.W. and Fogarasi, M.: "Pressure Drop in Wells Producing Gas and Condensate," *J. Cdn. Pet. Tech.* (Oct.–Dec. 1975) 28.
23. Asheim, H.: "MONA, An Accurate Two-Phase Well Flow Model Based on Phase Slippage," *SPEPE* (May 1986) 221.
24. Chierici, G.L., Ciucci, G.M., and Sclocchi, G.: "Two-Phase Vertical Flow in Oil Wells—Prediction of Pressure Drop," *JPT* (Aug. 1974) 927.
25. Poettmann, F.H. and Carpenter, P.G.: "The Multiphase Flow of Gas, Oil and Water Through Vertical Flow Strings with Application to the Design and Gas-Lift Installations," *Drill. & Prod. Prac.,* API, Dallas (1952) 257.

26. Fancher, G.H., and Brown, K.E.: "Prediction of Pressure Gradients for Multiphase Flow in Tubing," *Trans.*, AIME (1963) **228,** 59.
27. Hagedorn, A.R.: "Experimental Study of Pressure Gradients Occurring during Continuous Two-Phase Flow in Small Diameter Vertical Conduits," PhD dissertation, U. of Texas, Austin (1964).
28. Baxendell, P.B.: "The Calculation of Pressure Gradients in High Rate Flowing Wells," *JPT* (Oct. 1961) 1023.
29. Orkiszewski, J.: "Predicting Two-Phase Pressure Drops in Vertical Pipes," *JPT* (June 1967) 829.
30. Espanol, H.J.H.: "Comparison of Three Methods for Calculating a Pressure Traverse in Vertical Multi-Phase Flow," MS thesis, U. of Tulsa, Tulsa, OK (1968).
31. Messulam, S.A.G.: "Comparison of Correlations for Predicting Multiphase Flowing Pressure Losses in Vertical Pipes," MS thesis, U. of Tulsa, Tulsa, OK (1970)
32. Camacho, C.A.: "Comparison of Correlations for Predicting Pressure Losses in High Gas-Liquid Ratio Vertical Wells," MS thesis, U. of Tulsa, Tulsa, OK (1970).
33. Duns, H. Jr. and Ros, N.C.J.: "Vertical Flow of Gas and Liquid Mixtures in Wells," *Proc.*, 6th World Pet. Cong. (1963) 451.
34. Brill, J.P.: "Discontinuities in the Orkiszewski Correlation for predicting pressure Gradients in Wells," *J. Energy Res. Tech.* (March, 1989) **41,** 34.
35. Beggs, H.D. and Brill, J.P.: "A Study of Two-Phase Flow in Inclined Pipes," *JPT* (May 1973) 607.
36. Palmer, C.M.: "Evaluation of Inclined Pipe Two-Phase Liquid Holdup Correlations Using Experimental Data," MS thesis, U. of Tulsa, Tulsa, OK (1975).
37. Mukherjee, H. and Brill, J.P.: "Pressure Drop Correlations for Inclined Two-Phase Flow," *J. Energy Res. Tech.* (Dec. 1985).
38. Aziz, K., Govier, G.W., and Fogarasi, M.: "Pressure Drop in Wells Producing Oil and Gas," *J. Cdn. Pet. Tech.* (July–Sept. 1972) 38.
39. Kabir, C.S. and Hasan, A.R.: "Performance of a Two-Phase Gas/Liquid Flow Model in Vertical Wells," *JPSE* (1990) **4,** 273.
40. Ansari, A.M. *et al.*: "Supplement to paper SPE 20630, A Comprehensive Mechanistic Model for Upward Two-Phase Flow in Wellbores," paper SPE 28671 available at SPE headquarters, Richardson, TX.

Nomenclature

a = coefficient defined in Eq. 55
A = cross-sectional area of pipe, L, m^2
b = coefficient defined in Eq. 56
c = coefficient defined in Eq. 57
C = constant factor relating friction factor to Reynolds number for smooth pipes
C' = coefficient defined in Eq. 48
d = pipe diameter, L, m
e = error function
E_1 = average percentage error, %
E_2 = absolute average percentage error, %
E_3 = standard deviation, %
E_4 = average error, m/Lt^2, psi
E_5 = absolute average error, m/Lt^2, psi
E_6 = standard deviation, m/Lt^2, psi
f = friction factor
F_E = fraction of liquid entrained in gas core
F_{rp} = relative performance factor, defined in Eq. 112
g = gravity acceleration, m/s^2
h = local holdup fraction
H = average holdup fraction
L = length along the pipe, m
n = number of well cases
n' = exponent to account for the swarm effect on bubble rise velocity
N_{Re} = Reynolds number
p = pressure, m/Lt^2, psi
q = flow rate, L^3/t m^3/s
S = wetted perimeter, L, m
v = velocity, L/t m/s
V = volume, L^3, m^3
X = Lockhart and Martinelli parameter
Y = Lockhart and Martinelli parameter
Z = empirical factor defining interfacial friction
β = length ratio, defined in Eq. 31
δ = film thickness, L, m
δ = ratio of film thickness to diameter
$\overline{\Delta}$ = difference
ε = absolute pipe roughness, L, m
θ = angle from horizontal, rad or deg
λ = no-slip holdup fraction
μ = dynamic viscosity, kg/m·s, kg/m^{-s}
ν = kinematic viscosity, L^2/t, m^2/sq
ρ = density, m/L^3, kg/m^3
σ = surface tension, m/t^2, dyne/cm
τ = shear stress, m/Lt^2, N/m^3
ϕ = dimensionless groups defined in Eqs. 94 and 95

Subscripts

a = acceleration
A = average
c = Taylor bubble cap, core
$crit$ = critical
e = elevation
f = friction
F = film
g = gas
H = hydraulic
i = ith element
I = interfacial
L = liquid
LS = liquid slug
m = mixture
M = modified
max = maximum
min = minimum
N = Nusselt
p = pipe
r = relative
s = slip
S = superficial
SU = slug unit
t = total
TB = Taylor bubble
TP = two-phase

Superscript

* = developing slug flow

SI Metric Conversion Factor

in.	×2.54*	E+00 = cm

*Conversion factor is exact.

SPEPF

Original SPE manuscript received for review Sept. 2, 1990. Revised manuscript received Sept. 29, 1993. Paper accepted for publication Dec. 6, 1993. Paper (SPE 20630) first presented at the 1990 SPE Annual Technical Conference & Exhibition held in New Orleans, Sept. 23–26.

A.M. Ansari, a senior petroleum engineer, joined Pakistan Petroleum Ltd. in 1989. He holds a BS degree in mechanical engineering from NED U., Karachi, and an MS degree in petroleum engineering from the U. of Tulsa. **Nicholas D. Sylvester** is dean of engineering at the U. of Akron. He holds a BS degree from Ohio U. and a PhD degree from Carnegie-Mellon U., both in chemical engineering. Previously he served as dean of engineering and applied sciences and chairman of petroleum engineering at the U. of Tulsa. Sylvester has numerous publications in the areas of two-phase and non-Newtonian fluid flow as well as oil field pollution control. **Cem Sarica** is a research associate in the petroleum engineering department at the U. of Tulsa. He holds BS and MS degrees in petroleum engineering from Istanbul Technical U., and a PhD degree in petroleum engineering from the U. of Tulsa. He was an assistant professor of petroleum engineering at Istanbul Technical U. before joining the U. of Tulsa. His research interests are multiphase flow in pipes, oil and gas production, and fluid flow in porous media. **Ovadia Shoham** is an associate professor of petroleum engineering at the U. of Tulsa. He received his PhD degree in mechanical engineering from Tel Aviv U., his MS degree in chemical engineering from the U. of Houston, and his BS degree in chemical engineering from the Technion in Israel. Shoham currently teaches and conducts research in the area of modeling two-phase flow in pipes and its application in oil and gas production, transportation, and separation. He has over fifty publications in the areas of two-phase flow and production operations. Shoham served in several capacities in the Tulsa U. Fluid Flow Projects (1982–1991), including Director of Research. He was a member of the Production Operation Technical Committee (1990–1992) and served as a member of the planning committee of the Forum Series on Multiphase Flow in 1992. **James P. Brill** is the F.M. Stevenson professor of petroleum engineering at the U. of Tulsa and founder and Executive Director of the Tulsa U. Fluid Flow Projects. He holds a BS degree from the U. of Minnesota and a PhD in petroleum engineering from the U. of Texas at Austin. He currently teaches and conducts research in the areas of two-phase flow in pipes and production design and has published extensively in these areas. Brill was a member of the Distinguished Lecturer Committee, a 1982 Distinguished Lecturer, 1978–81 Engineering Manpower Committee member, a member of the Education and Professionalism Committee for the 1971 and 1976 Annual Meetings, and a member of the Education and Accreditation Committee during 1967–70. He has served as an SPE representative to the ABET Engineering Accreditation Commission and ex-officio member of the Education and Accreditation Committee since 1990.

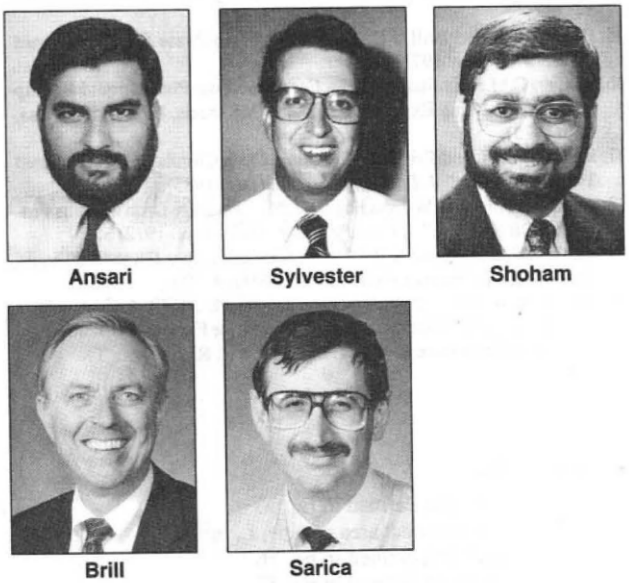

Predicting Two-Phase Pressure Drops in Vertical Pipe

J. ORKISZEWSKI*

ESSO PRODUCTION RESEARCH CO.
HOUSTON, TEX.

ABSTRACT

A method is presented which can accurately predict, with a precision of about 10 percent, two-phase pressure drops in flowing and gas-lift production wells over a wide range of well conditions. The method is an extension of the work done by Griffith and Wallis[11] and was found to be superior to five other published methods. The precision of the method was verified when its predicted values were compared against 148 measured pressure drops. The unique features of this method over most others are that liquid holdup is derived from observed physical phenomena, the pressure gradient is related to the geometrical distribution of the liquid and gas phase (flow regimes), and the method provides a good analogy of what happens inside the pipe. It takes less than a second to obtain a prediction on the IBM 7044 computer.

INTRODUCTION

The problem of accurately predicting pressure drops in flowing or gas-lift wells has given rise to many specialized solutions for limited conditions, but not to any generally accepted one for broad conditions. The reason for these many solutions is that the two-phase flow is complex and difficult to analyze even for the limited conditions studied. Under some conditions, the gas moves at a much higher velocity than the liquid. As a result, the down-hole flowing density of the gas-liquid mixture is greater than the corresponding density, corrected for down-hole temperature and pressure, that would be calculated from the produced gas-liquid ratio. Also, the liquid's velocity along the pipe wall can vary appreciably over a short distance and result in a variable friction loss. Under other conditions, the liquid is almost completely entrained in the gas and has very little effect on the wall friction loss. The difference in velocity and the geometry of the two phases strongly influence pressure drop. These factors provide the basis for categorizing two-phase flow. The generally accepted categories (flow regimes) of two-phase flow are bubble, slug, (slug-annular) transition and annular-mist.** They are ideally depicted in Fig. 1 and briefly described as follows.

BUBBLE FLOW (FIG. 1A)

The pipe is almost completely filled with the liquid and the free-gas phase is small. The gas is present as small bubbles, randomly distributed, whose diameters also vary randomly. The bubbles move at different velocities depending upon their respective diameters. The liquid moves up the pipe at a fairly uniform velocity and, except for its density, the gas phase has little effect on the pressure gradient.

SLUG FLOW (FIG. 1B)

In this regime, the gas phase is more pronounced. Although the liquid phase is still continuous, the gas bubbles coalesce and form stable bubbles of approximately the same size and shape which are nearly the diameter of the pipe. They are separated by slugs of liquid. The bubble velocity is greater than that of the liquid and can be predicted in relation to the velocity of the liquid slug.[12] There is a film of liquid around the gas bubble. The liquid velocity is not constant—whereas the liquid slug always moves upward (in the direction of bulk flow); the liquid in the film may move upward but possibly at a lower velocity, or it may move downward. These varying liquid velocities will result not only in varying wall friction losses, but also in a "liquid holdup" which will influence flowing density. At higher flow velocities, liquid can even be entrained in the gas bubbles. Both the gas and liquid phases have significant effects on the pressure gradient.

TRANSITION FLOW (FIG. 1C)

The change from a continuous liquid phase to a continuous gas phase occurs in this region. The liquid slug between the bubbles virtually disappears, and a significant amount of liquid becomes entrained in the gas phase. Although the effects of the liquid are significant, the gas phase is more predominant.

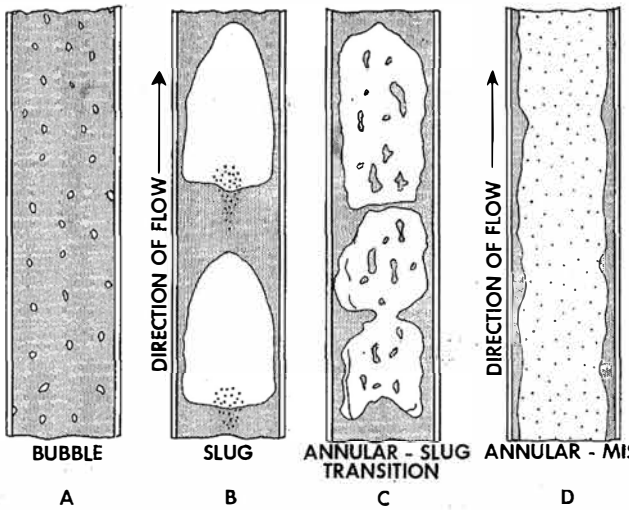

FIG. 1—GEOMETRICAL CONFIGURATIONS IN VERTICAL FLOW.

Original manuscript received in Society of Petroleum Engineers office August 8, 1966. Revised manuscript of SPE 1546 received March 1, 1967. Paper was presented at 41st Annual Fall Meeting held in Dallas, Tex., Oct. 2-5, 1966.

*Presently with International Petroleum Co. Ltd., Talara, Peru.

[11]References given at end of paper.

**All four regimes could conceivably exist in the same well. An example would be a deep well producing light oil from a reservoir which is near its bubble point. At the bottom of the hole, with little free gas present, flow would be in the bubble regime. As the fluid moves up the well, the other regimes would be encountered because gas continually comes out of solution, and the pressure continually decreases. Normally, however, flow is in the slug regime and rarely in mist, except for condensate reservoirs or steam-stimulated wells.

ANNULAR-MIST FLOW (FIG. 1D)

The gas phase is continuous. The bulk of the liquid is entrained and carried in the gas phase. A film of liquid wets the pipe wall, but its effects are secondary. The gas phase is the controlling factor.

To cope with the complex problem, the many published methods were analyzed to determine whether any one method was broad enough, or had the ingredients to be broad enough, to accurately predict pressure drops over a wide range of well conditions. The methods were first categorized. Certain methods were selected from each category to predict pressure drops for two selected well cases whose flow conditions were significantly different from those originally used in developing the various methods. Finally, the predicted pressure drops using the more promising methods were compared against known values taken from 148 cases having widely varying conditions of rate, GOR, tubing size, water cut and fluid properties.

BASIS FOR SELECTING METHODS STUDIED

Based upon similarity in theoretical concepts, the published methods were first divided into three categories. From each category certain methods were selected, based on whether they were original or unique, and were developed from a broad base of data. The discriminating features of the three categories are shown.

CATEGORY 1 (REFS. 1, 3-6, 9)

Liquid holdup is not considered in the computation of the density. The density is simply the composite density of the produced (top-hole) fluids corrected for down-hole temperature and pressure. The liquid holdup and the wall friction losses are expressed by means of an empirically correlated friction factor. No distinctions are made among flow regimes.

CATEGORY 2 (REFS. 7, 8, 10)

Liquid holdup is considered in the computation of the density. The liquid holdup is either correlated separately or combined in some form with the wall friction losses. The friction losses are based on the composite properties of the liquid and gas. No distinctions are made among flow regimes.

CATEGORY 3 (REFS. 2, 11-13)

The calculated density term considers liquid holdup. Liquid holdup is determined from some concept of slip velocity (the difference between the gas and liquid velocities). The wall friction losses are determined from the fluid properties of the continuous phase. Four distinct flow regimes are considered.

Of the 13 methods categorized, two from each category were selected for further study. The methods of Poettmann and Carpenter,[1] and Tek[4] were picked from Category 1. Most of the methods in this category are extensions of the Poettmann-Carpenter work. In the second category, the Hughmark and Pressburg method[8] was selected; the Hagedorn and Brown method[10] was not available at the time of the initial screening, but it was included in the final detailed evaluation. There are really only two methods in Category 3. The Griffith[12] and the Griffith and Wallis[11] methods are synonymous; the Nicklin, Wilkes, and Davidson method[13] is for special conditions and parallels the work of Griffith-Wallis. The other method is that of Duns and Ros.[2]

RESULTS OF THE COMPARISON

The five methods initially selected, whose results were hand calculated, were compared by determining the deviation between predicted and measured pressure drops for the first two well conditions listed in Table 1. Fig. 2 compares the predictions for Well 1. The results were similar for Well 2. The most accurate methods (Duns-Ros and Griffith-Wallis) were then programmed for machine computation and further tested against 148 well conditions.*

Neither method proved accurate over the entire range of conditions used. Although the Griffith-Wallis method was reliable in the lower flow-rate range of slug flow, it was not accurate in the higher range. The Duns-Ros method exhibited the same behavior except that it was also inaccurate for the high-viscosity oils in the low flow-rate range. The Griffith-Wallis method appeared to provide the better foundation for an improved general solution although its predicted values were in greater error (21.9 percent) than Duns and Ros (2.4 percent). The heart of this method, prediction of slip velocity, is derived from physical observation. However, since friction drop was

*The data in Table 1 are from 22 Venezuelan heavy-oil wells. In addition to the data presented in Table 1, the data used are from the publications of Poettmann and Carpenter,[1] Baxendell and Thomas,[3] Fancher and Brown,[6] and Hagedorn and Brown.[9] These represent 126 additional pieces of data.

TABLE 1—PHYSICAL CONDITIONS AND FLOW RATES OF HEAVY-OIL WELLS STUDIED

Well No.	Oil Rate (B/D)	GOR (scf/bbl)	Water Cut (%)	Oil Gravity (°API)	Measured Depth (ft)	Wellhead Pressure (psig)	Flow String Diameter (in.)	Measured Δp (psi)
1	320	4020	30	10.3	4360	250	8.76	810
2	175	6450	17	9.5	4360	300	8.76	925
3	1065	765	—	15.1	3825	550	2.992	650
4	1300	252	—	14.6	3940	150	"	850
5	3166	1430	—	14.4	3800	700	"	550
6	1965	232	—	14.4	3720	300	"	900
7	1165	957	—	15.6	4240	700	"	850
8	1965	1500	—	13.5	4570	850	"	650
9	2700	267	—	15.6	4175	300	"	1200
10	855	185	—	12.9	4355	250	"	1450
11	2320	1565	—	13.6	4670	910	"	740
12	2480	858	—	18.6	4575	650	"	900
13	1040	472	—	18.6	4400	400	"	950
14	1490	341	—	13.0	4065	500	"	1050
15	1310	335	—	13.6	3705	500	"	950
16	1350	185	—	12.9	4160	150	"	1350
17	788	222	—	16.0	4210	350	"	1400
18	1905	962	—	14.1	4487	580	"	720
19	967	193	—	13.3	4766	250	"	1300
20	1040	385	—	12.5	4505	250	"	1100
21	1585	865	—	12.9	4692	400	"	750
22	1850	575	—	18.7	3924	700	"	800

negligible in the work, the method for predicting friction losses is an approximation and therefore open to improvement. On the other hand, the Duns and Ros work in this range (which they termed plug flow) is presented as a complex set of interrelated parameters and equations, and is therefore difficult to relate to what physically occurs inside the pipe.

The Griffith-Wallis work was extended to include the high-velocity flow range. In modifying the method, a parameter was developed to account for (1) the liquid distribution among the liquid slug, the liquid film and entrained liquid in the gas bubble and (2) the liquid holdup at the higher flow velocities. This parameter served to better approximate wall friction losses and flowing density, and was principally correlated from the earlier published data of Hagedorn and Brown.[9] The data from Table 1 were also used to determine the effects of pipe diameter on the parameter. The details of the parameter evaluation are given in Appendix C and a brief description of the modified Griffith-Wallis method is outlined in Appendix A.

The results of the study, summarized in Table 2, are presented as the deviations between predicted and measured values for the modified Griffith-Wallis, the Duns-Ros and the then recently published Hagedorn-Brown[10] methods. (The Hagedorn-Brown method was included because of the excellent accuracies reported and the broad data range presented.) Plots of the individual predicted and measured values for the three methods are shown in Figs. 3 through 5. When the three methods are compared against the various grouped data sources (Table 2), only the modified Griffith-Wallis method is sufficiently accurate (average error) and precise (standard deviation) over the entire range of conditions. None of the 148 well conditions studied were in mist flow or wholly in (annular-slug) transition. The breakdown of wells by flow regimes includes seven partly in slug and transition, 26 partly in slug and bubble, four completely in bubble and 111 completely in slug flow.

CONCLUSIONS

For general engineering work, the modified Griffith-Wallis method will predict pressure drops with sufficient accuracy and precision over a wide range of well conditions. I recommend its use. However, the method should be used with discretion for those well conditions which were not sufficiently evaluated (e.g., flow in the casing annulus and in the mist-flow regime). The method's precision might be further improved if the liquid phase distribution could be more rigorously analyzed.

This method is accurate over a broader range than previous correlations. For a prediction method to be general, it must be expressed in terms of flow regime and liquid distribution. The other methods, which were not de-

TABLE 2—SUMMARY OF DEVIATIONS BETWEEN MEASURED AND PREDICTED PRESSURE DROPS

	Prediction Method		
	This Method	Duns and Ros	Hagedorn and Brown
Over-all Results			
(148 Well conditions)			
Avg. error, percent	— 0.8	+ 2.4	+ 0.7
Std. deviation, percent	10.8	27.0	24.2
Results from Grouped Data Sources			
Table 1 — Heavy-Oil Wells (22 Wells, low to medium velocities, 10 to 20° API oils)			
Avg. error, percent	— 1.2	+22.7	+16.4
Std. deviation, percent	10.4	18.7	41.4
Baxendell-Thomas[3] (1 Well, 25 rates mostly high velocities, 34° API oil)			
Avg. error, percent	— 2.1	+ 2.3	+ 8.7
Std. deviation, percent	11.1	20.0	12.7
Fancher-Brown[6] (1 Well, 20 rates medium to high velocities, 95 percent water cut)			
Avg. error, percent	+ 0.3	+ 1.7	+ 5.4
Std. deviation, percent	11.8	32.1	10.8
Hagedorn-Brown[9] (1 Well, medium to high velocities, 16 water runs, 16 oil runs of 10 to 100 cp oil)			
Avg. error, percent	+ 0.1	—16.9	+ 1.2
Std. deviation, percent	8.2	36.6	10.3
Poettmann-Carpenter[1] (49 Wells, low to medium velocities, 15 wells high water cut, rest 36 to 54° API oils)			
Avg. error, percent	— 1.0	+ 5.8	—13.0
Std. deviation, percent	12.0	12.4	22.2

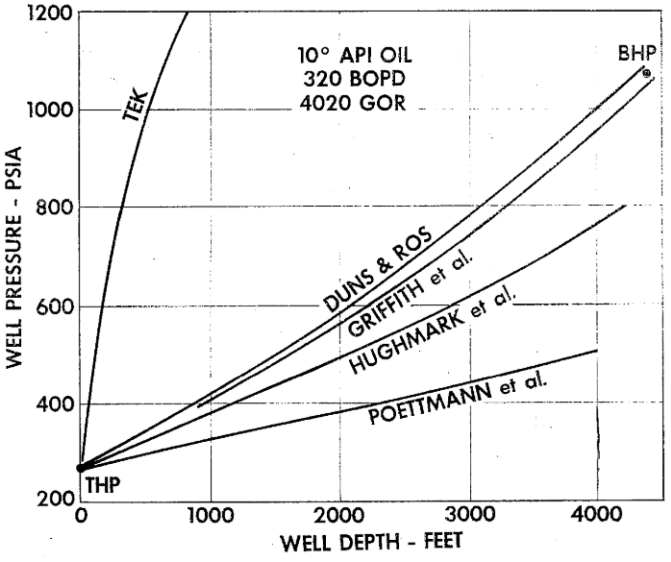

FIG. 2—COMPARISON OF PRESSURE PROFILES CALCULATED BY VARIOUS METHODS FOR WELL 1 (TABLE 1).

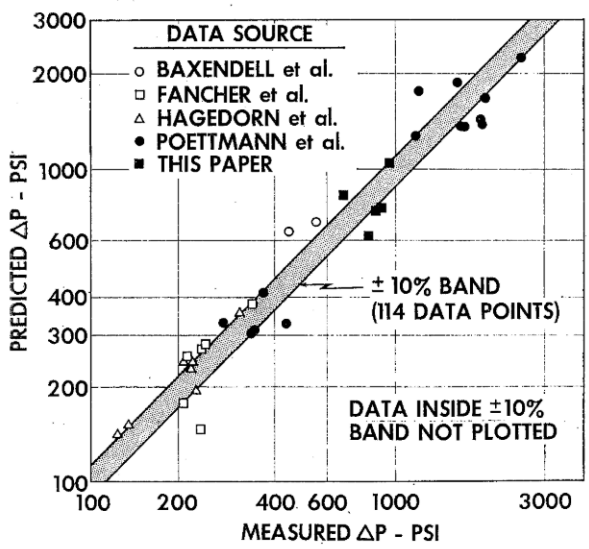

FIG. 3—THIS WORK (MODIFIED GRIFFITH AND WALLIS PREDICTION).

veloped in this manner, are only useful in the range of conditions from which they were developed.

NOMENCLATURE

A_p = flow area of pipe, sq ft
B_o = oil formation volume factor, bbl/STB
C_1, C_2 = parameters used to calculate bubble rise velocities from Eq. C-5, dimensionless, to be evaluated from Figs. 8 and 9
d_h = hydraulic pipe diameter ($4 \times A_p$/wetted perimeter), ft
D = depth from wellhead, ft
ΔD = increment of depth, ft
f = Moody friction factor, dimensionless, to be evaluated from Fig. 6
F_g = flowing gas fraction, dimensionless
g = acceleration of gravity, ft/sec^2
g_c = gravitational constant, ft-lb(mass)/lb(force)-sec^2
$(L)_B$ = bubble-slug boundary, dimensionless
$(L)_M$ = transition-mist boundary, dimensionless
$(L)_S$ = slug-transition boundary, dimensionless
N_b = 1,488 $v_b d_h \rho_L/\mu_L$, bubble Reynolds number, dimensionless
N_{Re} = 1,488 $v D_h \rho/\mu$, Reynolds number, dimensionless
p = pressure, psia
Δp = pressure drop, psi
$\overline{p}$ = average pressure, psia
p_{pc} = pseudo-critical pressure, psia
p_r = reduced pressure, dimensionless
P = pressure, lb/sq ft
q = volumetric flow rate, cu ft/sec
q_o = oil rate, B/D
R = produced GOR, scf/STB
R_s = solution gas, scf/STB
T_{pc} = pseudo-critical temperature, °R
T_r = reduced temperature, dimensionless
$\overline{T}$ = average temperature, °F
v = fluid velocity, ft/sec
v_b = bubble rise velocity (velocity of rising gas bubble relative to preceding liquid slug), ft/sec
v_{bz} = base bubble rise velocity for Eq. C-9, ft/sec
v_s = slip velocity (difference between average gas and liquid velocities), ft/sec
v_{gD} = $q_g (\sqrt[4]{\rho_L/g\sigma})/A_p$, dimensionless gas velocity
z = gas compressibility factor, dimensionless
γ = fluid specific gravity, dimensionless
Γ = liquid distribution coefficient, to be evaluated from Eqs. C-11 through C-16, dimensionless
μ = viscosity, cp
ξ/D = Moody pipe relative roughness factor (Fig. 7) and Duns-Ros mist flow factor (Eqs. C-21 and C-22), dimensionless
ρ = density, lb/cu ft
$\overline{\rho}$ = average flowing density, lb/cu ft
τ_f = friction-loss gradient, lb/sq ft/ft
σ = surface tension, lb/sec^2

SUBSCRIPTS

g = gas
L = liquid
o = oil
t = total

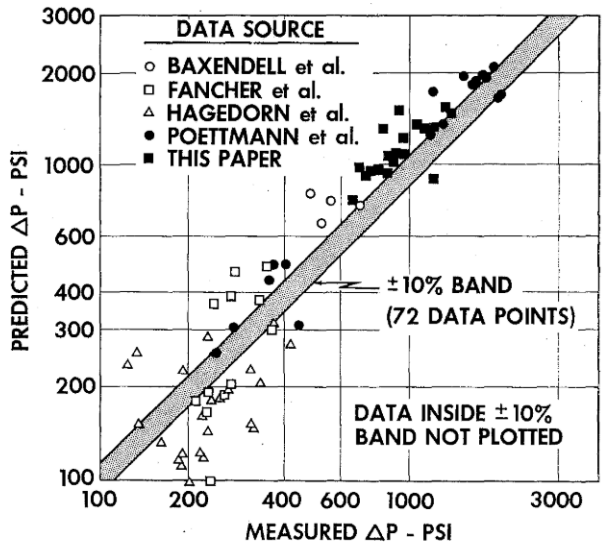

FIG. 4—DUNS AND ROS PREDICTION.[2]

ACKNOWLEDGMENT

The author wishes to thank the Creole Petroleum Corp. for supplying data in Table 1 from 22 Venezuelan heavy-oil wells.

REFERENCES

1. Poettmann, F. H. and Carpenter, P. G.: "The Multiphase Flow of Gas, Oil, and Water Through Vertical Flow Strings", *Drill. and Prod. Prac.*, API (1952) 257.
2. Duns, H., Jr., and Ros, N. C. J.: "Vertical Flow of Gas and Liquid Mixtures from Boreholes", *Proc.*, Sixth World Pet. Congress, Frankfort (June 19-26, 1963) Section II, Paper 22-PD6.
3. Baxendell, P. B. and Thomas, R.: "The Calculation of Pressure Gradients in High-Rate Flowing Wells", *J. Pet. Tech.* (Oct., 1961) 1023-1028.
4. Tek, M. R.: "Multiphase Flow of Water, Oil, and Natural Gas Through Vertical Flow Strings", *J. Pet. Tech.* (Oct., 1961) 1029-1036.
5. Yocum, B. T.: "Two-Phase Flow in Well Flowlines", *Pet. Eng.* (Nov., 1959) B-40.
6. Fancher, G. H., Jr., and Brown, K. E.: "Prediction of Pressure Gradients for Multiphase Flow in Tubing", *Soc. Pet. Eng. J.* (March, 1963) 59-69.
7. Baker, W. J. and Keep, K. R.: "The Flow of Oil and Gas Mixtures in Wells and Pipelines: Some Useful Correlations", *J. Inst. of Pet.* (May, 1961) **47**, No. 449, 162-169.
8. Hughmark, G. A. and Pressburg, B. S.: "Hold-Up and Pressure Drop with Gas-Liquid Flow in a Vertical Pipe", *AIChE J.* (Dec., 1961) **7**, No. 4, 677-682.
9. Hagedorn, A. R. and Brown, K. E.: "The Effect of Liquid Vis-

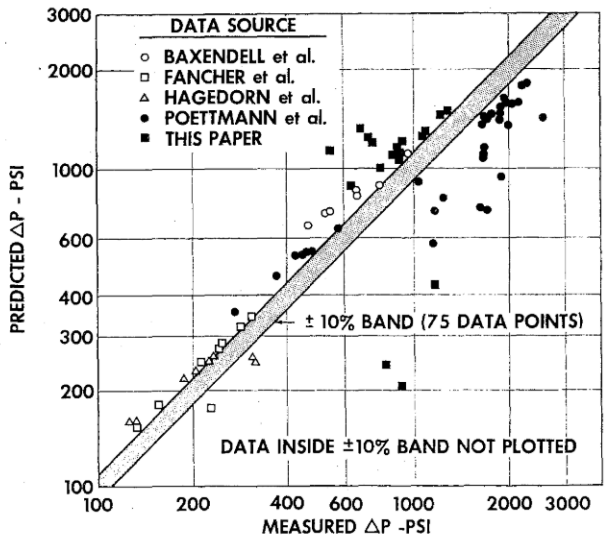

FIG. 5—HAGEDORN AND BROWN PREDICTION.[10]

cosity on Two-Phase Flow", *J. Pet. Tech.* (Feb., 1964) 203-210.

10. Hagedorn, A. R. and Brown, K. E.: "Experimental Study of Pressure Gradients Occurring During Continuous Two-Phase Flow in Small Diameter Vertical Conduits", *J. Pet. Tech.* (April, 1965) 475-484.
11. Griffith, P. and Wallis, G. B.: "Two-Phase Slug Flow", *J. Heat Transfer; Trans.*, ASME (Aug., 1961) 307-320.
12. Griffith, P.: "Two-Phase Flow in Pipes", Special Summer Program, Massachusetts Institute of Technology, Cambridge, Mass. (1962).
13. Nicklin, D. J., Wilkes, J. O. and Davidson, J. F.: "Two-Phase Flow in Vertical Tubes", *Trans.*, AIChE (1962) **40**, 61-68.
14. Stanley, D. W.: "Wall Shear Stress in Two-Phase Slug Flow", MS Thesis, Massachusetts Institute of Technology, Cambridge (June, 1962).
15. Moody, L. F.: "Friction Factors in Pipe Flow", *Trans.*, ASME (1944) **66**, 671-684.
16. Frick, T. C.: *Petroleum Production Handbook—Vol. II, Reservoir Engineering*, McGraw-Hill, New York (1962).

APPENDIX A

DESCRIPTION OF MODIFIED GRIFFITH AND WALLIS METHOD*

The fluid pressure drop in a vertical pipe is the sum effect of the energy lost by friction, the change in potential energy and the change in kinetic energy. This energy balance, which is basic to all pressure-drop calculations, can be generally written as

$$-dP = \tau_f dD + (g\rho/g_c)dD + (\rho v/g_c)dv \quad , \quad . \quad . \quad \text{(A-1)}$$

where P = pressure, lb/sq ft,
τ_f = friction-loss gradient, lb/sq ft/ft,
D = depth, ft,
g = acceleration of gravity, ft/sec^2,
g_c = gravitational consant, ft-lb(mass)/lb(force)-sec^2,
ρ = fluid density, lb/cu ft,
v = fluid velocity, ft/sec.

The procedure was credited to Griffith and Wallis because slug flow occurred in 95 percent of the cases studied. Although the mist-flow regime could not be evaluated, the Duns-Ros method was used because it appeared to be more accurate and logical than the Martinelli method recommended by Griffith. In two-phase flow, both τ_f and ρ are influenced by the flow regime type, and all three terms are functions of temperature and pressure. Therefore, to use Eq. A-1, (1) the flow string must be incremented so the fluid properties do not change markedly within any of the increments, (2) the flow regime type and corresponding variables of $\bar{\rho}$ and τ_f must be determined for each increment and (3) each increment must be evaluated by an iterative procedure.

The kinetic energy term is significant only in the mist-flow regime.[2] In mist flow $v_L << v_g$, the kinetic energy term may be expressed[1] more simply (using the gas law).

$$(\rho v/g_c)dv = -\frac{w_t q_g}{g_c A_p^2 P} dP \quad , \quad . \quad . \quad . \quad . \quad . \quad . \quad . \quad \text{(A-2)}$$

where A_p = pipe area, sq ft,

w_t = total mass flow rate, lb/sec,**

q_g = gas volumetric flow rate, cu ft/sec.**

With the above conditions and Eq. A-2, Eq. A-1 may then be expressed in a more convenient form.***

$$\Delta p_k = \left[\frac{1}{144} \frac{\bar{p} + \tau_f}{1 - w_t q_g / 4{,}637 A_p^2 \bar{p}} \right]_k \Delta D_k \quad , \quad \text{(A-3)}$$

where for average temperature-pressure conditions at increment k,

$\bar{p}$ = average fluid density, lb/cu ft,
Δp = pressure drop, psi,
$\bar{p}$ = average pressure, psia.

Since temperature is related to depth, Eq. A-3 may be incremented by either fixing ΔD and solving for Δp, or vice versa. However, since pressure usually has a greater influence on the average fluid properties than temperature, Δp should be fixed because the change in average fluid properties would then be more gradual in going from one increment to another. The value of Δp should be around 10 percent of the absolute pressure, which is known for one point in the increment, but should not be greater than 100 psi for that increment.

Pressure drops can be calculated, using Eq. A-3 in the following manner.

1. Pick a point in the flow string (e.g., wellhead or bottom-hole) where the flow rates, fluid properties, temperature and pressure are known.
2. Estimate the temperature gradient of the well.
3. Fix the Δp at about 10 percent of the measured or previously calculated pressure, which may be at either the top or bottom of the increment. Find average pressure of increment.
4. Assume a depth increment ΔD and find average depth of increment.
5. From the temperature gradient, determine average temperature of increment.
6. Correct fluid properties for temperature and pressure.
7. Determine the type of flow regime from Appendix B.
8. Based on Step 7, determine the average density ($\bar{\rho}$) and the friction loss gradient (τ_f) from Appendix C.
9. Calculate ΔD from Eq. A-3.
10. Iterate, if necessary, starting with Step 4 until assumed ΔD equals calculated ΔD.
11. Determine values of p and D for that increment.
12. Repeat procedure from Step 3 until the sum of the ΔD's equals the total length of the flow string.

A detailed example of the above calculated procedure is given in Appendix D.

APPENDIX B

DETERMINATION OF FLOW REGIME

Griffith and Wallis have defined the boundary between bubble and slug flow,[11] and Duns and Ros have defined the boundaries for the remaining three regimes.[2] The flow regime may be determined by testing whether the variables q_g/q_t *or* v_{gD}, or both, fall within the limits prescribed.

*This method is a composite of the following:

Method	Flow Regime
Griffith[12]	Bubble
Griffith and Wallis[11]	Slug (density term)
This work	Slug (friction gradient term)
Duns and Ros[2]	Transition
Duns and Ros[2]	Annular-mist

**All volumetric (q) and mass (w) flow rates are those of the produced fluids that are corrected for temperature, pressure and gas solubility.

***$\triangle Z$ is taken as positive downward. The pressure should be made discontinuous with depth should the denominator approach zero, or become negative, to estabish the shock front that characterizes sonic velocities.

Limits	Flow Regime
$q_g/q_t < (L)_B$	Bubble
$q_g/q_t > (L)_B$, $v_{gD} < (L)_S$	Slug
$(L)_M > \tilde{v}_g > (L)_S$	Transition
$v_{gD} > (L)_M$	Mist

The above variables are defined as

$$v_{gD} = q_g(\sqrt[4]{\rho_L/g\,\sigma})/A_p \quad . \quad . \quad . \quad . \quad . \quad . \quad . \quad . \quad . \quad (B\text{-}1)$$

$$(L)_B = 1.071 - (0.2218\ v_t^2/d_h, \text{ with the limit } (L) \geq 0.13 \quad . \quad . \quad . \quad . \quad . \quad . \quad . \quad . \quad . \quad (B\text{-}2)$$

$$(L)_S = 50 + 36\ v_{gD}\ q_L/q_g \quad . \quad . \quad . \quad . \quad . \quad . \quad . \quad . \quad (B\text{-}3)$$

$$(L)_M = 75 + 84\ (v_g\ q_L/q_g)^{0.75} \quad , \quad . \quad . \quad . \quad . \quad . \quad . \quad . \quad (B\text{-}4)$$

where v_{gD} = dimensionless gas velocity,

v_t = total fluid velocity (q_t/A_p), ft/sec,

ρ_L = liquid density, lb/cu ft,

σ = liquid surface tension, lb/sec^2.

APPENDIX C

EVALUATION OF AVERAGE DENSITY AND FRICTION LOSS GRADIENT

In the first four sections of this Appendix, the variables $\overline{\rho}$ and τ_f are defined for bubble flow, slug flow, transition and mist flow. The second section, while the most complex, is also the most important since slug flow had been encountered in over 95 percent of the gas-lift or flowing wells studied. The last section of this Appendix describes how τ_f was developed for the slug flow regime.

BUBBLE FLOW (REF. 12)

The void fraction of gas (F_g) in bubble flow can be expressed as

$$F_g = \frac{1}{2}\left[1 + \frac{q_t}{v_s A_p} - \sqrt{(1 + q_t/v_s A_p)^2 - \frac{4q_g}{v_s A_p}}\right], \quad . \quad . \quad . \quad . \quad . \quad . \quad . \quad . \quad . \quad (C\text{-}1)$$

where v_s = slip velocity in ft/sec. Griffith suggested that a good approximation of an average v_s is 0.8 ft/sec.* Thus, with Eq. C-1, the average flowing density can be computed as

$$\overline{\rho} = (1 - F_g)\ \rho_L + F_g \rho_g \quad . \quad . \quad . \quad . \quad . \quad . \quad . \quad (C\text{-}2)$$

The friction gradient is

$$\tau_f = f_{\rho L} v_L^2/2g_c d_h \quad , \quad . \quad . \quad . \quad . \quad . \quad . \quad . \quad . \quad . \quad (C\text{-}3)$$

where

$$v_L = q_L/[A_p\,(1 - F_g)]\,.$$

The friction factor f is obtained from Fig. 6 by using a Moody relative-roughness factor obtained from Fig. 7. The Reynolds number is calculated as $N_{Re} = 1{,}488\ \rho_L d_h v_L/\mu_L$; where d_h = hydraulic pipe diameter, ft, and μ_L = liquid viscosity, cp.

SLUG FLOW (REF. 11)

The average density term is

$$\overline{\rho} = \frac{w_t + \rho_L v_b A_p}{q_t + v_b A_p} + \Gamma\,\rho_L \quad , \quad . \quad . \quad . \quad . \quad . \quad . \quad . \quad (C\text{-}4)$$

*Athough the method is simple, it is reasonably precise. For the four wells that were wholly in bubble flow, the standard deviation was 5.1 percent, whereas the deviation was 9.8 percent for those wells partly in bubble and slug.

where Γ is a coefficient correlated from oilfield data. Griffith and Wallis correlated the bubble rise velocity v_b by the relationship

$$v_b = C_1 C_2 \sqrt{g\,d_h} \quad , \quad . \quad . \quad . \quad . \quad . \quad . \quad . \quad . \quad . \quad . \quad (C\text{-}5)$$

where C_1 is expressed in Fig. 8 as a function of bubble Reynolds number $(N_b = 1{,}488\ v_b d_h \rho_L/\mu_L)$, and C_2 is expressed in Fig. 9 as a function of both N_b and liquid Reynolds number.

$$N_{Re} = 1{,}488\ \rho_L d_h v_t/\mu_L \quad , \quad . \quad . \quad . \quad . \quad . \quad . \quad . \quad . \quad (C\text{-}6)$$

where v_t equals total velocity of liquid and gas (q_t/A_p), ft/sec.

Fig. 9 was extrapolated** so that v_b could be evaluated at the higher Reynolds numbers. When C_2 cannot be read

**The parallel work of Nicklen, Wilkes and Davidson[13] provided the basis for the extrapolation. It showed that bubble rise velocity was independent of N_b in the Reynolds number range of 9×10^3 to 1×10^5. The correlation of bubble rise velocity was found comparable to Eq. C-5 when N_b was around 8×10^3. The results were incorporated into the above extrapolation.

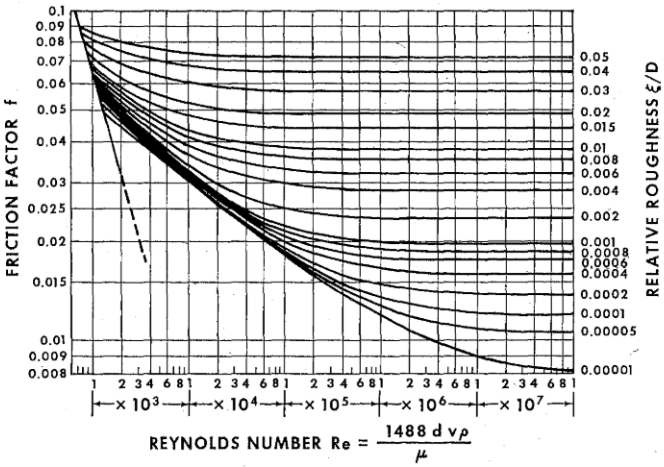

FIG. 6—MOODY FRICTION FACTOR.[15]

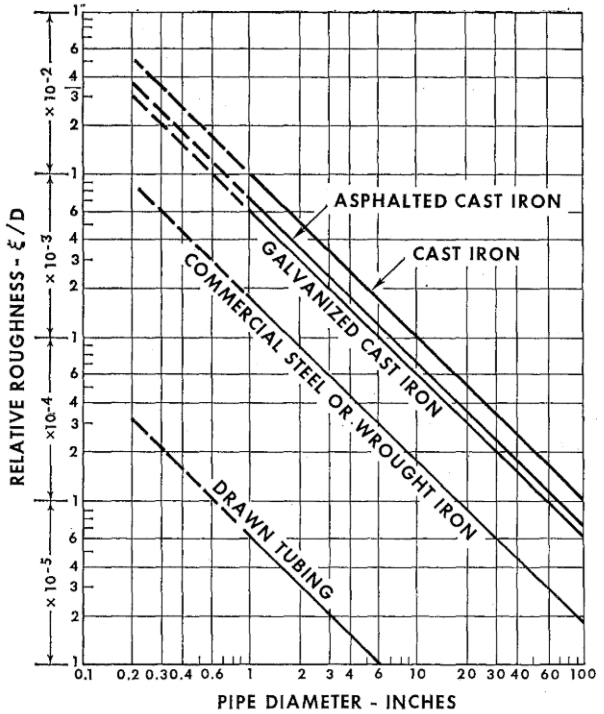

FIG. 7—EFFECT OF PIPE DIAMETER AND MATERIAL ON RELATIVE ROUGHNESS.[15]

from Fig. 9, the extrapolated values of v_b may be calculated from the following set of equations.

When $N_b \leq 3{,}000$,

$$v_b = (0.546 + 8.74 \times 10^{-6} N_{Re}) \sqrt{gd_h} \quad . \quad . \quad . \quad (C\text{-}7)$$

When $N_b \geq 8{,}000$,

$$v_b = (0.35 + 8.74 \times 10^{-6} N_{Re}) \sqrt{gd_h} \quad . \quad . \quad . \quad (C\text{-}8)$$

When $3{,}000 < N_b < 8{,}000$,

$$v_{bi} = (0.251 + 8.74 \times 10^{-6} N_{Re}) \sqrt{gd_h},$$

$$v_b = \frac{1}{2} v_{bi} + \sqrt{v_{bi}^2 + \frac{13.59\,\mu_L}{\rho_L \sqrt{d_h}}} \quad . \quad . \quad . \quad . \quad . \quad (C\text{-}9)$$

The wall friction-loss term, which has been independently derived, is expressed as

$$\tau_f = \frac{f\rho_L v_t^2}{2g_c d_h}\left[\frac{q_L + v_b A_p}{q_t + v_b A_p} + \Gamma\right] \quad . \quad . \quad . \quad . \quad . \quad (C\text{-}10)$$

The friction factor is obtained from Fig. 6 and is a function of the Reynolds number given by Eq. C-6 and the ξ/D obtained from Fig. 7. The liquid distribution coefficient Γ may be determined by the equation which meets the following conditions.

Continuous Liquid Phase	v_t	Use Equation
Water	<10	C-11
Water	>10	C-12
Oil	<10	C-13
Oil	>10	C-14

$$\Gamma = [(0.013 \log \mu_L)/d_h^{1.38}] - 0.681 + 0.232 \log v_t - 0.428 \log d_h \quad . \quad . \quad . \quad . \quad . \quad . \quad . \quad . \quad (C\text{-}11)$$

$$\Gamma = [(0.045 \log \mu_L)/d_h^{0.799}] - 0.709 - 0.162 \log v_t - 0.888 \log d_h \quad . \quad . \quad . \quad . \quad . \quad . \quad . \quad . \quad (C\text{-}12)$$

$$\Gamma = [0.0127 \log (\mu_L + 1)/d_h^{1.415}] - 0.284 + 0.167 \log v_t + 0.113 \log d_h \quad . \quad . \quad . \quad (C\text{-}13)$$

$$\Gamma = [0.0274 \log (\mu_L + 1)/d_h^{1.371}] + 0.161 + 0.569 \log d_h - \log v_t \{[0.01 \log (\mu_L + 1)/d_h^{1.571}] + 0.397 + 0.63 \log d_h\} \quad , \quad . \quad . \quad . \quad . \quad . \quad (C\text{-}14)$$

but is constrained by the limits

$$\Gamma \geq -0.065\, v_t \quad , \quad . \quad . \quad . \quad . \quad . \quad . \quad . \quad . \quad . \quad (C\text{-}15)$$

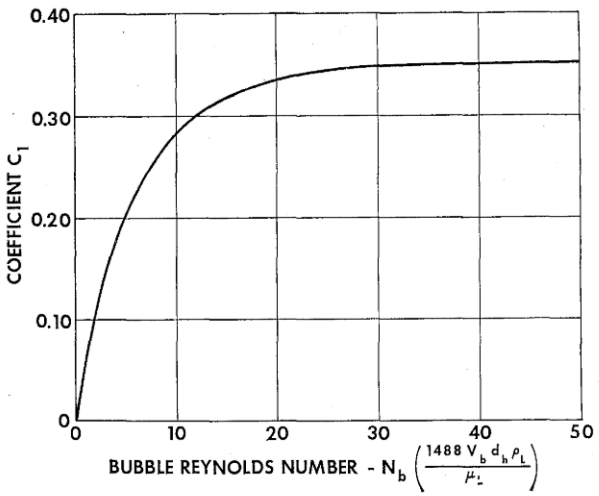

FIG. 8—GRIFFITH AND WALLIS' C_1 VS BUBBLE REYNOLDS NUMBER.

and when $v_t > 10$,

$$\Gamma \geq -\frac{v_b A_p}{q_t + v_b A_p}\left(1 - \frac{\bar{\rho}}{\rho_L}\right) \quad . \quad . \quad . \quad . \quad . \quad (C\text{-}16)$$

The above constraints eliminate pressure discontinuities between flow regimes.

TRANSITION FLOW

Duns and Ros approximated $\bar{\rho}$ and τ_f for transition flow. The method is first to calculate these terms for both slug and mist flow, and then linearly weight each term with respect to v_{gD} and the limits of the transition zone $(L)_S$ and $(L)_M$. The terms v_{gD}, $(L)_M$ and $(L)_S$ are defined in Appendix B. The average density term would be

$$\bar{\rho} = \frac{(L)_M - v_{gD}}{(L)_M - (L)_S}\left[\bar{\rho}\right]_{slug} + \frac{v_{gD} - (L)_S}{(L)_M - (L)_S}\left[\bar{\rho}\right]_{mist} \quad . \quad . \quad . \quad . \quad . \quad . \quad . \quad . \quad . \quad . \quad (C\text{-}17)$$

The friction gradient term would be weighted similarly. A more accurate friction-loss prediction is claimed if the gas volumetric flow rate for mist flow is taken as

$$q_g = A_p (L)_M (\rho_L/g\sigma)^{-1/4} \quad . \quad . \quad . \quad . \quad . \quad . \quad . \quad (C\text{-}18)$$

MIST FLOW

The average flowing density for mist flow is given in Eq. C-2. Since there is virtually no slip between the phases, F_g is

$$F_g = 1/(1 + q_L/q_g) \quad . \quad . \quad . \quad . \quad . \quad . \quad . \quad . \quad . \quad (C\text{-}19)$$

Duns and Ros express the friction-loss gradient as

$$\tau_f = f\,\rho_g v_g^2/2g_c d_h \quad , \quad . \quad . \quad . \quad . \quad . \quad . \quad . \quad (C\text{-}20)$$

where v_g is the superficial gas velocity, and f is again obtained from Fig. 6 as a function of gas Reynolds number ($N_{Re} = 1{,}488\, p_g d_h v_g/\mu_g$) and a correlated form of the Moody relative roughness factor ξ/D that was developed by Duns and Ros. In their correlation, they limit ξ/D to being no smaller than 10^{-3} but no greater than 0.5. Between these limits, ξ/D is determined from Eq. C-21 if N_w is less than 0.005 and from Eq. C-22 if N_w is greater than 0.005.

$$\xi/D = 34\,\sigma/(\rho_g v_g^2 d_h) \quad . \quad . \quad . \quad . \quad . \quad . \quad . \quad . \quad . \quad (C\text{-}21)$$

$$\xi/D = 174.8\,\sigma\,(N_w)^{0.302}/(\rho_g v_g^2 d_h) \quad , \quad . \quad . \quad . \quad . \quad (C\text{-}22)$$

where $N_w = 4.52 \times 10^{-7} (v_g \mu_L/\sigma)^2\, \rho_g/\rho_L$.

DEVELOPMENT OF τ_f FOR SLUG FLOW

A new method was developed to correlate the friction-loss gradient for slug flow because neither the Griffith and Wallis method, nor the Stanley[14] method (an outgrowth of the Griffith-Wallis work) proved accurate for the well conditions studied. (The Griffith-Wallis data were taken

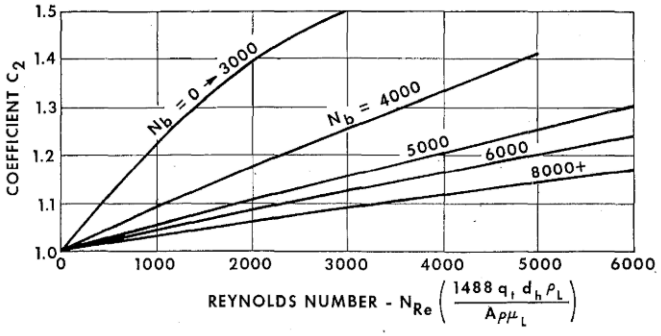

FIG. 9—GRIFFITH AND WALLIS' C_2 VS BUBBLE REYNOLDS AND REYNOLDS NUMBERS.

from low-flow velocity tests in which friction losses were minor and liquid entrainment was negligible.) This new method accounted for the complex nature of friction loss in slug flow by the introduction of a correlated liquid distribution function Γ (Eq. C-10) which implicitly accounts for the following physical phenomena.

1. Liquid is distributed in three places: the slug, the film around the gas bubble and in the gas bubble as entrained droplets. A change in this distribution will change the net friction losses.

2. The friction loss has essentially two contributions, one from the liquid slug and the other from the liquid film.

3. The bubble rise velocity approaches zero as mist flow is approached.

Values of the liquid distribution coefficient were calculated from the data of Hagedorn and Brown[9] by using Eq. A-3 of Appendix A and Eqs. C-4 through C-10 of Appendix C. (These data were selected because they covered a wide range of conditions for each of the four liquids used.) These values correlate with total fluid velocity and liquid viscosity. Fig. 10 shows the results where the fluid is water, and Fig. 11 shows the results where the fluids are oil. Coefficients were also calculated for the heavy-oil wells shown in Table 1, but these values were small and scattered because τ_f was small in comparison to $\overline{\rho}$. Nevertheless, the results were sufficiently grouped to show that pipe diameter (d_h) is another independent variable.

Neither the reversal in slopes nor the data scatter as seen in Figs. 10 and 11 can be resolved without additional experimental work. It is probable, however, that the slope reversal may be due to liquid entrained in the gas phase

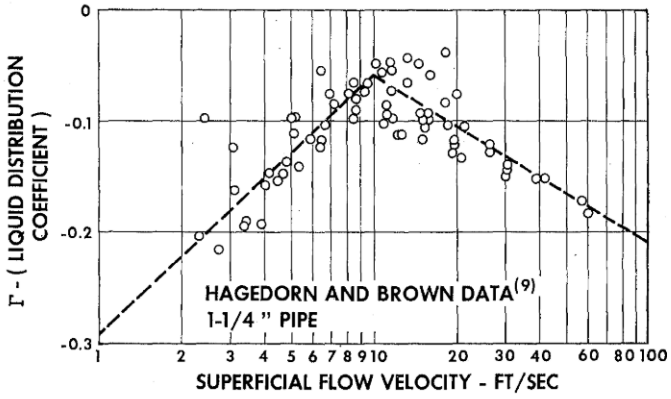

FIG. 10—EFFECT OF VELOCITY ON WATER DISTRIBUTION COEFFICIENT.

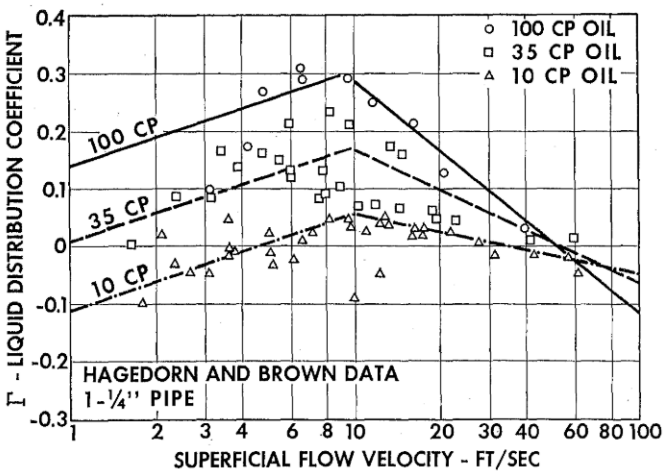

FIG. 11—OIL DISTRIBUTION COEFFICIENT AFFECTED BY BOTH VELOCITY AND VISCOSITY.

TABLE 3 — FLOW RATES AND PHYSICAL CONDITIONS OF HEAVY-OIL WELL 22

Oil Rate (q_o)	1,850 STB/D	Oil Specific Gravity (γ_o)	0.942
Produced GOR (R)	575 scf/ STB	Gas Specific Gravity (γ_g)	0.75
Total depth (D)	3,890 ft	Wellhead Pressure	670 psia
Tubing diameter (d_h)	0.249 ft	Tubing Area A_p	0.0488 sq ft
Temperatures:		Dead Oil Viscosity:	
Wellhead	126F	at 100F	89 cp
Reservoir	150F	at 210F	8.8 cp

and that the data scatter may be attributable to such additional parameters as liquid velocity, GOR and interfacial tension.

APPENDIX D

EXAMPLE OF TWO-PHASE PRESSURE DROP CALCULATION

An example calculation of the modified Griffith-Wallis method is presented to illustrate the details of the procedure outlined in Appendix A. In this example we will predict the pressure drop for heavy-oil Well 22 (Table 1). The input well data required for the calculation are given in Table 3. In addition, we will need the following correlations* that correct fluid properties for pressure and temperature:

Gas pseudo-critical properties (Katz *et al.*) T_{pc}, p_{pc}.

Gas compressibility (Brown *et al.*) z.

Live oil viscosity (Chew and Connally) μ.

Oil formation volume factor (Standing) B_o.

Solution gas (Lasater) R_s.

For calculational convenience, the temperature-viscosity-depth data contained in Table 3 should be plotted. The temperature-depth plot is shown in Fig. 12, and log viscosity-log temperature plot is shown in Fig. 13.

The detailed procedure for the calculation of the pressure drop for the first increment ($k = 1$) is as follows.

1. Based on the 670-psia wellhead pressure, fix Δp at 100 psi. Assume ΔD to be 540 ft. The average pressure ($\overline{p}$) and depth ($\overline{D}$) of increment k is then:

$$\overline{p}_k = p_{k-1} + \frac{\Delta p_k}{2} = 670 + \frac{100}{2} = 720 \text{ psia}$$

$$\overline{D}_k = D_{k-1} \frac{\Delta D_k}{2} = 0 + \frac{540}{2} = 270 \text{ ft.}$$

The average temperature ($\overline{T}$), read from Fig. 12 is 127.5F.

*These are conveniently found in Frick's *Petroleum Production Handbook, Vol. II* (Ref. 16).

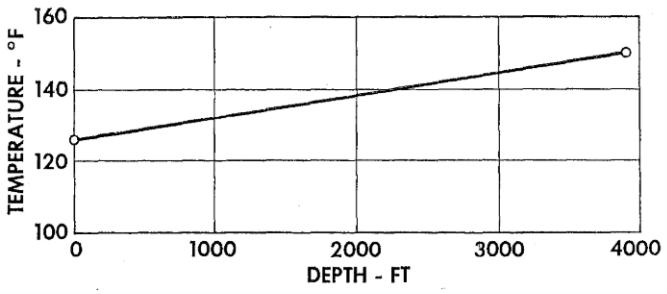

FIG. 12—TEMPERATURE VS DEPTH — WELL 22.

2. With the condition determined in Step 1, the fluid properties are corrected for temperature and pressure.

From Frick[16] the following values are obtained.

$R_s = 115$ scf/bbl (page 19-9).*

$B_o = 1.073$ bbl/STB (page 19-25).

$p_{pc} = 665$ psia (page 17-6).

$T_{pc} = 415$R (page 17-6).

$\mu = 18$ cp** (page 19-40).

The gas compressibility c is determined as

$$T_r = \frac{\overline{T} + 460}{T_{pc}} = \frac{587.5}{415} = 1.42$$

$$p_r = \frac{\overline{p}}{P_{pc}} = \frac{720}{665} = 1.08,$$

and from Frick (page 17-15),

$z = 0.875$.

The corrected volumetric flow rates are

$$q_L = 6.49 \times 10^{-5} q_o B_o = 6.49 \times 10^{-5} (1{,}850)\ (1.073)$$
$$= 0.129 \text{ cu ft/sec}$$

$$q_g = 3.27 \times 10^{-7} z\, q_o\, (R - R_s)\, \frac{(\overline{T} + 460)}{\overline{p}}$$
$$= 3.27 \times 10^{-7} (0.875)\ (1{,}850)\ (575 - 115)\ (587.5)/720$$
$$= 0.199 \text{ cu ft/sec}$$

$$q_t = 0.128 + 0.199 = 0.328 \text{ cu ft/sec}.$$

The corrected mass flow rates are

$$w_L = q_o\ (4.05 \times 10^{-3} \gamma_o + 8.85 \times 10^{-7} \gamma_g R_s)$$
$$= 1{,}850\ [4.05 \times 10^{-3} (0.942) + 8.85 \times 10^{-7}\ (0.75)\ (115)]$$
$$= 7.20 \text{ lb/sec}$$

$$w_g = 8.85 \times 10^{-7} q_o \gamma_g (R - R_s)$$
$$= 8.85 \times 10^{-7} (1{,}850)\ (0.75)\ (575 - 115)$$
$$= 0.565 \text{ lb/sec}$$

$$w_t = 7.20 + 0.57 = 7.77 \text{ lb/sec}.$$

*Parentheses indicate the page number in Frick's book[16], where the various correlations are found.

**Live oil viscosity. Dead oil viscosity, a parameter in the correlation, is read from Fig. 13.

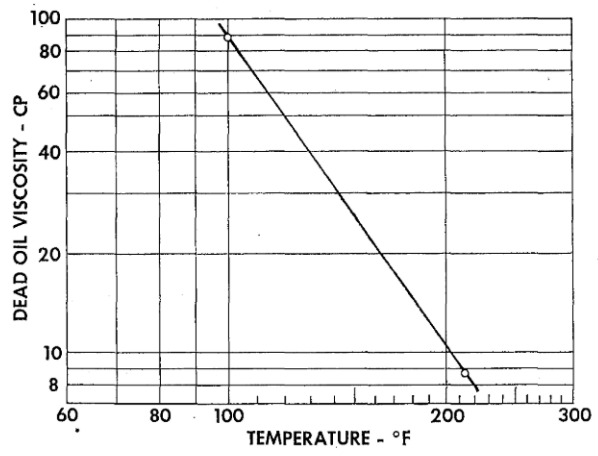

FIG. 13—DEAD OIL VISCOSITY VS TEMPERATURE — WELL 22.

The corrected densities are

$$\rho_L = w_L/q_L = 7.20/0.129 = 55.8 \text{ lb/cu ft}$$
$$\rho_g = w_g q_g = 0.565/0.199 = 2.84 \text{ lb/cu ft}.$$

3. The variables described in Appendix B are calculated and then are tested against the boundary limits to determine the flow regime.

Test Variables:

$$v_t = q_t/A_p = 0.328/0.0488 = 6.72 \text{ ft/sec}.$$

$$q_g/q_t = 0.199/0.328 = 0.607.$$

$$v_{gD} = 0.199 \left[\sqrt[4]{0.534\ (55.8)}\right]/0.0488 = 9.53 \quad \text{(B-1)}$$

Boundary Limits:

$$(L)_B = 1.071 - \frac{0.2218\ (6.72)^2}{0.249} \quad \text{(B-2)}$$

$(L)_B = -22$. Since $(L)_B$ has the limit of 0.13,

$\therefore (L)_B = 0.13$.

$$(L)_S = 50 + 36\ (9.53)\ (0.129)/0.199 = 272 \quad \text{(B-3)}$$

Because $q_g/q_t > (L)_B$ and $v_{gD} < (L)_S$, the fluids are in slug flow.

4. The equations given in the Slug Flow section of Appendix C are used to calculate $\overline{\rho}$ and τ_f.

Determine Reynolds number, bubble Reynolds number and slip velocity (v_b).

$$N_{Re} = 1{,}488\ (55.8)\ (0.249)\ (6.72)/18 = 7{,}720 \quad \text{(C-6)}$$

Since the bubble rise velocity is a nonlinear correlation, iteration is necessary. Therefore, assuming $v_b = 1.75$, bubble Reynolds number is

$$N_b = 1{,}488\ (55.8)\ (0.249)\ (1.75)/18 = 2{,}010.$$

C_2 cannot be read from Fig. 9. Thus the extrapolation equation (Eq. C-7) is used since $N_b < 3{,}000$.

$$v_b = [0.546 + 8.74 \times 10^{-6}\ (7{,}720)]\sqrt{32.2\ (0.249)}$$
$$= 1.74 \text{ ft/sec}.$$

Determine liquid distribution coefficient Γ and friction factor f. Eq. C-13 is used to evaluate Γ since $v_t < 10$:

$$\Gamma = \left[\frac{0.0127 \log (18 + 1)}{(0.249)^{1.415}}\right] - 0.284 + 0.167 \log 6.72$$
$$+ 0.113 \log 0.249 = -0.097.$$

Test limiting Γ with Eq. C-15:

$$-0.097 \geq -0.065\ (6.72)$$
$$\geq -0.436;$$

therefore, $\Gamma = -0.097$.

The ξ/D value from Fig. 7 is 0.0006. With this value and the calculated N_{Re} of 7,720, a friction factor of 0.034 is read from Fig. 6.

Evaluate $\overline{\rho}$ with Eq. C-4:

$$\overline{\rho} = \frac{7.77 + 55.8\ (1.74)\ (0.0488)}{0.328 + 1.74\ (0.0488)}$$
$$+ (-0.097)\ (55.8) = 24.9 \text{ lb/cu ft}.$$

Evaluate τ_f with Eq. C-10:

$$\tau_f = \frac{0.034\ (55.8)\ (6.72)^2}{64.4\ (0.249)}\left[\frac{0.129 + 1.74\ (0.0488)}{0.328 + 1.74\ (0.0488)} - 0.097\right]$$
$$= 2.26 \text{ lb/sq ft/ft}.$$

5. The depth increment from Eq. A-3 is

$$\Delta D_1 = 144 \left[\frac{\Delta p_1 \left(1 - \frac{w_t q_g}{4{,}637 A_p^2 \overline{p}} \right)}{\overline{\rho} + \tau_f} \right]_1$$

$$= 144 \left[\frac{100 \left(1 - \frac{7.77 (0.199)}{4{,}637 (0.0488)^2 (720)} \right)}{24.9 + 2.3} \right]_1 = 529 \text{ ft.}$$

The true value of ΔD_1 is near 529 ft. The calculation will converge very closely to this value even when the assumed ΔZ is off by $\pm$ 10 percent of the assumed value (540 ft) because, under these well conditions, the pressure gradient is primarily controlled by the relatively temperature-insensitive density head. However, under those circumstances where the friction gradient, which is temperature sensitive, is significant, iteration would be necessary should the calculated value of ΔD differ from the assumed value by +10 percent.

6. The top of the next increment is fixed at 529 ft and 770 psi, and Steps 1 through 6 are repeated for the new conditions.

7. The procedure is continued until $\Sigma \Delta D$ is equal to the total depth. The calculated pressure profile is compared against the measured profile in Fig. 14. ★★★

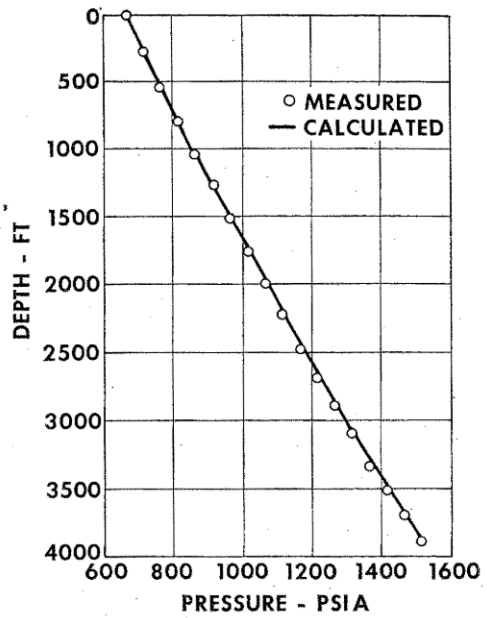

FIG. 14—CALCULATED VS MEASURED PRESSURE DROP — WELL 22.